DIGITAL SIGNAL PROCESSING TECHNIQUES

FOR LANDMINE DETECTION

BY

PEILIN YAO

A Thesis Submitted to the Faculty of Graduate Studies in Partial

Fulfillment of the Requirements for the Degree of

MASTER OF SCIENCE

Department of Electrical and Computer Engineering

University of Manitoba

Winnipeg, Manitoba

DIGITAL SIGNAL PROCESSING TECHNIQUES

FOR LANDMINE DETECTION

BY

PEILIN YAO

A Thesis Submitted to the Faculty of Graduate Studies in Partial

Fulfillment of the Requirements for the Degree of

MASTER OF SCIENCE

Department of Electrical and Computer Engineering
University of Manitoba
Winnipeg, Manitoba

Acknowledgements

I would like to thank my advisor Dr. Gabriel Thomas and Dr.Giuseppe LoVetri for giving me the opportunity to work on this project and for guiding me all throughout my research at the University of Manitoba. Thank you!

During my research, Mr.Corral and Mr. Su helped me greatly in the Lab, not only in GPR raw data preparation, but also thoughtful suggestions and comments. My thanks also go to the members of the GPR projects, Mr. Phelan, Mr. Jeffrey and Mr. Gilmore for their help in carrying out GPR system successfully.

I want to take this opportunity to thank Dr. Pradeepa Yahampath (ECE) and Dr. Ken Snelgrove (Civil Engineering) for accepting as the committee members.

Finally, I want to thank all my friends in Winnipeg for the wonderful time I spent with them, which I will cherish for the rest of my life.

Table of Contents

List of Figures

Abstract

Ground Penetrating Radar (GPR) emits into the ground, through a wideband antenna, an electromagnetic wave covering a large frequency band. Reflections from the soil caused by dielectric variations (such as the presence of an object) are measured. However, GPR systems do not include automatic detection and recognition algorithms, an important feature for applying GPR to landmine detection. The radar group at the University of Manitoba has developed a GPR system for Landmine detection. This system itself does not have any digital signal processing (DSP) algorithms for landmine detection and recognition. In this research effort, DSP methods for landmine detection are investigated. These techniques include: a Linear Prediction (LP) algorithm, the Total Least Square (TLS) algorithm [5], the simplex method and the cross-correlation techniques.

In the first part of this thesis, the finite-difference time-domain (FDTD) method, which is widely accepted for modeling the time domain scattering from buried objects, is used to generate the simulated GPR data for the evaluation of the implemented DSP techniques. Clutter is modelled using a damped exponential model. An Iterative (IT) algorithm [5] is used to decompose the data into its clutter and object contributions.

The LP algorithm, with adaptive processing for the general-purpose landmine detection, and the IT algorithm proposed by Gupta [5] for landmine detection/range estimation are implemented and tested. Analysis of the false alarms as a function of the signal to noise ratio (SNR) is given based on the simulation results. The cross-correlation alarm generator, which reduces the time consumption due to the iterative loop, is

introduced, and its performance for the false alarms as a function of SNR is provided. A dynamic rank calculation for the clutter decomposition is discussed.

Could these methods be used to detect non-metal landmines from experimental data collected using this GPR system? Using this stepped-frequency, continuous wave (SFCW) GPR system, we collected GPR raw data from non-metal landmines. The implemented DSP techniques are investigated, and the parameters of the landmines that algorithms are good at detecting are estimated. The LP algorithm was modified in order to improve its performance. The time delays from the ground surface in the IT algorithm and from the mine were estimated as well.

In our experiments, using a threshold calculated in an area where no landmines are buried, the LP algorithm is able to generate alarms that appear as landmines. The lower the threshold is set, the higher the generated false alarm rate is. With the cross-correlation alarm generator, the false alarm ratio of the IT algorithm is reduced by up to 60%. The implemented IT algorithm is able to detect the non-metal square landmine and to estimate their ranges.

Contributions

The main goal of this research is to apply DSP techniques to detect a non-metal landmine buried underground by using the existing GPR system developed at the University of Manitoba. This thesis investigates DSP algorithms for general-purpose non-metal landmine detection in the cross-range and for a square landmine detection both in cross-range and in depth.

GPR raw data were collected directly from the GPR system without any signal processing. Pre-processing of these GPR raw data focuses on background noise reduction. An LP algorithm is introduced to reduce any deterministic signal based on the layered ground model. Adaptive average background estimation method is used to remove the strong noise. After pre-processing, GPR data is ready for further DSP processing.

Two alarm generators, linear prediction alarm generator and cross-correlation alarm generator, generate alarms for any possible landmines. An LP alarm generator is a general-purpose method based on *error energy change* in the cross-range. The LP algorithm is improved in order to obtain a better result. If a landmine reference signature is available, a cross-correlation alarm generator can be used to generate alarms and reduce the processing time introduced by the IT algorithm.

On each alarmed cross-range scan position, the implemented IT algorithm decomposes the GPR raw data into a clutter set and an object related contribution set. With a reference signature, the number of alarms is reduced further. This thesis introduces a dynamic rank calculation method for the clutter estimation and estimates time delay calculation for the surface contribution. The landmine related parameters are

estimated to calculate the depth of the buried object. Experiments on the measured GPR data prove that these algorithms are able to detect the non-metal square landmine. Estimation of the depth of the landmines is also provided.

Chapter 1 Introduction and Motivation

1.1 The Landmine Threat

Landmines, since the First World War, have proved to be an effective military weapon. Antitank mines disrupt vehicular traffic, while antipersonnel mines protect antitank mines, defend areas, and deny access to bridges and other assets. Under some circumstances, landmines are used to control military and civilian movement across political borders. Although landmines are seen as an effective and inexpensive weapon, they represent a threat to public safety, i.e., to innocent bystanders and civilians. They undermine peace and stability and leave behind maimed individuals who require continuing health care and may cease to be fully productive members of the society.

It is estimated that there are from 50 to 70 million uncleared mines within at least 70 countries. About 26,000 people are killed or maimed every year by landmines [16]. For example, in Angola, one of every 334 individuals is a landmine amputee, and Cambodia has greater than 25,000 amputees due to mine blasts. The lives of over 22 million people are impeded from returning to normalcy by landmines. The US Department of State (1998) provides further information on the global landmine crisis [17].

1.2 The Landmine Detection Problem

Antipersonnel mines come in all shapes and sizes, and can be encased in metal, plastic, wood or nothing at all. They can be embedded in a field cluttered with various materials and objects, buried underground at various depths, scattered on the surface, planted within buildings, or covered by plant overgrowth.

Because mines are made of a variety of explosive materials, a landmine detection system should be able to detect mines regardless of the type of explosives used. Mines come in a variety of shapes and in various types of casings. Therefore, a detection system should either be insensitive to the geometrical shape of the mine and the type of casing material, or preferably, provide imaging information. The latter feature can enable the system to better distinguish mines from background clutter, such as rocks, metal shreds, etc. This, in turn, will reduce the false-positive alarm rate and the time wasted in trying to clear an innocuous object that appears to be a mine. On the other hand, it is vital that the detection system can find the mine, if it is there. Because mines can be buried at different depths under the ground surface, the detection system should not be overly sensitive to the depth of burial. The operator of a detection system should be able to avoid close proximity to the position of the mine to minimize the possibility of inadvertent triggering of the mine. Detection should also be performed at a reasonable operational speed, and at not too prohibitive a cost. This requires that the system must be accurate, not too slow and not too expensive.

In summary, mine detection involves dealing with a wide variety of mine material and shapes, different soil types and terrain, and non-uniformity of clutter. It is expected that the characteristic signature of a buried mine may vary widely depending on local circumstances. It may, therefore, be difficult to apply a particular technique unless the nature of the mine, soil and background clutter is well known. It is inconceivable that a single detection technology will be able to meet all needs.

1.3 Research in Landmine Detection

Landmines are a threat to human lives. Several methods have been developed for landmine detection. They are based on metal detectors, snifters, thermograph techniques and GPR.

Metal detectors attempt to obtain information on buried mines by emitting into the soil a time-varying magnetic field to induce an eddy current in metallic objects; this in turn generates a detectable magnetic field. However, landmines typically contain only a very small amount of metal, possibly in the firing pin, while many others contain no metal at all.

Biological sniffing by dogs is also used. Dogs have greater olfactory senses compared to humans, especially for small trace quantities, and can be trained to detect the presence of explosives. This is, in effect, a material characterization process as dogs are sniffing the vapours emitted from the explosive material. This technique requires, however, extensive training, and the dogs' limited attention span makes it difficult to maintain continuous operation. **Electronic chemical sniffers** can also be used, though they are not as sophisticated as dogs in terms of their detection abilities. Moreover, minefields are usually saturated with residual vapour emissions from recently detonated explosives, which may add to the chemical clutter of the area, thereby confusing the dogs' senses.

The **thermography technique** essentially measures the thermal emissivity of the ground and interprets changes in emissivity as being caused by the presence of a foreign object; therefore, material characterization information is not provided. However, this technology has the advantages of being passive, can be performed remotely, by aerial

search, and can cover a large area in a short time. Infrared thermography is best suited for identifying minefields (global area search), rather than searching for individual mines (local area search). It cannot work when the soil and mine are in thermal equilibrium, and therefore is generally limited for use either at sunset or sunrise when a temperature gradient can be established at the ground surface.

The difference in the reflectance and polarization of soil when disturbed by laser energy may be used to identify the presence of an anomaly [1]. This requires a powerful laser, complex data interpretation and provides no material characterization information.

Ground Penetrating Radar emits into the ground, through an antenna, an electromagnetic wave. Some GPR systems cover a large frequency band, called wide-band GPR system. Reflections from the soil caused by dielectric variations (such as the presence of an object) are measured. Further data processing allows the display of horizontal slices or three-dimensional representations.

Used for about 15 years in civil engineering and geology to detect buried objects and to analyze soil, this technology is well researched. This abundant research, however, does not include GPR systems that use automatic recognition algorithms, a feature important for applying GPR to mine detection. In recent years, researchers have investigated the application of GPR to mine detection. Although promising, the technology has limitations. In particular, the range resolution needed to detect small objects requires GHz frequencies, which results in decreased soil penetration.

Another constraint is cost. Compared to other technologies, especially the ones currently being used, GPR systems can be expensive. Although a GPR system can be

expensive, it is a potential solution for the problem of landmine detection. And low-cost solutions have been proposed [18].

How could the GPR be used to detect the mines while it is receiving very strong reflection from the surroundings? And how about other subsurface objects such as rocks? A subsurface object has a relative dielectric constant, which will be different from that of the ground, and this dielectric discontinuity will also be detected by the GPR. As two objects with different relative dielectric constants will differ in their scattering characteristics, it is feasible that they can be differentiated by a GPR system.

1.4 The proposed GPR system for landmine detection

A GPR system, as shown in Figure 1-1, has been developed at the University of Manitoba for research and development of DSP algorithms for mine detection. The system consists of a microwave network analyzer, an antenna and a motor for controlling the cross-range scan. A personal computer is used to control the motor and receive data from the network analyzer. The purpose of this system is to collect a set of standard GPR raw data and make it available in a database, called Master database, for researchers to develop DSP algorithms for buried object detection. For details about the Master database, please refer to [19].

A single double-ridged horn antenna is used as the transmitter and the receiver. It operates in the range of 1~12.4 GHz. The targeted object is an anti-personal mine shown in Figure 1-2. However, other objects such as rocks are buried too. These objects are randomly scattered on the sand surface before they are buried at different depths.

Our approach has concentrated on applying DSP techniques with this GPR system to the detection of subsurface mines.

This thesis is organized into seven chapters. Chapter 1 describes the motivation and general research efforts for landmine detection. Chapter 2 reviews various existing signal-processing techniques. In Chapter 3, the DSP techniques used in our research are discussed, including improvements of these methods. The FDTD method, which is used to generate simulated GPR data, is introduced in Chapter 4. The simulated GPR data is used to investigate the DSP methods of interest for landmine detection. Random noise is added for the investigation of false alarms as a function of signal-to-noise ratio (SNR). Problems and solutions are also discussed in this chapter. In Chapter 5, the measured GPR data is used to investigate the LP algorithm; the problems encountered in our experiments are described, and solutions to these problems are discussed, too. Before the linear prediction (LP) algorithm is used, the GPR raw data is pre-processed to remove the average background noise. The results of these experiments are presented and discussed. The IT algorithm for clutter decomposition and range estimation on GPR raw data is discussed in Chapter 6. A cross-correlation alarm generator is introduced and experimental results are provided. Finally, in Chapter 7, Conclusions and Future work, summarizes the concepts developed, reports results, highlights possible future work, and provides conclusions from this research effort.

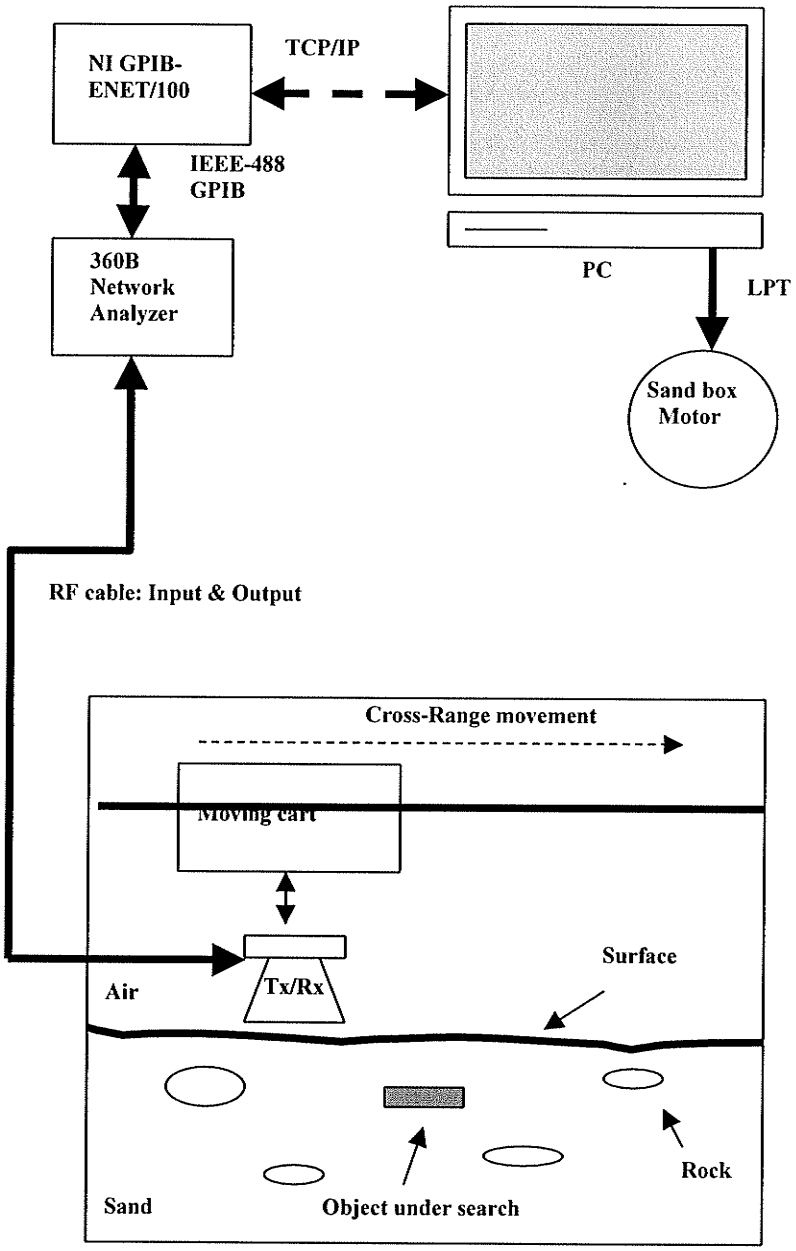

Figure 1-1 GPR system architecture for landmine detection at the University of Manitoba

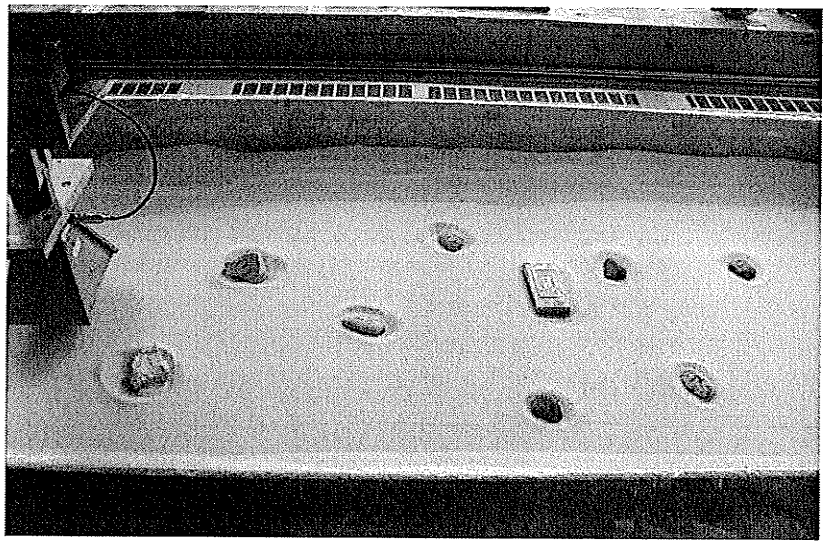

Figure 1-2. Objects placed on the surface to show their coordinates before burying.

Chapter 2 Review of Existing Signal Processing Techniques

Recently, considerable efforts have been put into the development of GPR systems [18]. The coherent clutter component from the ground surface return consists of the dominant clutter contribution and originates at the ground surface. The clutter reduction techniques discussed below, which estimate the coherent component of the clutter, can reduce the coherent component of the ground clutter. The other remaining clutter is still present in the data, which can be further reduced by statistical techniques.

2.1 Conventional methods for clutter reduction

Early time gating is an efficient method for removing the surface clutter from the reflection of deeply buried targets. Choosing an appropriate time gate is very challenging, especially for targets close to the surface. In such cases, the target contributions may be removed due to the overlapping returns of shallow targets and the ground surface. If the GPR system has a high range resolution, then this method may be very useful for removing the dominant clutter.

There are two methods for **average background estimation**. One is **complex average subtracting** [6]. This method uses the mean of a number of measurements taken in an area where it is known no buried objects exist. Subtracting the average may not lead to sufficient clutter reduction because the ground is an inhomogeneous medium and its statistical properties vary with position along the surface. Inhomogeneous aspects of the ground make returns vary from scan position to scan position. Background estimation will be affected by the presence of an object and thus the estimation will not be accurate. The other method is a **moving average estimate of the background** [6],

which uses adaptive algorithms to adjust the estimated background according to the environments.

The early time peak, which is usually due to the ground surface response, can be synthesized in the time domain using a sinc-approximation and subsequently subtracted [5]. However, the presence of shallow targets leads to a change in the amplitude and location of the early time estimation. An improved peak subtraction approach uses a superposition of damped exponentials in the frequency domain to estimate the early time contributions from lossy media. The Prony method [5, 20] has been used to estimate the necessary exponential parameters. The estimated early time clutter can then be subtracted from the data.

2.2 Statistical techniques used for incoherent clutter reduction

If one assumes that incoherent clutter can be represented as a random process with known statistics, then the following methods can be used for clutter reduction.

- **Use of a whitening filter**

The clutter statistics are determined from many realizations of a rough surface. The whitening filter [9] is used as a linear prediction error filter. The limitation of this technique is that the ground medium's statistical properties vary with every position along the surface. Any mismatch in the clutter statistics used to design the filter degrades the performance of the whitening filter.

- **Kalman filtering**

Kalman filtering has been used for parameter estimation in the presence of random noise. It detects sudden changes that occur at the unknown points. In this approach,

parameters are considered as being constant with some fluctuations. The system used at the Technische Universität Ilmenau [4] simulates an array of 6 emitting and receiving antenna. The data are acquired in the frequency domain, between 1 and 6 GHz. This method focuses on the pre-processing of GPR data. It is suggested that for this method to work, the clutter must show a certain amount of correlation.

- **Nonlinear optimization**

Using an impulse radar system with pulse repetition frequency of 250 KHz, Brunzell [6] subtracted the background noise from a handheld GPR return and applied an energy detector to detect shallow objects under the ground. This technique assumes stable ground reflection. It is unsatisfactory in practice because the background is unstable, i.e., background changes from scan to scan.

A subspace decomposition technique has been used for the elimination of ground-reflected clutter from the GPR data [7]. It is based on the generalized singular value decomposition. The proposed model, which uses a low-order polynomial, is for slow spatial variations. The method was applied to the depth interval that contained the ground bounce. The GPR data was obtained by an impulse radar system, which was developed by the Ohio State University.

Deming in [8] proposes the use of the maximum likelihood adaptive neural system to detect landmines. This method requires that the clutter and mine signature models be well defined. The time domain GPR data was obtained by an impulse radar system with center frequency of 400 MHz at University of Oklahoma.

- **Linear Prediction method**

The use of LP [10] for modeling clutter assumes stationary clutter, and computation of the LP coefficients is done over the clutter area assuming no buried landmines. The proposed weighted LP algorithm deals with a non-stationary clutter environment, and the LP coefficients are computed adaptively. In the paper, the ground penetrating radar is FSCW radar, which sends out stepped radio frequency signals to the ground and measures the return. The bandwidth of the radar hardware is in the order of a few Gigaherts (GHz).

- **Hidden Markov Models**

Hidden Markov Models are stochastic models for complex, non-stationary stochastic processes that produce time sequences of random observations as a function of states. The technique proposed in [11] uses a time-domain radar called GEO-CENTERS EFGPR, which is GEO-CENTERS energy focusing GPR. In this model, the landmine signature is used for detection.

2.3 Other methods for clutter reduction in GPR systems

- **Iterative technique for clutter reduction in GPR system**

An ultra-wideband GPR system is used in [5] where only a small spot on the ground surface is illuminated. The clutter is assumed to be rough surface scattering, surface-target interaction terms as well as some inhomogeneties. This new algorithm decomposes the GPR return into its clutter and target contribution. The clutter reduction algorithm yields an estimation of the depth of the subsurface target. A damped exponential model is used. An adaptive estimation of unknown parameters is

accomplished by the iterative process, which has two coupled iterative loops. The Prony technique is also used for this parameter estimation. An appropriate time window is required to separate the early time clutter contribution from the late time clutter. It is claimed that this technique has the potential for real world applications. Their experimental GPR data were acquired using frequencies between 1 GHz and 5 GHz in increments of 100 MHz through a near field probe antenna.

2.4 DSP methods used in this thesis

In summary, an accurate estimation of the clutter is crucial for all of the above techniques. Finding an accurate estimate is indeed a very challenging task due to the uncertainty and variation in the ground scattering. Generally speaking, two kinds of commonly used GPR systems for landmine detection are pulse radar and SFCW radar. With our ultra-wideband network analyzer, which can generate a step frequency signal from 1 GHz to 12 GHz, we will use linear prediction algorithm (based on layered earth model) and average background estimation technique to reduce (pre-processing) the background noise from the GPR raw data. After the pre-processing, LP algorithm will be investigated for general cross-range landmine detection (*error energy detection*). On each scan position, *TLS-Prony* in frequency domain for clutter estimation. The IT method with the reference signature of a landmine [5] is used for the specific landmine detection, and this technique can provide range estimation as well. The block diagram of the DSP techniques used is shown in Figure 2-1.

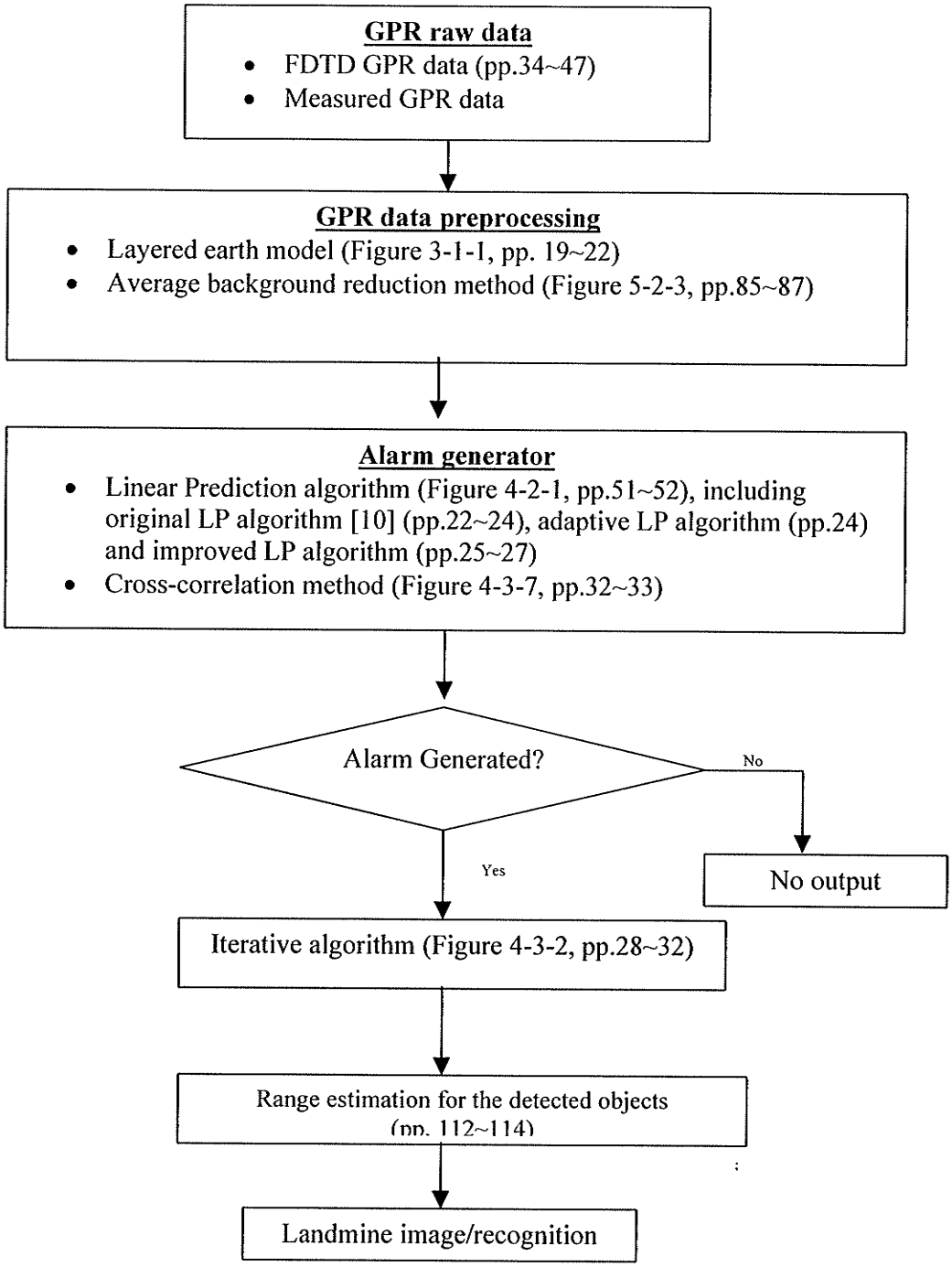

Figure 2.1 Blocks diagram of DSP techniques used in this thesis

Chapter 3 Introduction to Various Applicable DSP Techniques

As mentioned in Chapter 2, the LP algorithm [10] and the IT algorithm [5] are used in our system and have been investigated further to meet our system needs for landmine detection. The LP algorithm generates alarms if the calculated *error energy* is above a threshold. The IT algorithm uses the *TLS-Prony* technique for clutter reduction and the simplex method[1] for range estimation. A layered geophysical model is helpful in understanding the wave propagation characteristics and in preprocessing the GPR data in order to remove deterministic signals. In this chapter, we will introduce the concepts of these techniques.

3.1 A geophysical model

A geophysical model [2] is proposed to represent the real earth in certain significant respects. If there is a useful connection between the behavior of the earth and the corresponding behavior of the model, the model can be useful in analyzing data from the earth and making geological decisions. The linear algorithm, which will be incorporated herein, is based on a *layered-delay model.*

There are two basic approaches to data processing: the deterministic approach and the statistical approach. The deterministic approach is concerned with the building of mathematical and physical models of, for example, a layered earth to better understand wave propagation. The statistical approach is concerned with the building of models involving random components. For example, deep reflecting objects are considered to have a random distribution.

[1] The MATLAB function "fminsearch" is used, [21].

A flat-layered earth is a well-know model used in geophysics, as depicted in figure 3-1-1. A horizontal line represents the surface, and below the surface there are media whose interfaces are parallel to the surface. There are *N+1* horizontal interfaces. The topmost interface is denoted by index 0, while the lowest interface is denoted by index *N*. Two electromagnetic plane waves are assumed to exist within each layer, one wave traveling upward and the other one traveling downward.

If a down-going propagating wave is incident on the top of interface *n*, then the reflection coefficient r_n is equal to the resulting up-going signal reflected from the top of interface *n*, and transmission coefficient τ_n is equal to the resulting down-going signal transmitted through interface *n*. If the up-going wave is on the bottom of the interface *n*, then the reflection coefficient is denoted as r_n' and transmission coefficients is denoted as τ_n' .

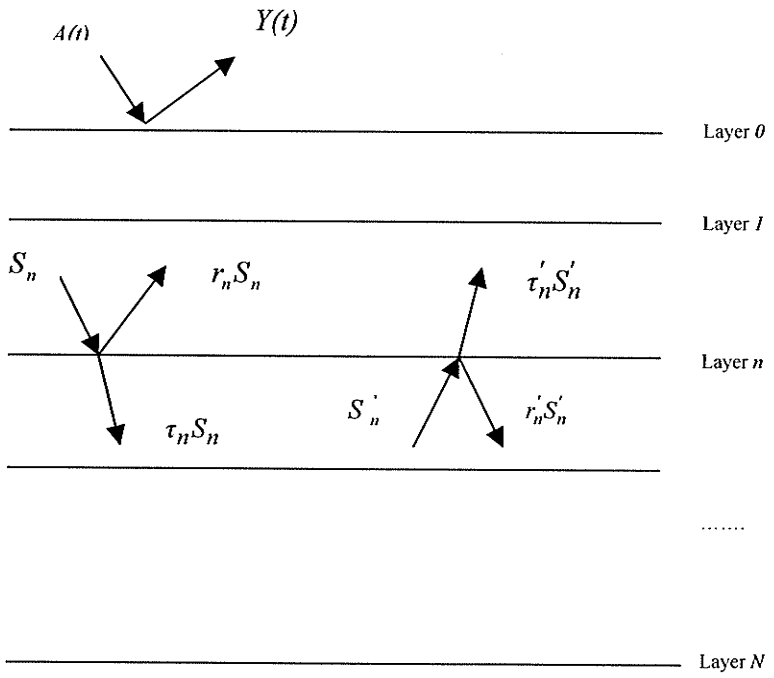

Figure 3-1-1: The layered system and the reflection / transmission coefficients for an interface

Using the sifting property $A(\tau) = \int_{-\infty}^{+\infty} A(t)\delta(t-\tau)dt$, any wave train can be represented by its generating function:

$$A(t) = A_0\delta(t-t_0) + A_1\delta(t-t_0-\Delta t) + A_2\delta(t-t_0-2\Delta t) + \ldots$$

Signal A_0 occurs at the time t_0, and A_1 occurs at a delay of one time unit $t_0 + \Delta t$, i.e., at a delay of the two-way travel time through the nearby layer. Then the received signal $Y(t)$ at the topmost surface at time $t = t_0$ is given by $Y_0 = r_0 A_0$. At time $t = t_0 + \Delta t$, the received signal Y_1 will be:

$$Y_1 = r_0 A_1 + \tau_0' r_1 \tau_0 A_0 = r_0 A_1 + \tau_0' r_1 \tau_0 Y_0 / r_0$$

Letting $b_1 = \tau_0' r_1 \tau_0 / r_0$ and $b_0 = r_0$, we have

$$Y_1 = b_0 A_1 + b_1 Y_0$$

Similarly, at time $t = t_0 + 2\Delta t$, we have

$$\begin{aligned} Y_2 &= r_0 A_2 + \tau_0' r_1 \tau_0 A_1 + \tau_0' \tau_1' r_2 \tau_1 \tau_0 A_0 \\ &= r_0 A_2 + \tau_0' r_1 \tau_0 (Y_1 - \tau_0' r_1 \tau_0 Y_0 / r_0)/r_0 + \tau_0' \tau_1' r_2 \tau_1 \tau_0 A_0 \\ &= r_0 A_2 + \tau_0' r_1 \tau_0 Y_1 / r_0 - (\tau_0' r_1 \tau_0)^2 Y_0 / (r_0)^2 + \tau_0' \tau_1' r_2 \tau_1 \tau_0 Y_0 / r_0 \end{aligned}$$

Letting $b_2 = \tau_0'\tau_1' r_2 \tau_1 \tau_0 / r_o - (\tau_0' r_1 \tau_0 / r_0)^2 = \tau_0'\tau_1' r_2 \tau_1 \tau_0 / r_0 - b_1^2$, i.e. $\tau_0'\tau_1' r_2 \tau_1 \tau_0 / r_0 = b_1^2 + b_2$, then, we have:

$$Y_2 = b_0 A_2 + b_1 Y_1 + b_2 Y_0$$

In general, summing all the contribution at $t = t_0 + n\Delta t$, we will have the reflected wave given as:

$$Y_n = b_0 A_n + b_1 Y_{n-1} + b_2 Y_{n-2} + \ldots + b_n Y_0$$

Suppose $A_{n+1} = 0$ at $t = t_0 + (n+1)\Delta t$, and then the above equation becomes the linear combination of the previous data.

$$Y_{n+1} = b_1 Y_n + b_2 Y_{n-1} + \ldots + b_n Y_1 + b_{n+1} Y_0 \qquad (3\text{-}1\text{-}1)$$

This equation justifies the "linear combination" model in the time-domain for the deterministic signal and which will be used in FDTD simulation. A least square algorithm is used to determine $b_1, b_2, \ldots, b_{n+1}$ for a particular ground reflection simulation.

3.2 Linear Prediction Algorithm

The LP algorithm calculates the *error energy* from the nearby cross-range scan position along the beam, as shown in Figure 3-2-1. On each scan position, the GPR system emits a sequence of continuous frequency waves stepped over several frequencies. Our current GPR system has up to 501 step frequencies from 1 GHz to 12.4 GHz. A Master database of many experiments has been compiled [19].

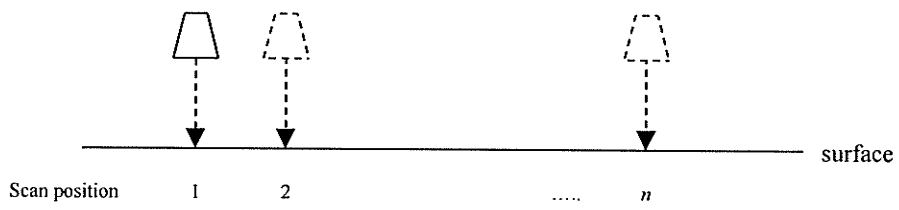

Figure 3-2-1 An application example using linear prediction algorithm

3.2.1 The basis of the linear prediction algorithm

Let $y(n) = [x_1(n) \quad x_2(n) \quad \ldots \quad x_L(n)]^T$ be a vector that contains the complex (i.e., magnitude and phase) GPR return at the cross-range scan position n. The element $x_i(n)$ is the received GPR phasor at step frequency f_i, i=1,2,…,L. L is the total number of step frequencies (L is 512 in our case). Given the current vector and a few previous vector samples, it is up to the LP algorithm to decide if $y(n)$ is from a landmine. The current vector $y(n)$ can be predicted from a linear combination of its past few vectors (for clutter only). We may assume that the clutter vector sample $y(n)$ satisfies the time-varying LP model:

$$y(n) = \sum_{k=1}^{p} a_k(n) y(n-k) + e(n) = \boldsymbol{Y}(n-1)\boldsymbol{a}(n) + e(n) \tag{3-2-1}$$

$$\tilde{y}(n) = \boldsymbol{Y}(n-1)\boldsymbol{a} \tag{3-2-2}$$

where k =1, 2, ..., p, p is the prediction order, and $\boldsymbol{Y}(n-1) = [y(n-1) \quad y(n-2) \quad \ldots \quad y(n-p)]$ is a scan data matrix of the last p scans. The LP coefficient vector to be determined is $\boldsymbol{a}(n) = [a_1(n) \quad a_2(n) \quad \ldots \quad a_p(n)]^T$. The vector $\mathbf{e}(n)$ is called the *prediction error vector*. The distribution of the sample vector $y(n)$ may not be Gaussian, but the LP error $e(n)$ can be approximated as a Gaussian distribution having zero mean and covariance matrix $\boldsymbol{C}$ [10]. Suppose that E[] indicates the average operation, then the covariance matrix $\boldsymbol{C}$ is calculated by:

$$\boldsymbol{C} = \mathrm{E}[(y(n) - \tilde{y}(n))(y(n) - \tilde{y}(n))^*]$$

where the superscript $*$ represents the complex conjugate transpose operation.. Using LSE to estimate the coefficients in equation (3-2-1) and to apply them to $\tilde{y}(n)$ in equation (3-2-2), we can obtain the collection of LP error $e(n)$ over a small area assuming no landmine existing, and then the estimation of the covariance matrix $\boldsymbol{C}$ is calculated using MATLAB function ***normfit*** (refer to section 4.2 for implementation details).

Letting $\xi(n)$ be the weighted prediction error energy which can be calculated by

$$\xi(n) = e(n)^* \boldsymbol{C}^{-1} e(n) = [y(n) - \tilde{y}(n)]^* \boldsymbol{C}^{-1} [y(n) - \tilde{y}(n)] \tag{3-2-3}$$

Taking the derivative of the above with respect to $\boldsymbol{a}(n)$ and setting this gradient to zero gives the solution (see [10] for details and Appendix IV for reference):

$$\boldsymbol{a}^o(n) = [\boldsymbol{Y}(n-1)^* \boldsymbol{C}^{-1} \boldsymbol{Y}(n-1)]^{-1} \boldsymbol{Y}(n-1)^* \boldsymbol{C}^{-1} y(n) \tag{3-2-4}$$

The error energy $\xi(n)$ will then be given by:

$$\xi(n) = y(n)^* \boldsymbol{C}^{-1} y(n) - y(n)^* \boldsymbol{C}^{-1} \boldsymbol{Y}(n-1) \boldsymbol{a}^o(n) \tag{3-2-5}$$

We then declare a detection of landmine if $\xi(n)$ is greater than some threshold. $\xi(n)$ is the minimum weighted prediction error energy, where the weighting matrix is given by $\boldsymbol{C}^{-1}$. Setting the derivative of $\xi(n)$ to zero in equation (3-2-3) means that a least square model is being used.

3.2.2 Threshold and weighting matrix

- **Adaptive threshold**

The prediction error energy $\xi(n)$ will typically vary from one set of p-scans to another because the statistics of the ground will vary. Using a fixed threshold will increase the false alarm rate or decrease the probability of detection. The mean $\mathrm{E}[\xi(n)]$ and variance $\mathrm{E}[|\xi(n) - E[\xi(n)|^2]$ are updated as follows:

$$\mathrm{E}[\xi(n)] = (1-\lambda)\,\mathrm{E}[\xi(n-1)] + \lambda \xi(n) \tag{3-2-6}$$

$$\mathrm{E}[|\xi(n) - \mathrm{E}[\xi(n)]|^2] = (1-\lambda)\,\mathrm{E}[|\xi(n-1) - \mathrm{E}[\xi(n-1)]|^2] + \lambda\,|\xi(n) - \mathrm{E}[\xi(n)]|^2$$

The normalized error energy $\xi(n)$ is:

$$\xi'(n) = \{\xi(n) - \mathrm{E}[\xi(n)]\} / \{\mathrm{E}[|\xi(n) - \mathrm{E}[\xi(n)]|^2]\}^{1/2} \tag{3-2-7}$$

A landmine is detected if $\xi'(n)$ is greater than the normalized error energy threshold. The parameter λ in equation (3-2-6) is chosen experimentally.

- **Weighting matrix**

The weighting matrix $\boldsymbol{W}$ is given by $\mathbf{C}^{-1}$:

$$\boldsymbol{W} = \boldsymbol{C}^{-1}$$

Because the prediction error $e(n)$ in the clutter may be highly correlated, the inverse of the covariance matrix $\boldsymbol{C}$ may have a singularity problem. To solve this, we first find the

principle components of the clutter. Then, we reduce the rank of $\boldsymbol{C}$ by calculating its eigenvector matrix $\boldsymbol{Q}$ and its related eigenvalue matrix $\boldsymbol{G}$. And finally, we form the weighting matrix **W** as follows:

$$\boldsymbol{W} = \boldsymbol{QGQ}^{*} \tag{3-2-8}$$

The eigenvalue matrix is given by $\boldsymbol{G} = diag\{\lambda_1, \lambda_2, ..., \lambda_L\}, \lambda_1 \geq \lambda_2 \geq ... \geq \lambda_L$. If we form a diagonal matrix of eigenvalues as:

$$\boldsymbol{D} = diag\{1/\lambda_1, 1/\lambda_2, ..., 1/\lambda_J, 0, ..., 0\}$$

where J is the largest integer such that $\lambda_1 / \lambda_J \leq k$, where k is a chosen parameter, the matrix $\boldsymbol{W}$ is then given by:

$$\boldsymbol{W} = \boldsymbol{QDQ}^{*} \tag{3-2-9}$$

Now the coefficients are calculated by

$$\boldsymbol{a}^{o}(\mathrm{n}) = [\boldsymbol{Y}(\mathrm{n}-1)^{*}\, \boldsymbol{WY}(\mathrm{n}-1)]^{-1} \boldsymbol{Y}(\mathrm{n}-1)^{*}\, \boldsymbol{Wy}(\mathrm{n}) \tag{3-2-10}$$

3.2.3 Improvement of the LP algorithm

If we let $\boldsymbol{W} = \boldsymbol{W}_h^{*}\boldsymbol{W}_h$, $\boldsymbol{y}_w(n) = \boldsymbol{W}_h \boldsymbol{y}(n)$ and $\boldsymbol{Y}_w(n-1) = \boldsymbol{W}_h \boldsymbol{Y}(n-1)$, where $\boldsymbol{W}_h = \boldsymbol{D}^{1/2}\boldsymbol{Q}$

Equation (3-2-10) becomes:

$$\boldsymbol{a}^{o}(\mathrm{n}) = [\boldsymbol{Y}_w(\mathrm{n}-1)^{*}\, \boldsymbol{Y}_w(\mathrm{n}-1)]^{-1} \boldsymbol{Y}_w(\mathrm{n}-1)^{*}\, \boldsymbol{y}_w(\mathrm{n}) \tag{3-2-11}$$

The coefficients $\boldsymbol{a}^{o}(\mathrm{n})$ can be physically interpreted as the ratio of correlated energy $\mathbf{Y}_w(\mathrm{n}-1)^{*}\mathbf{y}_w(\mathrm{n})$ over the previous correlated energy $\mathbf{Y}_w(\mathrm{n}-1)^{*}\mathbf{Y}_w(\mathrm{n}-1)$.

We calculate $\boldsymbol{Y}_w(\mathrm{n}-1)^{*}\boldsymbol{Y}_w(\mathrm{n}-1)$ by

$$
\begin{aligned}
&Y_w(\text{n-1})^* Y_w(\text{n-1}) \\
&=[y_w(n-1) \quad y_w(n-2) \quad \ldots \quad y_w(n-p)]^*[y_w(n-1) \quad y_w(n-2) \quad \ldots \quad y_w(n-p)] \\
&=\begin{bmatrix} y_w(n-1)^* y_w(n-1) & y_w(n-1)^* y_w(n-2) & \ldots & y_w(n-1)^* y_w(n-p) \\ y_w(n-2)^* y_w(n-1) & y_w(n-2)^* y_w(n-2) & \ldots & y_w(n-2)^* y_w(n-p) \\ \ldots\ldots & & & \\ y_w(n-p)^* y_w(n-1) & y_w(n-p)^* y_w(n-2) & \ldots & y_w(n-p)^* y_w(n-p) \end{bmatrix}
\end{aligned}
$$

(3-2-12)

The diagonal components, i.e., $y_w(n-i)^* y_w(n-i)$ in equation (3-2-12) are energies at the previous scan positions. $y_w(n-i)^* y_w(n-j), i \neq j$, are the cross-correlation products of different scan positions. The linear prediction coefficients not only depend on the previous energy received, but also depend on the cross-correlation at the different scan positions.

After the background signal is removed, the residue signal is assumed to have Gaussian distribution, which means the residue signals are independent from a scan position to another san position. Based on this assumption, we will have:

$$y_w(n-i)^* y_w(n-j) = 0, i \neq j \tag{3-2-13}$$

Then:

$$
\begin{aligned}
Y_w(n\text{-}1)^* Y_w(n\text{-}1) &= diag\{y_w(n-1)^* y_w(n-1), y_w(n-2)^* y_w(n-2), \ldots, y_w(n-p)^* y_w(n-p)\} \\
&= diag\{\text{energy}_{n-1}, \text{energy}_{n-2}, \ldots, \text{energy}_{n-p}\} \\
&= \boldsymbol{S}
\end{aligned}
$$

Here, we use the notation $\text{energy}_{n-i,n-j} = y_w(n-i)^* y_w(n-j)$ and $\text{energy}_{n-i} = y_w(n-i)^* y_w(n-i)$

$\boldsymbol{S}$ should have full rank, then

$$\boldsymbol{S}^{-1} = diag\{\text{energy}_{n-1}^{-1}, \text{energy}_{n-2}^{-1}, \ldots, \text{energy}_{n-p}^{-1}\}$$

and $Y_w(\text{n-1})^* y_w(\text{n}) = [y_w(\text{n-1}) \quad y_w(\text{n-2}) \ldots \quad y_w(\text{n-p})]^* y_w(\text{n})$

Then equation (3-2-11) becomes

$$a^{o}(\mathrm{n}) = \boldsymbol{S}^{-1}\boldsymbol{Y}_{w}(\mathrm{n}-1)^{*}\, y_{w}(\mathrm{n})$$

$$= [\frac{y_{w}(\mathrm{n}-1)^{*}\, y_{w}(\mathrm{n})}{\mathrm{energy}_{\mathrm{n-1}}} \quad \frac{y_{w}(\mathrm{n}-2)^{*}\, y_{w}(\mathrm{n})}{\mathrm{energy}_{\mathrm{n-2}}} \quad \cdots \quad \frac{y_{w}(\mathrm{n}-\mathrm{p})^{*}\, y_{w}(\mathrm{n})}{\mathrm{energy}_{\mathrm{n-p}}}]^{T}$$

$$a_{i}^{o}(n) = \frac{y_{w}(\mathrm{n}-\mathrm{i})^{*}\, y_{w}(\mathrm{n})}{\mathrm{energy}_{\mathrm{n-i}}} = \frac{\mathrm{energy}_{\mathrm{n-i,n}}}{\mathrm{energy}_{\mathrm{n-i}}}, i = 1,2,\ldots, p \qquad (3\text{-}2\text{-}14)$$

The above equation (3-2-14) indicates that the linear prediction coefficient is the ratio of cross-correlated energy over the energy received at the particular previous scan position. The coefficient $a_{i}^{o}(n)$ will be zero, this is because

$$y_{w}(n-i)^{*}\, y_{w}(n) = 0, \quad for \quad all \quad i \neq 0$$

Therefore, the new complex GPR return vector cannot be predicted by the previous returns. If this cross-correlation is small, the prediction will also be poor. Since $a_{i}^{o}(n) = 0$, equation (3-2-5) becomes

$$\xi(n) = y(n)^{*}\boldsymbol{C}^{-1}y(n)$$

The previous analysis has considered that GPR data at different scan positions are highly independent. However, if energy_{n-i} is close to zero, this can result in undetermined $a_{i}^{o}(n)$ values in equation (3-2-14). A new linear prediction formula for the coefficients can be determined by:

$$a_{i}(n) = \frac{\mathrm{energy}_{n-i,n}}{\sum_{\mathrm{k=1}}^{\mathrm{p}} \mathrm{energy}_{\mathrm{n-k}}}, i = 1,2,\ldots, p \qquad (3\text{-}2\text{-}15)$$

Here we have only modified the denominator of (3-2-14) so that no singularities occur. The advantage of equation (3-2-15) is that the linear prediction coefficients are calculated using correlation energy over the sum of the energies over the prediction area.

This will avoid the sudden change because of the very low energy or zero energy in some rare cases.

3.2.4 Summary of the LP algorithm

The linear prediction algorithm calculates the weighted prediction error of a clutter vector sample from a position so that significant error energy may indicate that the clutter has changed suddenly, indicating the possibility of having a landmine at that position. Because it does not use any knowledge of mine properties, it is a general algorithm for any landmine detection, but it has the disadvantage that it will be triggered by any abrupt change in soil properties, or by any buried object.

If the received GPR wave is independent from each scan position, the complex GPR return vector is unpredictable. The improved linear prediction algorithm in (3-2-15) is obtained for the specific case of zero error energy, which was more applicable to our problem (mostly homogeneous clutter). The improved linear prediction coefficients are modified to avoid the zero energy problems in equation (3-2-14).

3.3 TLS–Prony Method

The TLS algorithm [5] is used for ground bounce clutter estimation and reduction in the frequency domain. An exponential model is used to model the clutter and the Prony method estimates the parameters for clutter decomposition.

3.3.1 Concept of the TLS Method

In this GPR application, the received GPR raw data in the frequency domain, at each scan position, can be presented by:

$$y(\omega) = [y(\omega_1) \quad \ldots \quad y(\omega_L)] = [y_1 \quad \ldots \quad y_L] \tag{3-3-1}$$

where $\omega_i, i = 1,\ldots,L$ is a sequence of L continuous frequency steps. Each frequency measurement y_i has an error e_i. Equation (3-3-1) becomes:

$$y_n = ([y_{n-1} \quad \ldots \quad y_{n-k}] + [e_{n-1} \quad \ldots \quad e_{n-k}])\boldsymbol{a} + e_n \qquad k < n \le M \tag{3-3-2}$$

Then, the TLS method becomes finding a solution for the vector $\boldsymbol{a}$ such that $\sum_{i=0}^{k} e_{n-i}^2$ is a minimum.

If we define $\mathbf{x}$ as $[y_{n-1} \quad y_{n-2} \quad \ldots \quad y_{n-k}]$, $\mathbf{e}_{x,n} = [e_{n-1} \quad \ldots \quad e_{n-k}]$ and $e_{y,n} = e_n$, then Equation (3-3-2) becomes:

$$y_n = [\boldsymbol{x}_n + \boldsymbol{e}_{x,n}]\boldsymbol{a} + e_{y,n} \tag{3-3-3}$$

Let $\boldsymbol{e} = [e_{x,n} \mid e_{y,n}]$, then TLS problem becomes finding the vector $\boldsymbol{a}$ such that the norm of $\boldsymbol{e}$ is minimum.

If

$$y_n = \boldsymbol{x}_n \boldsymbol{a} = \sum_{i=1}^{k} a_i y_{n-i} \tag{3-3-4}$$

substituting y_n in Equation (3-3-4) to Equation (3-3-3), we have

$$0 = e_{x,n}\boldsymbol{a} + e_{y,n} = [e_{x,n} \mid e_{y,n}] \begin{bmatrix} a \\ 1 \end{bmatrix} \tag{3-3-5}$$

Using Prony method (provided by MATLAB) to estimate coefficient vector $\boldsymbol{a}$, $e_{x,n}$ will be minimized, which results in $e_{y,n}$ be minimized because of Equation (3-3-5). This indicates that the norm of $\boldsymbol{e}$, expressed as $\|e\| = (\sum_{i=0}^{K} e_i^2)^{1/2}$, is minimum if the coefficient vector $\boldsymbol{a}$ satisfies equation (3-3-4).

3.3.2 Exponential model

Using an exponential model [5], $y(\omega)$ becomes:

$$y(\omega) = \sum_{i=1}^{N} c_i e^{-\omega\gamma_i} e^{-j\omega t_i} \tag{3-3-6}$$

where $e^{-j\omega t_i}$ is a linear phase factor, c_i is a complex amplitude factor for the frequency independent component of the received signal, $e^{-\omega\gamma_i}$ is a damping factor with $\gamma_i \geq 0$, t_i is the time delay as the wave propagation toward the mine, and ω denotes frequency. Three parameters $[c_i, t_i, \gamma_i]$ will be estimated by the Prony method. ($N \geq 2$ is expected). The time delay parameter t_i can also be used to calculate the range of the buried landmine.

3.4 Modelling of the clutter and the landmine contribution

After the estimated clutter is removed, the residual GPR data is dominated by the contribution from the buried object if there is any. In this section we will introduce a *scattering model* for the buried object contribution and its parameters will then be estimated by the Simplex method.

3.4.1 An exponential model for Clutter and Target's scattering model

Similar to the clutter model, the **scattering model** is defined as:

$$t(\omega) = A_r e^{-\omega\gamma_r} e^{-j\omega\delta_r} T_r(\omega) \tag{3-4-1}$$

where a linear phase factor $e^{-j\omega\delta_r}$ is considered as the contribution from the mine at the time delay $\delta_r, \delta_r \geq 0$, and $T_r(\omega)$ represents a reference signature of a landmine.

The received GPR data $Gpr(\omega)$ can then be represented as:

$$Gpr(\omega) = c(\omega) + t(\omega) + n(\omega)$$

where $n(\omega)$ is additive Gaussian noises. If $\hat{c}(\omega)$ represents the estimated clutter from $c(\omega)$ defined in equation (3-3-6), the residual GPR data $R(\omega) = Gpr(\omega) - \hat{c}(\omega)$ is dominated by the mine contribution $t(\omega)$. The unknown parameter vector $\theta = [A_r \quad \gamma_r \quad \delta_r]$ for the mine are determined by minimizing the square error, known as least square error, between the object model and residual data.

$$E_r(\theta) = \sum_{\omega_1}^{\omega_n} | R(\omega) - t(\omega) |^2 = \sum_{\omega_1}^{\omega_n} | R(\omega) - A_r e^{-\omega\gamma_r} e^{-j\omega\delta_r} T_r(\omega) |^2 \qquad (3\text{-}4\text{-}2)$$

where ω_1 and ω_n are the start and end frequencies, and $\theta = [A_r \quad \gamma_r \quad \delta_r]$ is the unknown parameter vector to be estimated.

3.4.2 Simplex method for the parameter estimation

In section 3.4.1, the reflection from the mine is modeled by the reference signature $T_r(\omega)$ and unknown parameter vector $\boldsymbol{\theta} = [A_r \quad \gamma_r \quad \delta_r]$ in equation (3-4-1). The parameter vector $\boldsymbol{\theta}$ is estimated by using the Simplex method to minimize the error in equation (3-4-2).

The error function (3-4-2) is represented as a LSE. Why don't we directly use the LSE method to estimate these parameters? There are two reasons. One is that the simplex method requires only function evaluations. LSE is not very efficient in terms of the number of function evaluations that it requires. However, the Simplex Method may often be the best method to use. In the case of multiple dimensions, the LSE method sometimes does not converge to the minimum, but the simplex is constantly shrinking. The other reason is that the simulation results from the Simplex method, **fminsearch** in

MATLAB, and the LSE method, **lsqcurvefit** in MATLAB, indicated that the Simplex Method was more suitable than the LSE method in our case. Refer to Appendix I for details.

3.5 Cross-correlation technique with threshold

In section 3.4, a reference signature is used for mine detection and parameter estimation. With our high range resolution GPR radar, the cross-correlation technique with a reference signature in time domain can also be used to generate alarms.

Suppose that in time domain, *y(t)* and *x(t)* are two jointly stationary random processes, the cross-correlation of *y(t)* and *x(t)* is defined as:

$$Corr_{y,x}(\tau) = E[y(t)x(t)] = \int_{-\infty}^{\infty} y(t+\tau)x(t)dt \qquad (3\text{-}5\text{-}1)$$

In our GPR application, after the clutter is removed, the GPR residual data, in time domain, $R(t)$ can be represented by

$$R(t) = AT_r(t) + n(t) + r_c(t) \qquad (3\text{-}5\text{-}2)$$

where $n(t)$ is random noise, independent of the mine contribution $AT_r(t)$, and $r_c(t)$ is the residual clutter. $T_r(t)$ is a reference signature of the mine. The cross-correlation of $R(t)$ and $T_r(t)$ is:

$$E[R(t)T_r(t)] = E[AT_r(t)T_r^*(t)] + E[n(t)T_r^*(t)] + E[r_c(t)T_r^*(t)] \qquad (3\text{-}5\text{-}3)$$

Since $n(t)$ is independent from $T_r(t)$, the second term will be zero, i.e.

$$E[R(t)T(t)] = AE[\|T_r(t)\|^2] + E[r_c(t)T_r^*(t)] \qquad (3\text{-}5\text{-}4)$$

If the threshold is set to $E[r_c(t)T_r^*(t)]$, then, a target is detected if $E[R(t)T(t)] > threshold$. The threshold is an experimental result, which is obtained by illuminating a small area where no mine is expected.

Chapter 4 Implementation of DSP algorithms and Simulation results

In this chapter, the FDTD method is used to generate the simulated GPR data. In section 4.1, we first introduce the creation of FDTD GPR data, and then preprocess them for further processing. The linear prediction algorithm discussed in section 4.2 generates alarms for object detection without any knowledge of specific object type. The IT algorithm for specific object detection, described in section 4.3, consists of two steps: one is for removal ground reflection, and the other one for the estimation of target parameter, especially for the range estimation. The objectives of these simulations are to determine the adequacy of these DSP algorithms' implementation and their efficiency.

4.1 Introduction to FDTD GPR data

4.1.1 General geometry model for the FDTD simulations

The FDTD method is a powerful and simple method, which can easily produce numerically synthesized data for the GPR problem. The specific objects of interest are landmines, which, electrically, are lossy dielectric objects with minimal highly conducting parts.

In order to build a scattering model for the FDTD simulation software, we need to create the geometry of the problem first. An example of the problem data file is in Appendix II. Its geometry is shown in Figure 4-1-1 and Figure 4-1-2. Test points, from T1 to T17, are set between the current source and ground surface. To ensure the accuracy and stability of the 3-D FDTD computation, the numerical parameters for the problem must be chosen carefully.

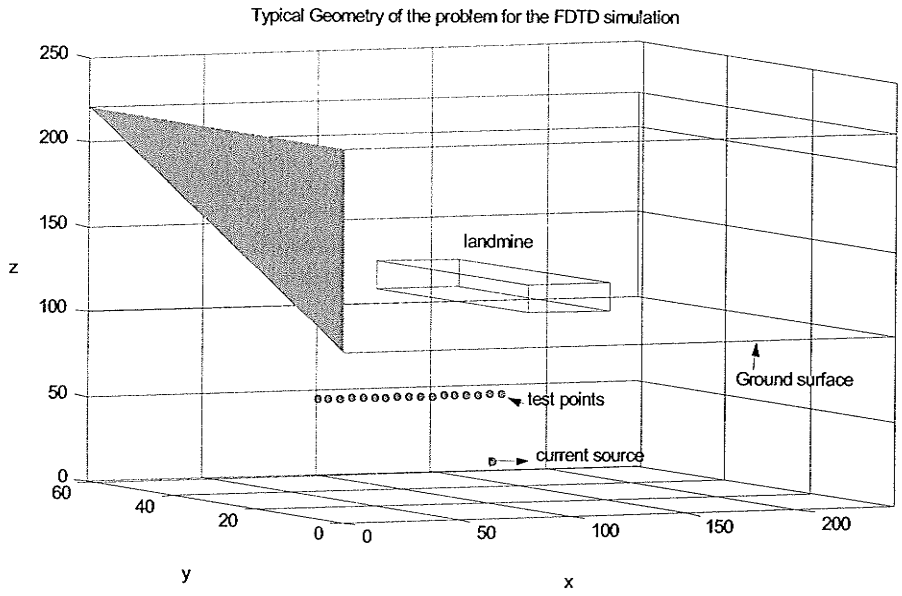

Figure 4-1- 1 Typical Geometry of the problem for the FDTD simulation

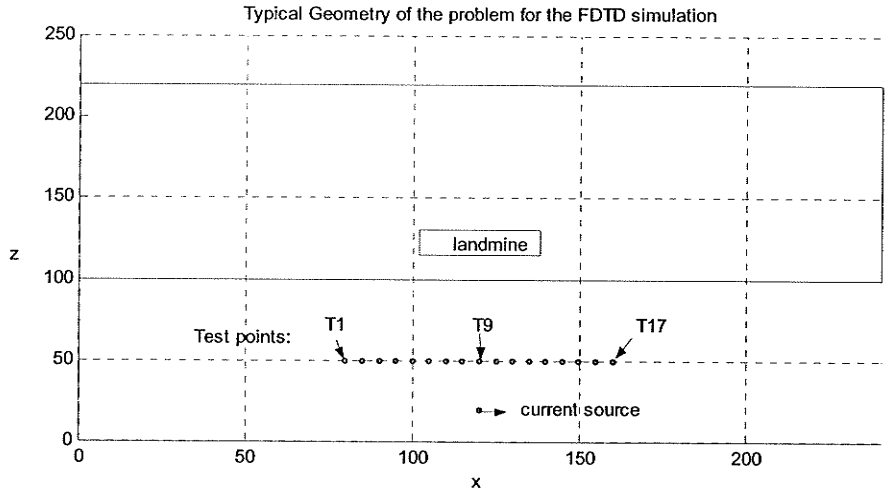

Figure 4-1- 2 x-z plane of the typical geometry of the problem

- **Cell size**

Cell size is determined based on the shortest wavelength. For example, if the GPR frequency is from 1GHz to 5GHz, the highest frequency $f_{\max}$ is 5GHz. The shortest wavelength is:

$$\lambda_{\min} = \frac{v_g}{f_{\max}}, \qquad v_g = \frac{c}{\sqrt{\varepsilon_r}} \tag{4-1-1}$$

v_g is the propagation speed and ε_r is the relative dielectric constant of the propagation media. The term c is the propagation speed in the air, i.e. 3×10^8. ε_r is around 3.15 for lossy sand [15] and 3.5 for plastic landmine [5]. Therefore,

$$\lambda_{\min} = \frac{V_g}{f_{\max}} = \frac{3*10^8}{5*10^9*\sqrt{3.5}} = 0.032 \text{ m}$$

The cell sizes in each of the three dimensions are denoted as: Δx, Δy, and Δz. To simplify the simulation, we chose a uniform grid with $\Delta x = \Delta y = \Delta z = \Delta h$. Δh gives more than 10 samples per shortest wavelength for a accurate result. In this example,

$$\Delta h = \Delta x = \Delta y = \Delta z = 0.0025\ m < 0.0032\ m$$

- Time steps

Once the cell size has been determined, the size of the time steps is calculated from the stability conditions. For a 3-D rectangular grid, the stability limit can be written as

$$\Delta t_{step} = \frac{1}{c\left(\frac{1}{\Delta x^2} + \frac{1}{\Delta y^2} + \frac{1}{\Delta z^2}\right)^{1/2}} \tag{4-1-2}$$

If $\Delta h = \Delta x = \Delta y = \Delta z = 0.0025\ m$, the calculated time step Δt_{step} is

$$\Delta t_{step} = \frac{\Delta h}{c\sqrt{3}} = \frac{0.0025}{3*10^8*\sqrt{3}} = 4.81\text{E-}12 \text{ sec}$$

- The derivative of a Gaussian wave

The source is an elemental current source having a Gaussian pulse shape in time.

$$f(t) = \begin{cases} 0 & t < 0 \\ a * e^{-\frac{(t-t_0)^2}{b^2}} & t \geq 0 \end{cases} \tag{4-1-4}$$

The first derivative of equation (4-1-4) is:

$$\frac{df(t)}{dt} = \begin{cases} 0 & t < 0 \\ -\dfrac{2a(t-t_0)}{b^2} * e^{-\frac{(t-t_0)^2}{b^2}} & t \geq 0 \end{cases} \qquad (4\text{-}1\text{-}5)$$

With parameter $a = 1.0$, $t_0 = 1E-9$ and $b = 0.18E-9$, the frequency bandwidth of the signal is 5GHz. Figure 4-1-3 and Figure 4-1-4 are the waveforms of equation (4-1-5) in time domain and frequency domain. The time duration of this wave is approximately 1.0ns. The time step, Δt_{step}, is 0.00481125ns. Therefore there are 207 samples in this period of time. The Gaussian pulse is well resolved in time.

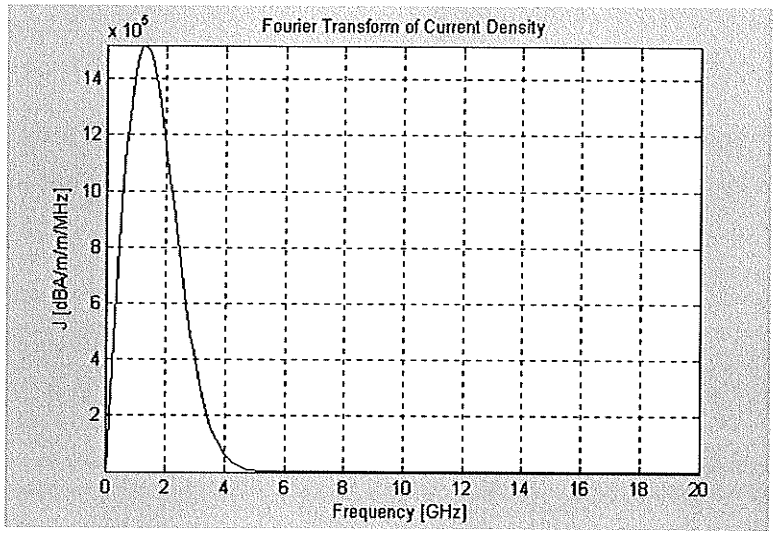

Figure 4- 1-3 Current source waveform in frequency domain

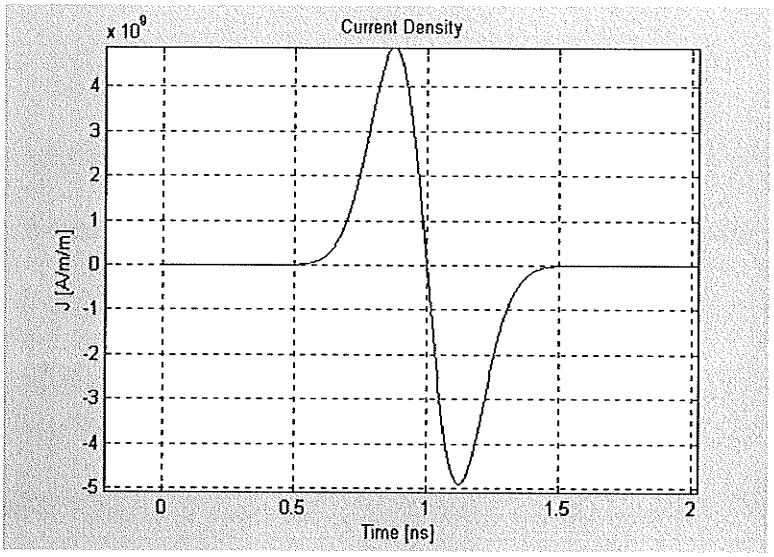

Figure 4- 1-4 Current source waveform in time domain

4.1.2 FDTD simulated GPR data

Based on the geometry of the problem example in Appendix II, the test points and the current source are in the x-z plane, but with different x locations, i.e. different distances to the object. Test point 9, shown in figure 4-1-2, is at the same position as the current source in the y-z plane.

There are three major components generated in the FDTD GPR data: the direct coupling between the current source and the receiver (i.e., the test points), contributions from the ground object and from the buried object. Three FDTD simulated GPR data are generated: ground only (no bomb buried under the ground) for the determination of ground contribution; a bomb buried under the ground surface; and no ground and no bomb for the determination of coupling.

In order to determine the initial time point for the reflection from the buried object surface, FDTD GPR data is analysed as below. The shortest distance between the current

source and ground surface is denoted as ΔR_1, ground surface to test point 9 as ΔR_2, and the distance between the buried object and ground surface is denoted as ΔR_3, as shown in Figure 4-1-5.

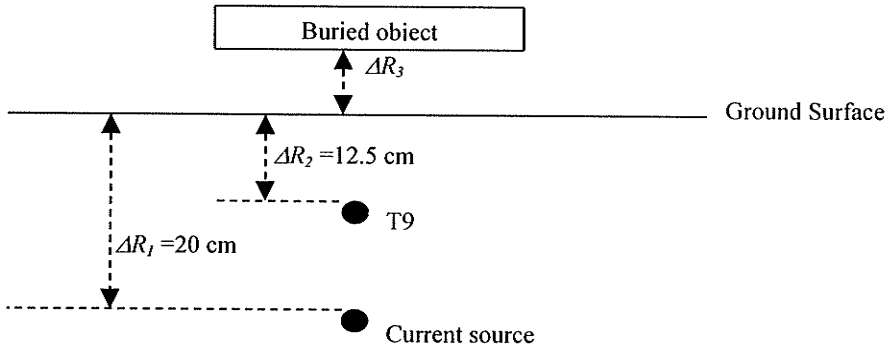

Figure 4-1- 5 x-z plane of the FDTD problem from Figure 4-1-2

The propagation time to reach ground surface from the current source is $\Delta R_1/c$. $\Delta R_2/c$ is the propagation time from ground surface to test point 9. Similarly, the propagation time to reach the buried object surface and be reflected back to ground surface is $2 \times \Delta R_3/v_g$. Therefore, the total propagation time t_p at test point 9 is the sum of the propagation times from the current source to the buried object plus the propagation time from the buried object to test point 9, i.e.,

$$t_p = \frac{\Delta R_1}{c} + \frac{\Delta R_2}{c} + \frac{2 \times \Delta R_3}{v_g} = \frac{\Delta R_1 + \Delta R_2 + 2 \times \Delta R_3 \times \sqrt{\varepsilon_r}}{c} = 1.0833\text{E-}9 + (4.4096\text{E-}11) \times \Delta R_3 \qquad (4\text{-}1\text{-}6)$$

In our FDTD simulation, ε_r for the ground object is set to 7. Adding the time delay $1ns$ for the Gaussian waveform, the time that requires for the buried object reflection to reach T9 should be

$$t_p + 1ns = 2.0833 + 0.044096 \times \Delta R_3 \quad (ns). \qquad (4\text{-}1\text{-}7)$$

We generate six FDTD simulated GPR data with different depth ΔR_3 for the buried objects, as listed in Table 4-1. The name of the FDTD GPR data is defined based on the following rules:

- 'T9' denotes test point 9.
- 'mine' or 'ground' indicates a landmine object or ground object involved.

According to the above definition, "***mine_ground_T9_*** ΔR_3" indicates FDTD GPR waveform received at test point 9 with a landmine buried under the ground in the depth of ΔR_3. "***ground_T9***" means ground only, no landmine is buried, and GPR waveform is received at test point 9. With no landmine and no ground, the GPR waveform at test point 9 is donated as "***non_T9***", the direct coupling from the current source at test point 9. The residual GPR data after subtracting "***non_T9***" from "***ground_T9***" is the reflection contributed by ground only, ***ground_only_T9***, as shown in Figure 4-1-6.

$$ground\_only\_T9 = ground\_T9 - non\_T9 \tag{4-1-8}$$

Similarly, "***mine+ground_T9_*** ΔR_3" denotes the contribution from ground plus the buried landmine after direct coupling is removed, as shown in Figure 4-1-7.

$$mine+ground\_T9\_\Delta R_3 = mine\_ground\_T9\_\Delta R_3 - non\_T9 \tag{4-1-9}$$

Finally, we can obtain the landmine-only reflection waveform, "***mine_only_T9_*** ΔR_3" by subtracting "***ground_only_T9***" from "***mine+ground_T9_*** ΔR_3",

$$mine\_only\_T9\_\Delta R_3 = mine+ground\_T9\_\Delta R_3 - ground\_only\_T9 \tag{4-1-10}$$

The FDTD waveforms for the landmine only are shown in Figure 4-1-8. We define the peak time step as the sample time at which the GPR waveform reaches its peak point. The peak time step is calculated by $(t_p + 1ns)/\Delta t_{step}$. The calculated peak time steps for the buried landmines with different depths are listed in table 4-1.

Table 4-1: Parameter for six generated FDTD GPR waveforms at test point 9.

Cells for landmine buried under the ground surface	ΔR_3 (cm)	Time delay (ns)	Calculated peak time step	FDTD simulated peak time step
5	1.25cm	2.3038	478	465
10	2.5cm	2.5243	524	511
15	3.75cm	2.7447	570	557
20	5.00cm	2.9652	616	603
25	6.25cm	3.1857	662	649
30	7.50cm	3.4062	707	695

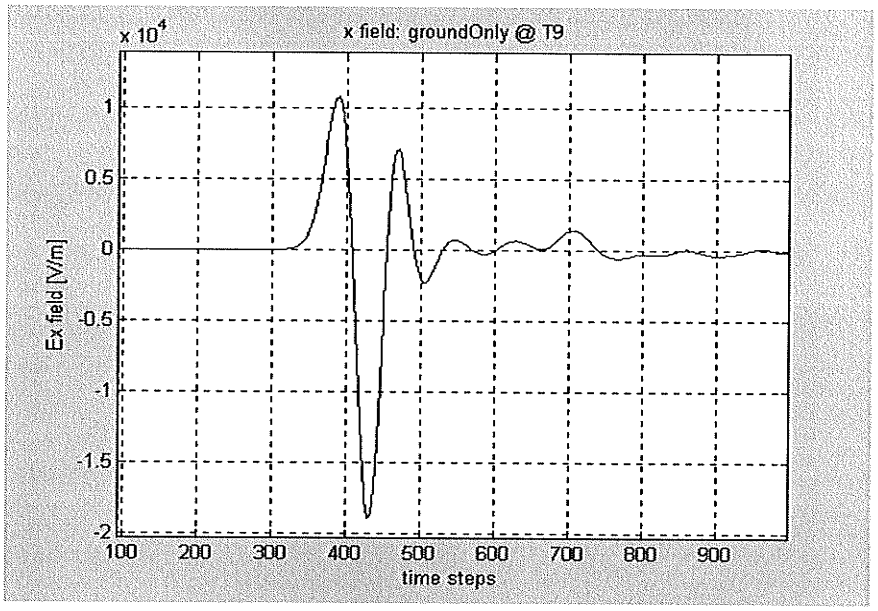

Figure 4-1-6 GPR waveform of ***ground_only_T9***

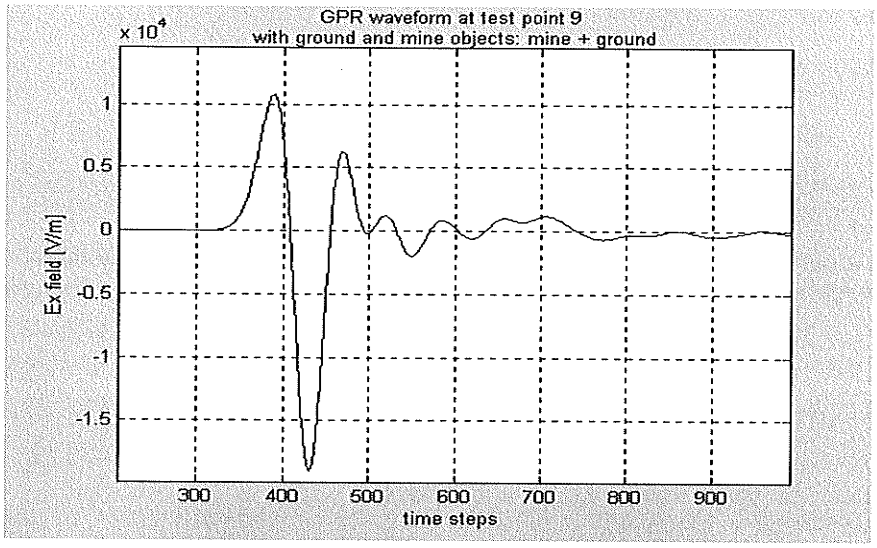

Figure 4-1-7 ***mine+ground_T9_ΔR₃*** with ΔR_3 =10

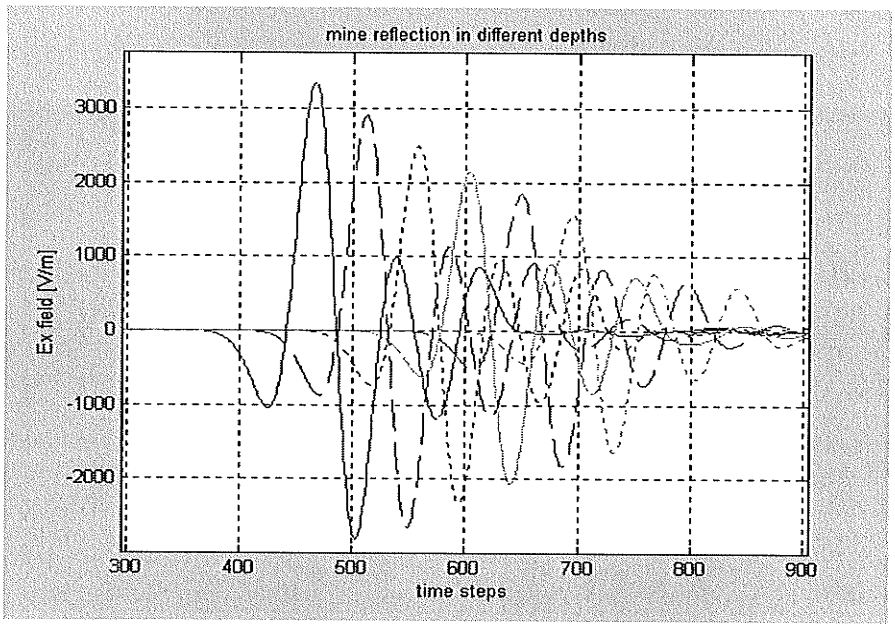

Figure 4-1-8 GPR waveform of ***mine_only_T9_ΔR₃*** with different ΔR_3

We notice that the calculated peak time step has an offset of 13 time steps from the corresponding simulated FDTD peak time step. For example, in the first row of table 4-1, subtracting 465 from 478 is 13. This is because the calculated peak time step is a reference point based on the current source center point (the center of the derivative of Gaussian waveform in Figure 4-1-4). And the simulated FDTD peak time step is the sample time at which the total received reflected waveform reaches its peak value. They are not the same. However, If we use the first row of table 4-1 as a reference, we can see that the number of peak time step increases 46 per 5-cell-increase in ΔR_3. For instance, 578-524 = 511-465 = 64. This proves that the simulated FDTD peak time step in FDTD waveform reflects the depth of the buried landmines.

4.1.3 Landmine signature

Landmine signature is used for object-oriented object detection. This signature should be unique, different from the other objects involved. There are only two objects in our simulation, a ground object and a buried landmine object. The landmine signature should be able to identify the landmine waveform from the reflection contributed by the ground object. The signature can be obtained from the landmine-only GPR waveform. In Figure 4-1-8, the reflection waveforms from the landmines buried in different depths have the same feature, which is different from the reflection from the ground, as shown in Figure 4-1-6. It can be used as the landmine signature. We normalized ***mine_only_T9_ΔR_3*** as a reference signature $t_{signature}(t_i)$, as shown in Figure 4-1-9. t_i is the time step.

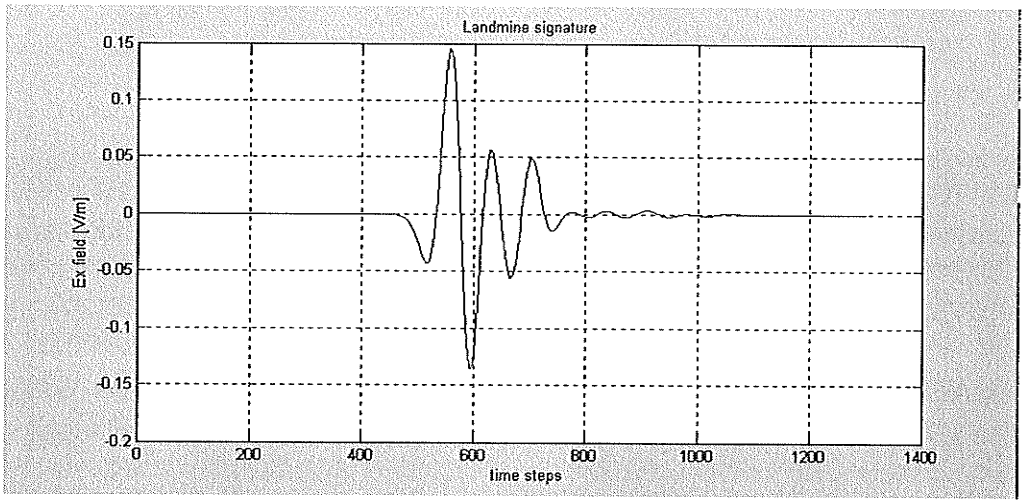

Figure 4-1-9 Landmine signature obtained after normalising the mine-only reflection waveform

4.1.4 Pre-processing of FDTD GPR data

The GPR waveforms with a landmine, as shown in Figure 4-1-6, is different from the GPR waveforms with no landmine, as shown in Figure 4-1-7. The contribution from the ground is much stronger than the reflection from the landmine. In order to detect the landmine, this ground surface reflection must be preprocessed (reduced) before any further processing.

Setting the prediction order to 24 for the linear algorithm in section 3.1, we calculate the estimated GPR data $\hat{y}(t_{j+1})$ based on the previous received GPR data $y(t_{j-i}), j > 24, j > i$ by using equation (3-1-1) as below:

$$\hat{y}(t_{j+1}) = \sum_{i=1}^{24} b_i y(t_{j-i}) \tag{4-1-11}$$

Then, we use the least square algorithm to determine the coefficients $\{b_i, i=1 \text{ to } 24\}$, i.e., b_i is chosen so that the *error* in equation (4-1-12) is minimum:

$$error = | y(t_{j+1}) - \sum_{i=1}^{24} b_j y(t_{j-i}) |^2, j > 24 \quad (4\text{-}1\text{-}12)$$

After the coefficients are obtained, we estimate the ground-only reflection, ***Esground***, by:

$$Esground(t_j) = \sum_{i=1}^{24} b_i y(t_{j-i}); j > 24 \quad (4\text{-}1\text{-}13)$$

Finally, subtracting ***Esground*** from the received GPR data, we get the residual GPR data as below:

$$\textbf{\textit{Residual\_ mine+ground\_T9\_}}\Delta R_3 = \textbf{\textit{mine+ground\_T9\_}}\Delta R_3 - \textbf{\textit{Esground}} \quad (4\text{-}1\text{-}14)$$

$$\textbf{\textit{Residual\_ ground\_only\_T9}} = \textbf{\textit{ground\_only\_T9}} - \textbf{\textit{Esground}} \quad (4\text{-}1\text{-}15)$$

The residual GPR waveform ***Residual_ mine+ground_T9_***ΔR_3, as shown in Figure 4-1-10, is generated after pre-processing of GPR data ***mine+ground_T9_***ΔR_3 with ΔR_3=25. It consists of contributions from the landmine and the residual ground contribution after the estimated ground reflection, ***Esground***, is removed. Comparing the Figure 4-1-7 with Figure 4-1-10, we can see the landmine GPR waveform is enhanced and the contribution from the ground surface is reduced significantly.

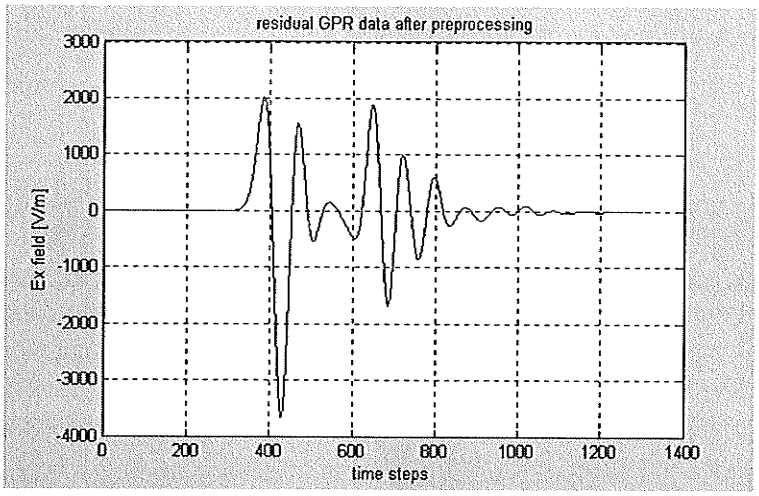

Figure 4-1-10 residual GPR data after pre-processing on ***mine+ground T9*** ΔR_3 with

Table 4-2 is constructed as if the landmines are buried under the ground surface with different depths at different scan positions. Figure 4-1-11(a) is the corresponding geometry. ***Prep_GPR_data_group*** is created based on table 4-2. ***Prep_GPR_data_group*** will be used in the further processing for landmine detection. The image of ***Prep_GPR_data_group***, as shown in Figure 4-1-12, reflects the range of the buried landmines according to their depths. The strongest (darkest) line at the time step of around 430 is the residual ground contribution after the preprocessing of GPR data.

Table 4-2: a grouped preprocessed GPR data

Cross-range scan position	1 ~15, 17~28, 30~41, 43~54, 56~67,69~80, 82~93	16	29	42	55	68	81
Residual GPR data	***Residual_ ground_only_T 9***	***Residual_ mine+ground_T9_*** ΔR_3					
		ΔR_3=5	ΔR_3=10	ΔR_3=15	ΔR_3=20	ΔR_3=25	ΔR_3=30

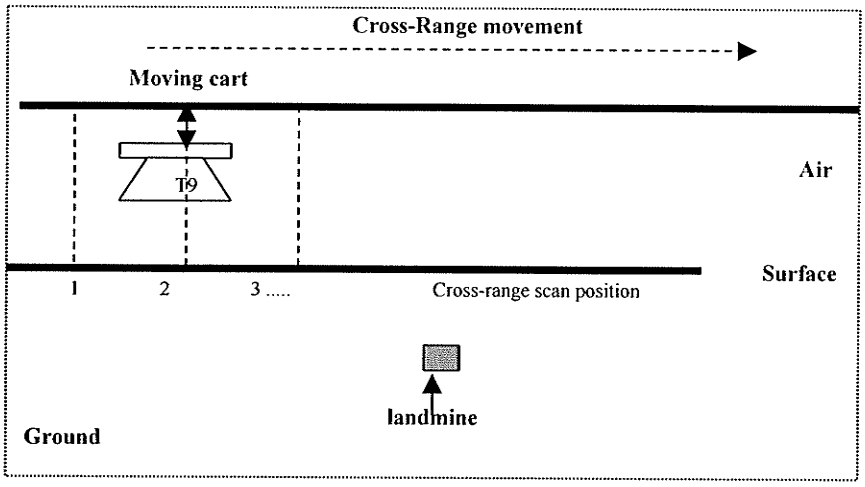

Figure 4-1-11(a) Geometry of a grouped FDTD data: ***Prep_GPR_data_group***

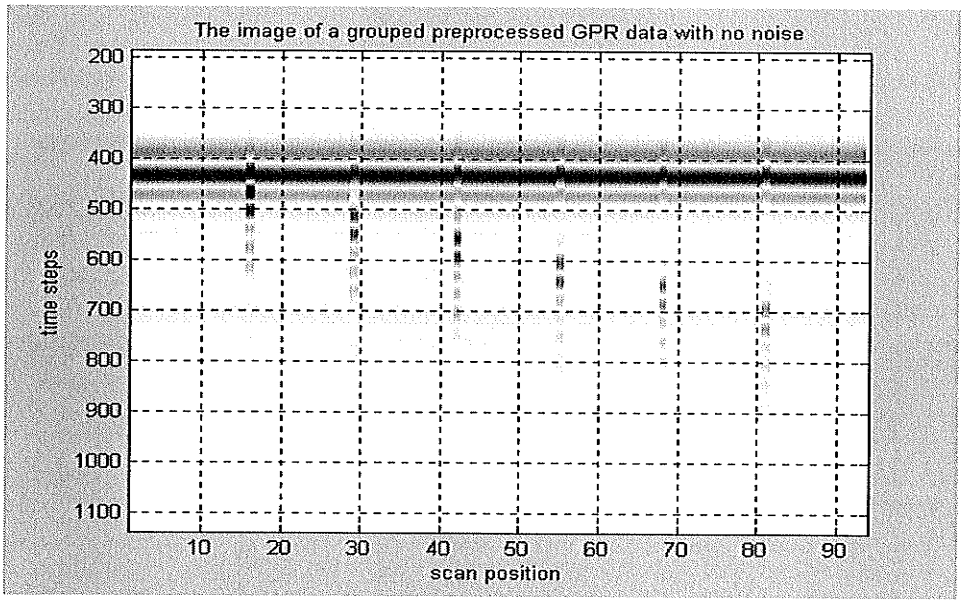

Figure 4-1-11(b) the image of a grouped pre-processed GPR data generated according to table 4-2

4.2 LP algorithm for landmine detection

The LP algorithm, described in Section 3.2, is a general method designed for landmine detection. In this section, the implementation of the LP algorithm is discussed. The pre-processed FDTD GPR data, ***Prep_GPR_data_group*** created in section 4.1.4, will be used as the input. The simulation results will be analysed.

4.2.1 Implementation of LP algorithm

Figure 4-2-1 is the implementation block diagram of the LP algorithm described in section 3.2.1. For the improved LP algorithm, the prediction coefficient vector $\boldsymbol{a}_{p\times 1}$ is calculated according to the equation (3-2-15). At the beginning, five parameters need to be determined. The prediction order p, the adaptive parameter λ and the scale factor ξ_scale are experimental values. The weighting matrix $\boldsymbol{W}_{m\times m}$ and the normalized error energy threshold $\xi'_{threshold}$ are calculated over a small area with no buried landmines. Figure 4-2-2 is the LP initiation block diagram for the calculation of $\boldsymbol{W}_{m\times m}$ and $\xi'_{threshold}$.

In Figure 4-2-2, $y_{m\times 1}(n)$ is the pre-processed GPR data at the cross-range scan position n. m denotes the total number of pre-processed GPR data in time domain. $\boldsymbol{Y}_{m\times p}(n-1)$ is generated by the pre-processed GPR data from the p previous scan positions, i.e.,

$$\boldsymbol{Y}_{m\times p}(n-1)=\{\, y_{m\times 1}(i), i=n-1, n-2, \ldots, n-p. \,\}. \tag{4-2-1}$$

The prediction coefficient vector $\boldsymbol{a}_{p\times 1}(n)$ and error energy $\boldsymbol{e}_{m\times 1}(n)$ are calculated by:

$$\boldsymbol{a}_{p\times 1}(n)=[\boldsymbol{Y}^{*}_{m\times p}(n-1)\boldsymbol{Y}_{m\times p}(n-1)]^{-1}\boldsymbol{Y}_{m\times p}(n-1)^{*}\, y_{m\times 1}(n) \tag{4-2-2}$$

$$\boldsymbol{e}_{m\times 1}(n)=y_{m\times 1}(n)-\boldsymbol{Y}_{m\times p}(n-1)\boldsymbol{a}_{p\times 1}(n) \tag{4-2-3}$$

Moving to the next scan position and updating $\boldsymbol{Y}_{m\times p}(n-1)$ with the latest pre-processed GPR data from the previous p scan positions, we obtain a series of $\boldsymbol{e}_{m\times 1}(n), n = p+1, p+2, \ldots$. The covariance of $\boldsymbol{e}_{m\times 1}(n)$ is $\boldsymbol{C}_{m\times m}$. The weighting matrix $\boldsymbol{W}_{m\times m}$ is calculated by

$$\boldsymbol{W}_{m\times m} = \boldsymbol{C}_{m\times m}^{-1} = (\boldsymbol{Q}_{m\times q}\Lambda_{q\times q}\boldsymbol{Q}_{q\times m}^{*})^{-1} \tag{4-2-5}$$

If the inverse of $\boldsymbol{C}_{m\times m}$ has singular problem, then the weighting matrix $\boldsymbol{W}_{m\times m}$ is calculated according to section 3.2.2. After estimating $\boldsymbol{W}_{m\times m}$, we can calculate the weighted error energy $\xi(n)$, and then normalise the error energy threshold $\xi'_{threshold}$ by:

$$\xi(n) = \boldsymbol{y}_{m\times 1}(n)^{*}\boldsymbol{W}_{m\times m}\boldsymbol{y}_{m\times 1}(n) - \boldsymbol{y}_{m\times 1}(n)^{*}\boldsymbol{W}_{m\times m}\boldsymbol{Y}_{m\times p}(n)\boldsymbol{a}_{p\times 1}(n) \tag{4-2-6}$$

$$\xi'_{threshold} = \xi\_scale \times \max\{[\xi(n) - \bar{\xi}]/(\mathrm{E}[|\xi(n) - \bar{\xi}|^2])^{1/2}\} \tag{4-2-7}$$

$\bar{\xi}$ is the mean of $\xi(n)$ and $\mathrm{E}[|\xi(n) - \bar{\xi}|^2]$ is the variance of $\xi(n)$.

After initialization, we obtain the weighting matrix $\boldsymbol{W}_{m\times m}$ and the normalised error energy threshold $\xi'_{threshold}$ as the parameters of the LP algorithm in Figure 4-2-1. The prediction coefficient vector $\boldsymbol{a}_{p\times 1}(n)$ and the weighted error energy $\xi(n)$ are estimated by:

$$\boldsymbol{a}_{p\times 1}(n) = [\boldsymbol{Y}_{m\times p}(n-1)^{*}\boldsymbol{W}_{m\times m}\boldsymbol{Y}_{m\times p}(n-1)]^{-1}\boldsymbol{Y}_{m\times p}(n-1)^{*}\boldsymbol{W}_{m\times m}\boldsymbol{y}_{m\times 1}(n) \tag{4-2-8}$$

$$\xi(n) = \boldsymbol{y}_{m\times 1}(n)^{*}\boldsymbol{W}_{m\times m}\boldsymbol{y}_{m\times 1}(n) - \boldsymbol{y}_{m\times 1}(n)^{*}\boldsymbol{W}_{m\times m}\boldsymbol{Y}_{m\times p}(n-1)\boldsymbol{a}_{p\times 1}(n) \tag{4-2-9}$$

We then normalize the weighted error energy $\xi(n)$ as $\xi'(n)$:

$$\xi'(n) = [\xi(n) - \bar{\xi}]/\{\mathrm{E}[|\xi(n) - \bar{\xi}|^2]\}^{1/2} \tag{4-2-10}$$

where $\bar{\xi}$ is the mean of $\xi(n)$ and $E[|\xi(n)-\bar{\xi}|^2]$ the variance of $\xi(n)$. The LP algorithm generates an alarm if

$$\xi'(n) > \xi'_{threshold} \tag{4-2-11}$$

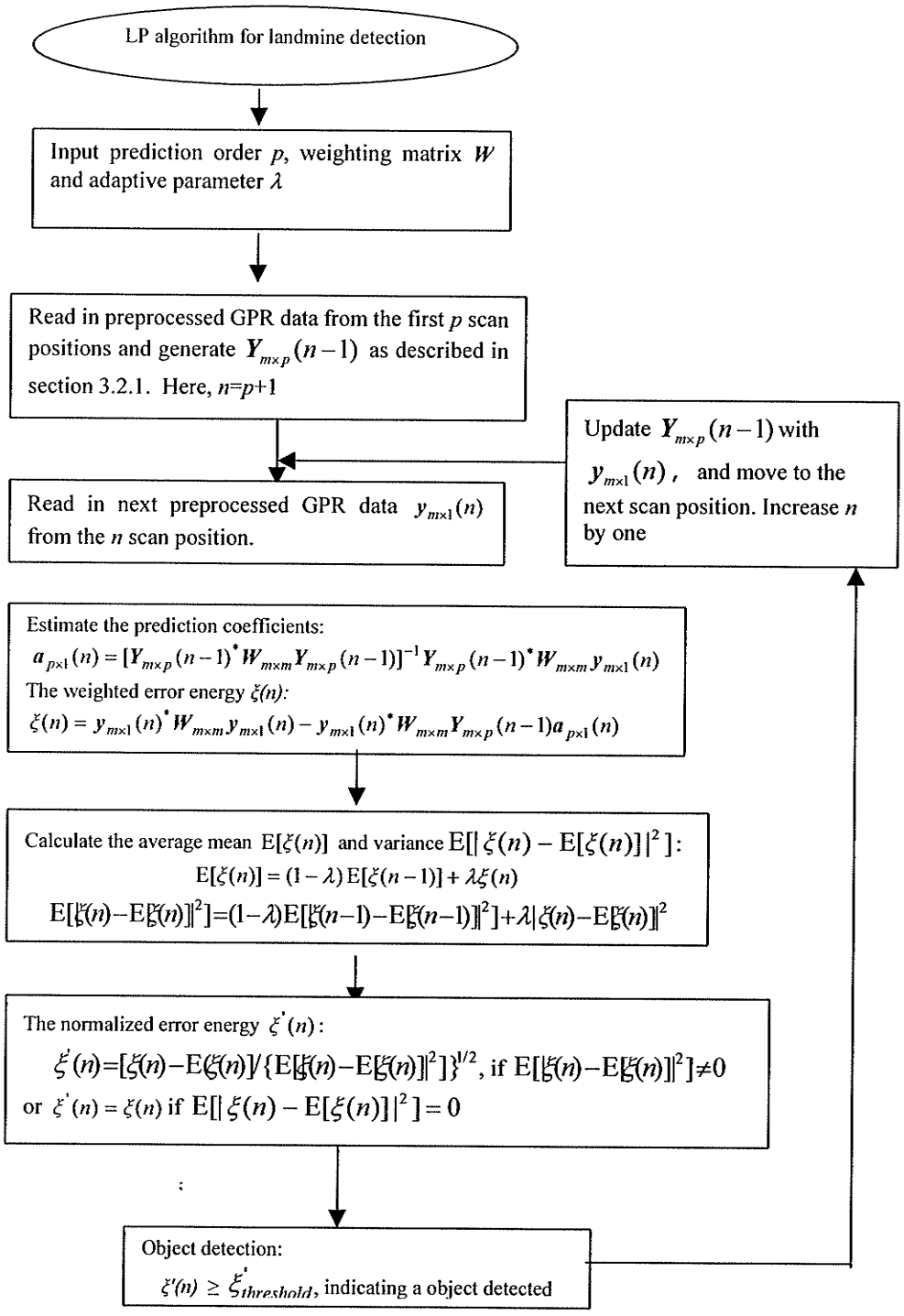

Figure 4-2-1 Block diagram of the Linear Prediction Algorithm

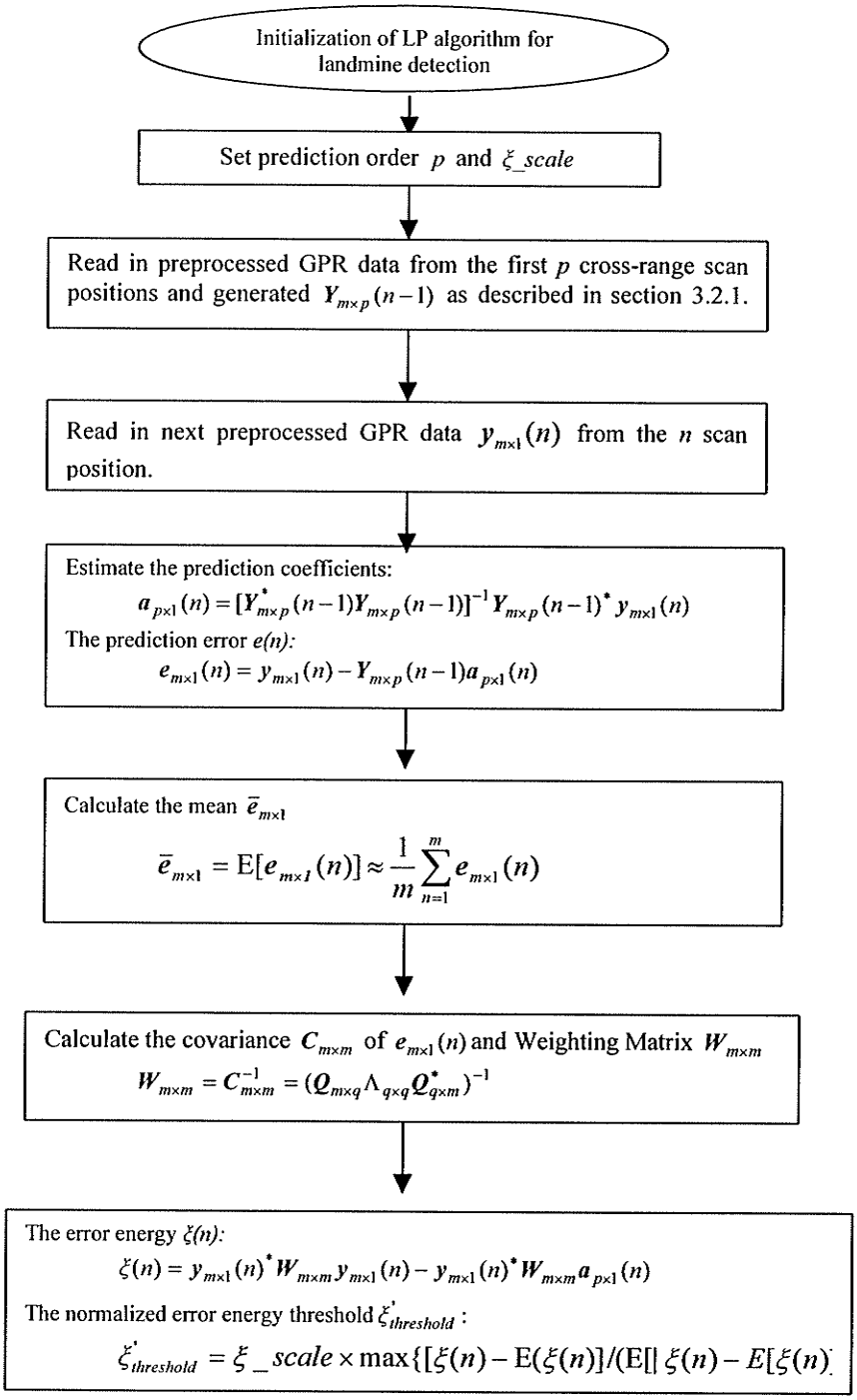

Figure 4-2-2 Initiation of parameters for LP algorithm over a small area

We use ***Prep_GPR_data_group*** as the input of the LP algorithm with p set to 5 and ξ_scale to 2. The adaptive parameter λ is set to 1 due to the ideal flat ground surface, and m is 1031. Figure 4-2-3 is the output of the LP algorithm. The normalized error energy generates six peaks at the cross-range scan positions of 16, 29, 42, 55, 68, and 81. The LP algorithm alarms six scan positions for landmine detection. Comparing with the cross-range scan positions of the buried landmines listed on table 4-2, we can see that the LP algorithm generates alarms for every buried landmines. The result is expected. If the object is buried closer to the ground surface, then the reflected signal is stronger. This demonstrates that the implemented linear prediction algorithm works well for the general landmine detection.

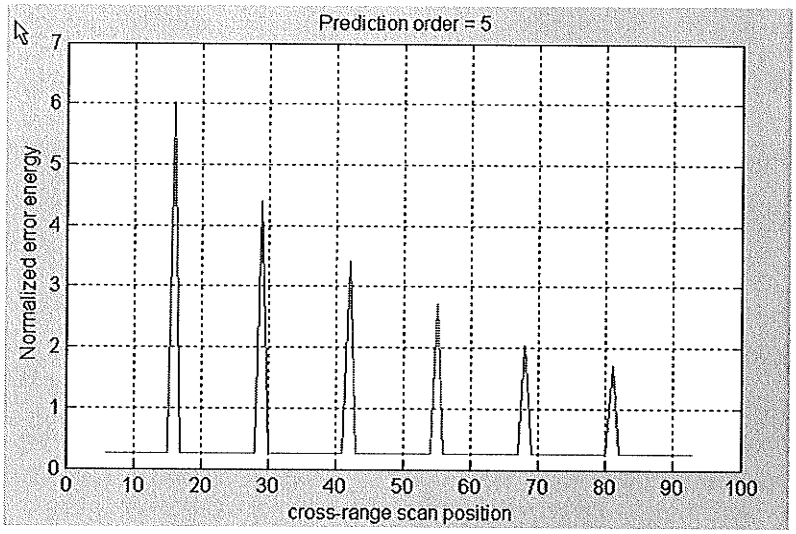

Figure 4-2-3 Output of LP algorithm with *Prep_GPR_data_group*

4.2.2 Simulation Results

In practice, noise from the system or from unknown resources is unavoidable. Normal distributed random numbers with zero mean were added to ***Prep_GPR_data_group*** in order to simulate noisy measured GPR data.

$$Prep\_GPR\_data\_group\_noise = Prep\_GPR\_data\_group + Noise \quad (4\text{-}2\text{-}12)$$

The added noise should have the same frequency bandwidth, i.e., 5GHz, as the preprocessed FDTD GPR data, ***Prep_GPR_data_group***, shown in Figure 4-2-4. The processing block diagram of the additional noise generator is shown as below:

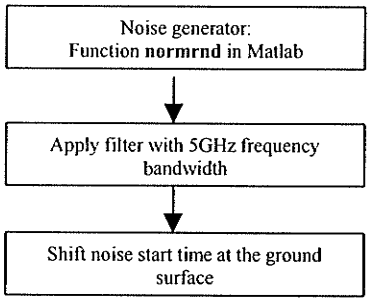

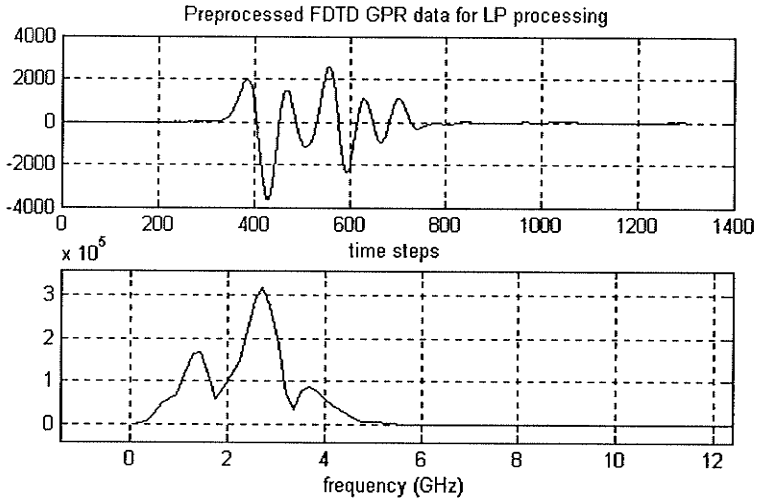

Figure 4-2-4 Pre-processed GPR data as an input of LP algorithm

Figure 4-2-5 (a) is an example of generated noise with 5GHz bandwidth. Figure 4-2-5 (b) is the image of simulated GPR data with noise, ***Prep_GPR_data_group_noise.***

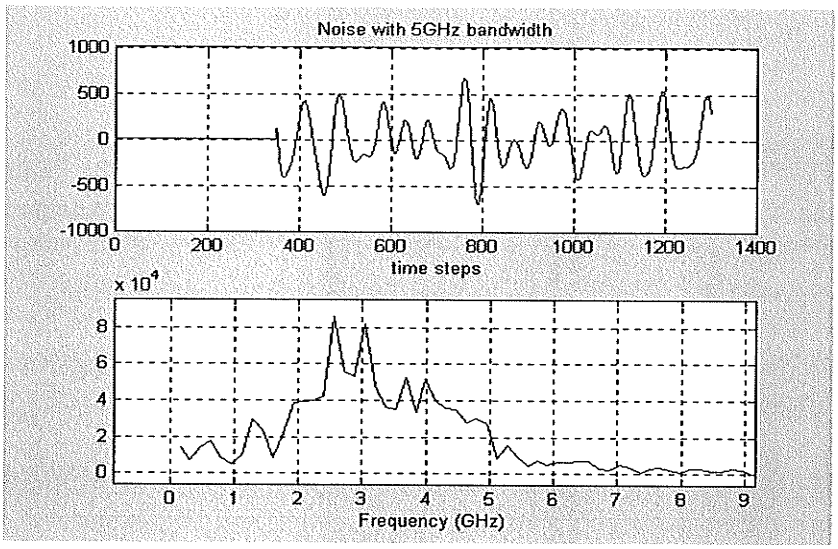

Figure 4- 2-5 (a) Generated noise with 5GHz bandwidth

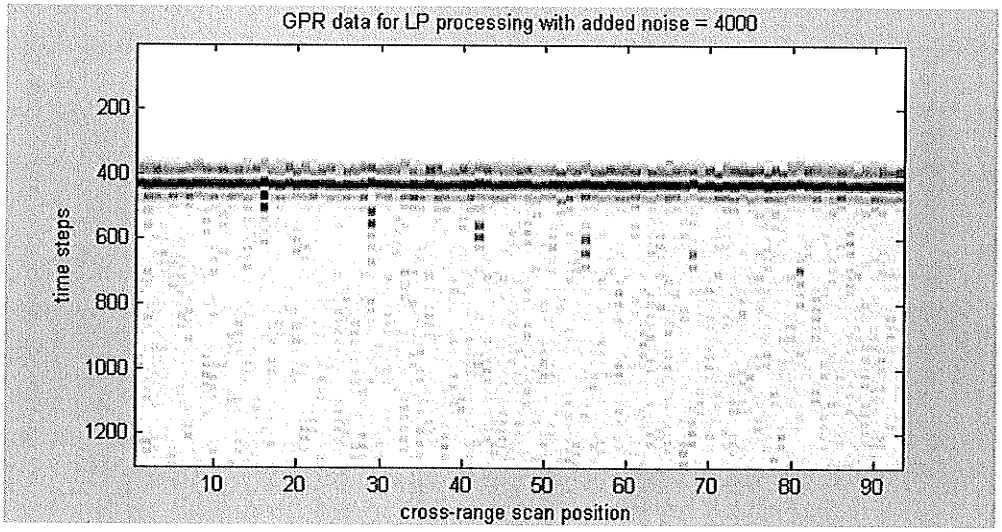

Figure 4-2-5(b) Image of simulated GPR data with added noise

The signal-to-noise ratio (SNR) is defined as:

$$SNR = 10 \log \frac{E_s}{E_n} \qquad (4\text{-}2\text{-}13)$$

E_s is the reflected signal energy from landmine only, i.e., ***mine_only_T9_ΔR_3***. E_n is the residual energy from the ground surface after signal preprocessing, ***Residual_ ground_only_T9,*** plus noise, ***Noise.*** Then we have:

$$E_s = \sum_{i=1}^{m} | \, \boldsymbol{mine\_only\_T9\_\Delta R_3}(i) \, |^2 \tag{4-2-14}$$

$$E_n = \sum_{i=1}^{m} | \, \boldsymbol{Residual\_\ ground\_only\_T9}\,(i) + \boldsymbol{Noise}\,(i) \, |^2 \tag{4-2-15}$$

Because the landmines are buried at different depths, their SNRs are different. In the above simulation, the calculated SNRs of ***Prep_GPR_data_group_noise*** with standard noise deviation of 4000 and 5500 are listed in table 4-3 and table 4-4. Figure 4-2-6 is an output of LP algorithm with noise deviation of 5500.

Table 4-3 SNRs with noise deviation of 4000

Cross-range scan position of buried object	16	29	42	55	68	81
SNR (dB)	0.9219	-0.45348	-1.6119	-2.4817	-3.6589	-4.3115

Table 4-4 signal-to-noise ratios (SNRs) with noise deviation of 5500

Cross-range scan position of buried object	16	29	42	55	68	81
SNR (dB)	-0.5896	-1.365	-3.1934	-3.8872	-4.8006	-5.2197

A false alarm is defined as an alarm that the LP algorithm generates at a cross-range scan position where there is no landmine buried. If $\xi'_{threshold}$ in the LP algorithm is set high, then the false alarm will be low and some of the landmines with low SNRs will not be detected.

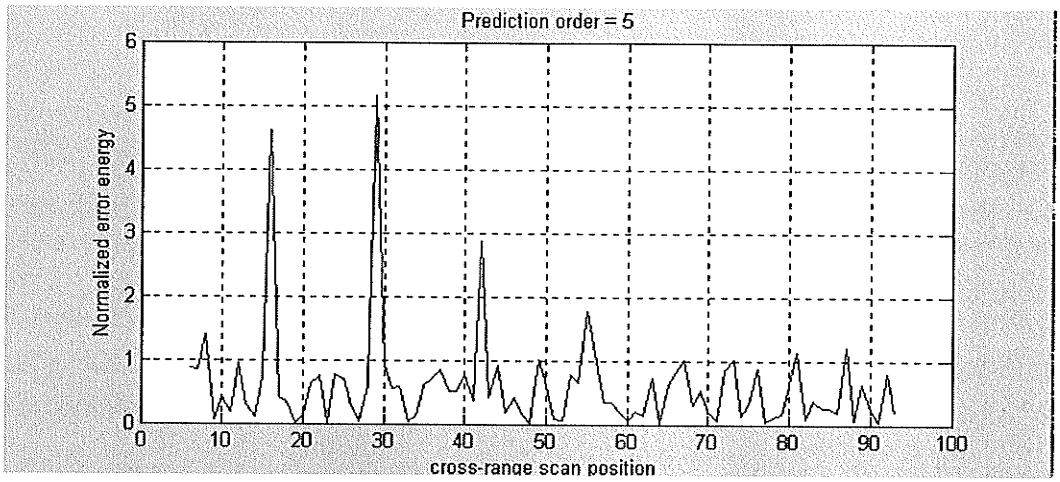

Figure 4-2- 6 Output of LP algorithm for landmine detection

For example, in Figure 4-2-6, if we set $\xi'_{threshold}$ to 2, then three landmines, located at the cross-range scan position 16, 29 and 42, would be detected with no false alarms generated, and the other three landmines, located at the cross-range scan position 55, 68 and 81, would be undetected. If $\xi'_{threshold}$ in the LP algorithm is set to 1.1, then four landmines, located at the cross-range scan position 16, 29, 42 and 55, are detected with one false alarm generated. The landmines with very low SNR are undetectable, such as the landmines at the scan position 68 and 81.

Table 4-5 is the simulation results for the number of detected landmines over SNR and the false alarms over SNR. $\overline{Snr}$ is averaged over 10 landmines buried in the same depth scattered at different cross-range scan positions, as shown in Figure 4-2-7.

$$\overline{Snr} = \frac{1}{10}\sum_{i=1}^{10} Snr\ (i) \qquad (4\text{-}1\text{-}16)$$

$Snr\ (i), i = 1,..., 10$, is the calculated SNR of the 10 landmines. The number of alarms is the total number of alarms generated by the LP algorithm, including false alarms.

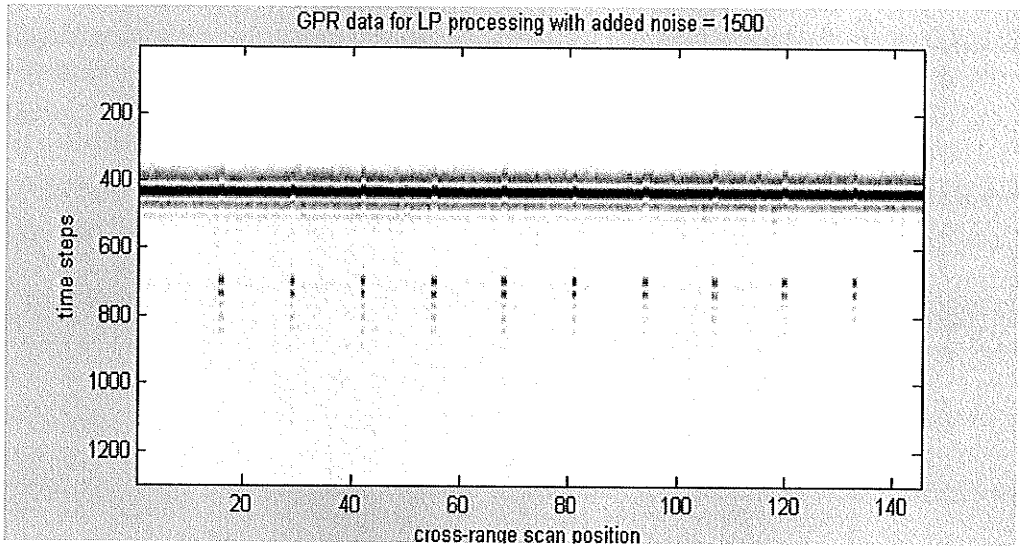

Figure 4-2-7 Image of 10 landmines buried in the same depth at different cross-range scan positions

Table 4-5 Generated alarms over averaged SNR and landmine detected over SNR

$\overline{S}nr$	Number of alarms	Number of Landmine detected	$\overline{S}nr$	Number of alarms	Number of Landmine detected
-4.725	14	10	-5.545	43	9
-4.722	11	10	-5.676	40	6
-4.736	11	10	-5.613	37	8
-4.981	31	10	-5.715	43	9
-5.005	24	10	-5.881	42	5
-5.004	26	10	-5.999	39	8
-5.018	26	10	-5.938	38	7
-5.011	25	9	-5.861	42	6
-5.143	23	9	-5.927	39	5
-5.196	30	10	-6.118	43	7
-5.184	23	10	-6.307	41	7
-5.144	29	9	-6.338	40	9
-5.328	35	8	-6.512	33	5
-5.426	33	9	-6.457	38	4
-5.491	29	9	-6.281	42	4
-5.522	43	8	-5.881	42	5
-5.627	36	9	-6.438	41	6

Figure 4-2-8 shows the curve generated according to table 4-5, and indicates that if the SNR is greater than -5dB, less than 95% of landmines will be detected. With a fixed threshold $\xi'_{threshold}$, if the SNR is set low, the number of false alarms will be high and the percentage of detected landmines over the total number of buried landmines will be low.

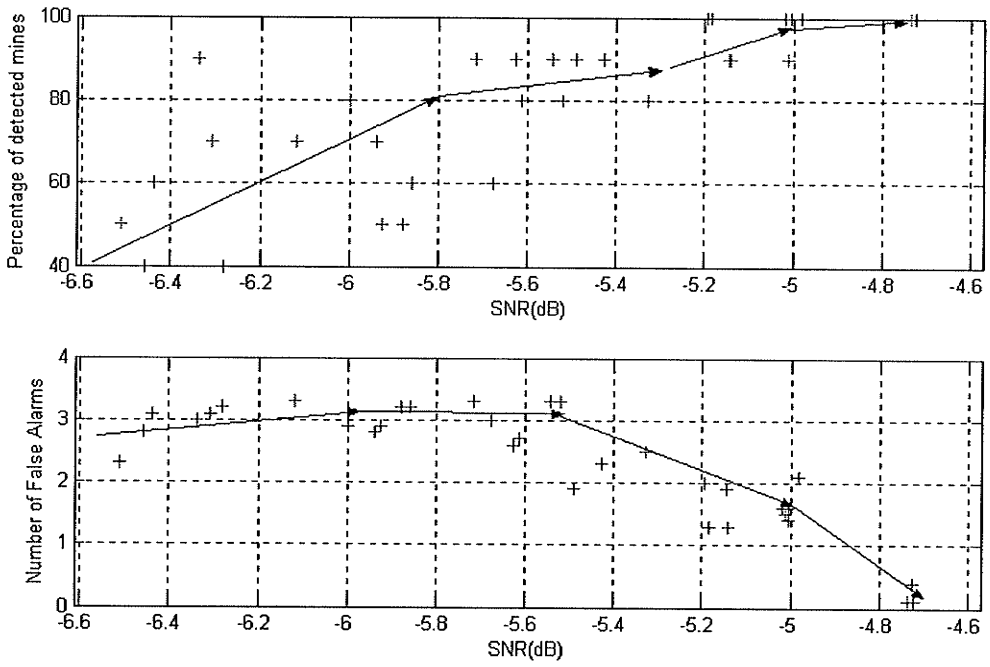

Figure 4-2-8 simulation results for false alarms over SNR and ratio of detected landmines over SNR

4.2.3 Summary

The purpose of this simulation was to determinate the adequacy of the implementation of the LP algorithm. Seven basic sets of pre-processed FDTD GPR data were generated, pre-processed and reconstructed to simulate the cross-range GPR data. Using these preprocessed FDTD GPR data as the inputs of the LP algorithm, the implemented LP algorithm was able to detect the buried objects at different cross-range scan positions. The output of the LP algorithm reflects the error energy in response to the depth of a buried object, i.e. if the landmine is closer to the ground surface, the output of the LP algorithm is stronger due to higher SNR.

In practice, noise from the GPR system or unknown resources is not avoidable. Random noise was generated to simulate the random contribution from a variety of environments. The landmine detection percentage and the total number of false alarms are functions of signal-to-noise ratio. If SNR is high, then the landmine detection percentage is high, and the number of false alarms is low. The simulation results were what we expected. According to our simulation results, if the SNR is lower than –5dB, the detection of landmine is not guaranteed. Lowering the landmine detection threshold will result in more false alarms.

The simulation results of the improved LP algorithm are almost the same as the original one. This is because the inputs of the LP algorithm are highly correlated, i.e., the equation (3-2-13) is not satisfied.

In our simulation, the generated FDTD GPR data is based on a simple geometry. We did not verify the effect of varying environment with adaptive threshold. More

complex geometry of problem models with rough surface or a simulated varying environment may be considered as a future work.

4.3 IT algorithm for object detection

4.3.1 Problem and solution for specific landmine detection and range estimation

In section 4.2, we simulate the linear prediction algorithm to generate alarms for general object detection. This method does not provide any further object-related information, such as depth. The IT algorithm in [5] is an object-oriented method that provides a way to estimate the depth of a buried object. The object's signature is required for the method.

The IT algorithm first uses the Prony technique to decompose the ground surface contribution from the received GPR data, and then uses the Simplex method, with the reference signature of interest, to estimate the target related parameters based on a damping exponential model. After the estimated ground surface contribution is removed, the residual GPR data is further cross-correlated with the object's signature and compared with the threshold for object detection. The detection block diagram for this procedure is shown in Figure 4-3-1, and the implementation block diagram of the IT algorithm is shown in Figure 4-3-2.

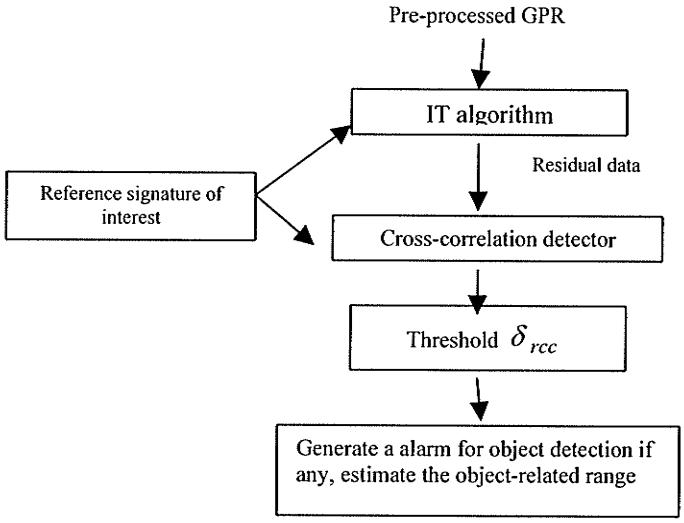

Figure 4-3-1 Block diagram for object detection with IT algorithm

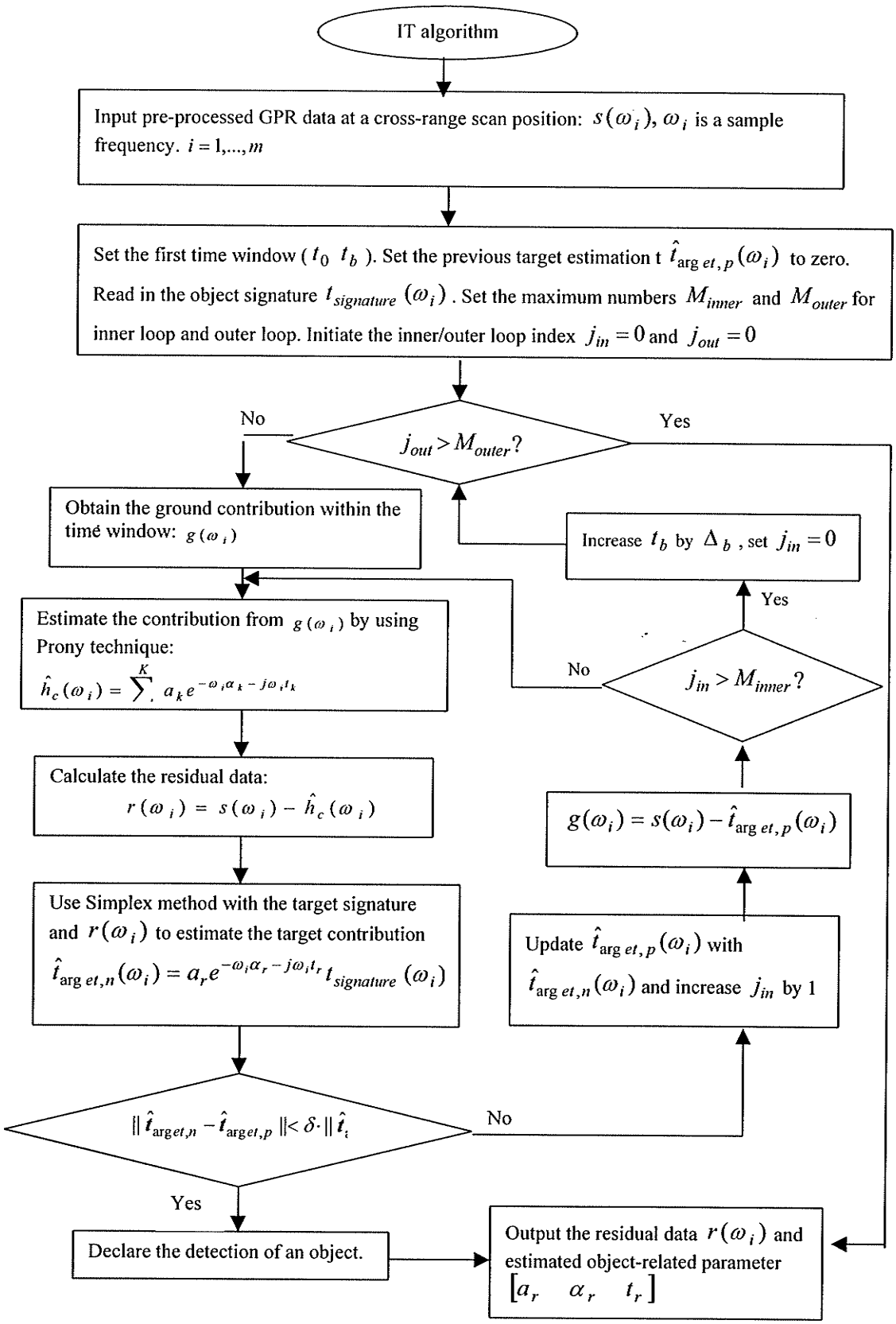

Figure 4.3.2 Implementation block diagram of IT algorithm

4.3.2 Implementation

The IT algorithm has two loops, an inner loop and an outer loop, denoted by j_{in} and j_{out} respectively. The outer loop controls the time window for the estimation of the ground surface contribution only. In this loop, m is the maximum number of sampled frequencies, t_0 and t_b are the start and end point of the time window. The first time window (t_0 t_b) must not include any contributions from the buried object. So the first t_b must be the chosen carefully. At the beginning, we set the previous estimated object contribution to zero, i.e, $\hat{t}_{\arg et,p}(\omega_i) = 0$. The maximum numbers for the inner loop M_{inner}, the outer loop M_{outer}, and the threshold δ for object detection are chosen experimentally.

The preprocessed FDTD GPR data, ***Residual_ mine+ground_T9_ΔR3,*** consists of the residual contribution from the ground surface and the contributions from the buried object. In the time domain or frequency domain, ***Residual_ mine+ground_T9_ΔR3*** can be represented as $s(t_i)$ or $s(\omega_i)$

$$s(t_i) = h_c(t_i) + t_{\arg et}(t_i), i = 1,..., m$$

$$s(\omega_i) = h_c(\omega_i) + t_{\arg et}(\omega_i), i = 1,..., m \qquad (4\text{-}3\text{-}1)$$

where $h_c(t_i)$ or $h_c(\omega_i)$ represents the ground surface contributions, and $t_{arget}(t_i)$ or $t_{arget}(\omega_i)$ are contributions from a buried object. t_i is the time step and ω_i the sample frequency. $m = 1031$ in our case. In Figure 4-1-10, we can see that the peak value from the ground surface contribution is located at the time step 420, so we choose $t_0 = 0$ and

$t_b = 420$ as the first window. The ground surface contribution within the first time window is $g(t_i) = s(t_i), i = 1,...420$. $g(\omega_i)$ is the FFT transform of $g(t_i)$.

After the ground surface contribution $g(\omega_i)$ is obtained, we use the damped exponential model, described in section 3.4.1, to estimate the contribution, $\hat{h}_c(\omega_i)$, based on $g(\omega_i)$. The estimate can be expressed as:

$$\hat{h}_c(\omega_i) = \sum_{k=1}^{K} a_k e^{-\omega_i \alpha_k - j\omega_i t_k} \tag{4-3-2}$$

where α_k is the damping factor, a_k is the coefficient of the model, K is the rank used by the Prony technique (we will discuss how to estimate the rank later), and t_k is the time delay. The residual data $r(\omega_i)$, obtained by removing $\hat{h}_c(\omega_i)$ from $s(\omega_i)$, should be dominated by the contributions from the buried object if any.

The buried object contribution is modelled as:

$$t_{\arg et}(\omega_i) = a_r e^{-\omega_i \alpha_r - j\omega_i t_r} t_{signature}\ (\omega_i) \tag{4-3-3}$$

where $t_{signature}\ (\omega_i)$ represents the target signature of interest as shown in Figure 4-1-9, α_r is the damping factor, and a_r the coefficient of the model. t_k is the time delay which can be used to estimate the range of the buried object. The square error between the object model and the residual data $r(\omega_i)$ is:

$$e_{rror} = \sum_{i=1}^{m} \| r(\omega_i) - a_r e^{-\omega_i \alpha_r - j\omega_i t_r} t_{signature}\ (\omega_i) \|^2 \tag{4-3-4}$$

Using the Simplex method to minimise e_{rror}, we obtain the latest estimated object contribution as:

$$\hat{t}_{\arg et,n}(\omega_i) = \hat{a}_r e^{-\omega_i \hat{\alpha}_r - j\omega_i \hat{t}_r} t_{signature}(\omega_i) \tag{4-3-5}$$

If the change between the previous estimated object contribution, $\hat{t}_{\arg et,p}(\omega_i)$, and the latest estimated object contribution, $\hat{t}_{\arg et,n}(\omega_i)$, is less than the threshold δ, i.e.,

$$\sum_{i=1}^{m} \| \hat{t}_{\arg et,n}(\omega_i) - \hat{t}_{\arg et,p}(\omega_i) \| < \delta \sum_{i=1}^{m} \| \hat{t}_{\arg et,p}(\omega_i) \| \tag{4-3-6}$$

We consider that a buried object has been detected. The object related parameters, $[\hat{a}_r \quad \hat{\alpha}_r \quad \hat{t}_r]$, and the residual data, $r(\omega_i)$, are outputted for further processing. If equation (4-3-6) is not satisfied and the inner loop does not reach its maximum number, we subtract the estimated object contribution from the pre-processed GPR data $s(\omega_i)$ to obtain the contributions from the ground:

$$g(\omega_i) = s(\omega_i) - \hat{t}_{\arg et,n}(\omega_i) \tag{4-3-7}$$

Afterwards the inner loop is increased by 1 and continued for the object detection from equation (4-3-2).

If the inner loop reaches its maximum number, then the algorithm exits from the inner loop to the outer loop and increase the time window by Δ_b. If the outer loop does not reach its maximum number, then the algorithm enters the inner loop again. If the outer loop does reach its maximum number and no object has been detected, then the algorithm stops and exit.

4.3.3 Implementation Problems and solutions

Three important parameters in the IT algorithm implementation are the rank of the Prony technique for clutter subtraction, the first time window for clutter-only estimation and the start point for the Simplex Method.

- The rank of the Prony technique

The rank, K in equation (4-3-2), is required by the Prony technique. The rank varies according to the complexity of the environment. It is hard to guess it around based on experiments. K can be calculated from the ground contribution, $g(\omega_i)$. In order to estimate the rank, we first make a data matrix $\boldsymbol{A}$ from $g(\omega_i)$, and then use the singular value decomposition (SVD) of the matrix to obtain the rank.

Vector $\boldsymbol{x}$ is the collection of the previous received ground contribution $g(t_{i-l}), l = 1,...,L$.

$$\boldsymbol{x} = [g(t_{i-1}) \quad g(t_{i-2}) \quad \cdots \quad g(t_{i-L})] \tag{4-3-8}$$

Using the linear prediction algorithm in time domain, we have:

$$g(t_i) = \boldsymbol{xa} = [g(t_{i-1}) \quad g(t_{i-2}) \quad \cdots \quad g(t_{i-L})][a_1 \quad a_2 \quad \cdots \quad a_L]^T \tag{4-3-9}$$

$\boldsymbol{a} = [a_1 \quad a_2 \quad \cdots \quad a_L]^T$ is the linear coefficient vector.

Similarly,

$$g(t_{i+1}) = \boldsymbol{xa} = [g(t_i) \quad g(t_{i-1}) \quad \cdots \quad g(t_{i-L+1})][a_1 \quad a_2 \quad \cdots \quad a_L]^T$$

Let $\boldsymbol{y} = \begin{bmatrix} g(t_{i-L+1}) \\ g(t_{i-L+2}) \\ \cdots \\ g(t_{i-L+M}) \end{bmatrix}_{M\times 1}$ and $\boldsymbol{X} = \begin{bmatrix} g(t_{i-1}) & g(t_{i-2}) & \cdots & g(t_{i-L}) \\ g(t_{i-2}) & g(t_{i-3}) & \cdots & g(t_{i-L+1}) \\ & & \cdots & \\ g(t_{i-M}) & g(t_{i-M+1}) & \cdots & g(t_{i-L+M-1}) \end{bmatrix}_{M\times L}$

Then, we have

$$\boldsymbol{y} = \boldsymbol{Xa} \tag{4-3-10}$$

The singular value decomposition (SVD) of the matrix $\boldsymbol{X}$ is:

$$\boldsymbol{X} = \boldsymbol{UDV}^*; \qquad \boldsymbol{D} = \begin{bmatrix} \boldsymbol{D}_{K\times K} & 0_{K\times(L-K)} \\ 0_{(M-K)\times K} & 0_{(M-K)\times(L-K)} \end{bmatrix} \tag{4-3-11}$$

U and V are unitary matrices and D is a diagonal matrix. The rank of data matrix X is K, therefore the number of the linear prediction coefficients is K. The implementation for the rank of data matrix is:

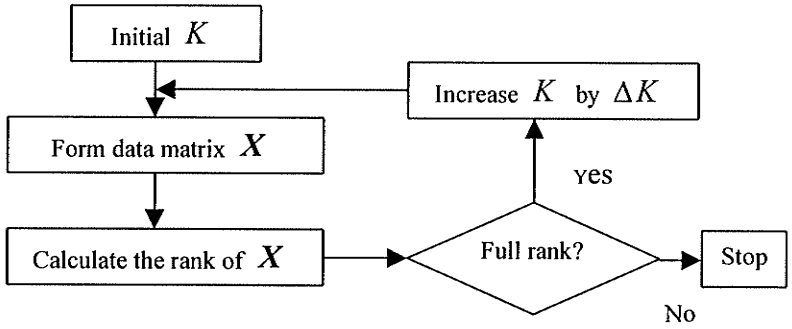

Figure 4-3-3 Rank calculation block diagram for the Prony technique

- The first time window for ground surface contribution only

The first time window must cover the contributions from the ground surface only. Initially, we searched the time step with the highest signal peak as the start of reflection from the ground surface. It is true for a deep buried non-metal landmine. But sometimes, this is not true for subsurface buried objects or landmines with a small metal piece. Based on the above consideration, the first window is chosen upon experiments. Implementation of the window search can be accomplished by two methods: one is based on an automatic search of the peak signal from the ground surface in a certain time area. The other one is to configure the first time window manually.

- The start point for Simplex Method

The Simplex method needs a start point. After the estimated ground surface contribution is removed, the residual GPR data, $r(\omega_i)$, is supposed to be dominated by the reflection from the buried objects. $r(\omega_i)$ can be rewritten as:

$$r(\omega_i) = h_c(\omega_i) - \hat{h}_c(\omega_i) + a_r e^{-\omega_i \alpha_r - j\omega_i t_r} t_{signature}(\omega_i), i = 1,...,m \quad (4\text{-}3\text{-}12)$$

Multiplying $\frac{t^*_{signature}(\omega_i)}{\| t_{signature}(\omega_i) \|^2}$ on both sides of the above equation, we have

$$r(\omega_i)\frac{t^*_{signature}(\omega_i)}{\| t_{signature}(\omega_i) \|^2} = [h_c(\omega_i) - \hat{h}_c(\omega_i)]\frac{t^*_{signature}(\omega_i)}{\| t_{signature}(\omega_i) \|^2} + a_r e^{-\omega_i \alpha_r - j\omega_i t_r} \quad (4\text{-}3\text{-}13)$$

$r(\omega_i)\frac{t^*_{signature}(\omega_i)}{\| t_{signature}(\omega_i) \|^2}$ should be dominated by the second term, $a_r e^{-\omega_i \alpha_r - j\omega_i t_r}$. Again, the Prony technique is used to estimate the parameters $[\hat{a}_r \quad \hat{\alpha}_r \quad \hat{t}_r]$ for the start point based on the strongest signal in the $r(\omega_i)\frac{t^*_{signature}(\omega_i)}{\| t_{signature}(\omega_i) \|^2}$.

4.3.4 Simulation Results

The purpose of the following simulation is to evaluate the adequacy of the implemented IT algorithm. We use the preprocessed FDTD GPR data with buried objects as the input. We expect that the ground surface contribution should be decomposed from the contributions of the landmines. Unlike the LP algorithm in section 4.2, the IT algorithm processes the received GPR data at a cross-range scan position. It does not need any GPR data from previous scan positions. In our simulation, the data in ***Residual_mine+ground_T9_ΔR_3***, listed in table 4-6, is used as the inputs of the algorithm. The geometry of these data, as shown in Figure 4-3-4, is created according to table 4-6.

We assume that the GPR system illuminates the area with a narrow beam width and the buried landmines are separated enough so that there are no contributions from the nearby landmines. For example, on the second cross-range scan position; the GPR receives contributions from the ground surface and from the landmine buried directly

under the scan position 2. No contributions from the closest landmine under the scan position 3 and scan position 1 are considered.

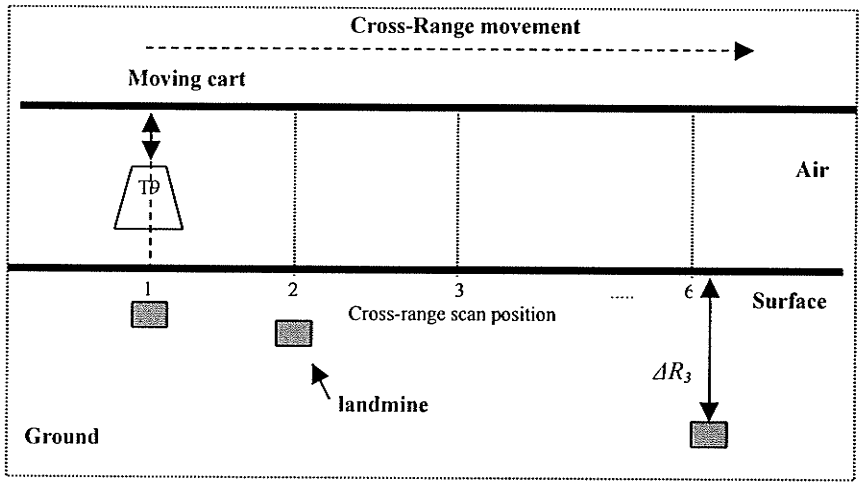

Figure 4-3-4 Geometry of the preprocessed FDTD GPR data set for IT simulation

Table 4-6: a set of preprocessed FDTD GPR data

Cross-range scan position	1	2	3	4	5	6
Residual_ mine+ground_T9_ ΔR_3 ΔR_3	5	10	15	20	25	30

Figure 4-3-5 is the images of the input and the output of the IT algorithm. From cross-range scan position 2 to 6 and from time step 390 to time step 450, the ground surface contributions are reduced significantly. At the cross-range scan position 1, the buried object is 1.25cm deep under the ground surface. The contributions from the ground surface and from the buried object are partly overlapped. The un-overlapped ground surface contribution, from time step 390 to time step 430, is reduced, too. We can conclude that the implemented algorithm does decompose the ground surface contributions from the contributions of the buried objects.

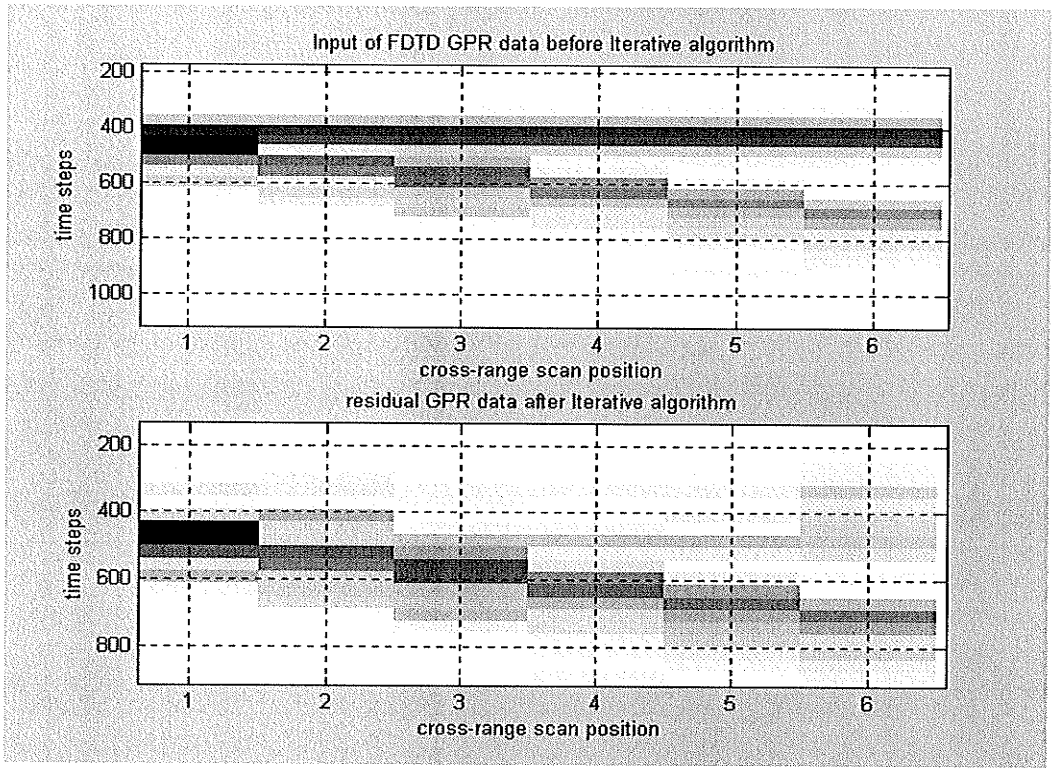

Figure 4-3-5 Images of input and output data of IT algorithm

4.3.5 Simulation problems and solutions

In our simulation, we faced the time consumption problem of the IT algorithm. In order to show this, the following example was set. The threshold δ was defined as 0.001 for ground-only preprocessed FDTD GPR data, ***Residual_ ground_only_T9***. No landmine was buried. The inner loop was set to 10 and the outer loop to 8. The algorithm did not detect an object as expected, but the consumption of CPU time was 3.249e+002 seconds, i.e. 5.41478 minutes for the detection procedure. For a cross-range scan area of 20 cm, if scan positions are 1cm apart equally, the number of total scan position would be 20, and the IT algorithm needs 1.8 hours to finish. If the threshold is set to 0.01, the algorithm generates the alarms at the ground-only scan position.

One of the solutions to this time consuming problem is to apply this algorithm on the alarmed scan positions only. The alarms can be generated by the LP algorithm for general landmine detection or by a *cross-correlation alarm generator* for specific landmine detection. Because a reference signature is also used in the algorithm, we prefer the second one. In this solution, Figure 4-3-1 is modified as indicated in Figure 4-3-6.

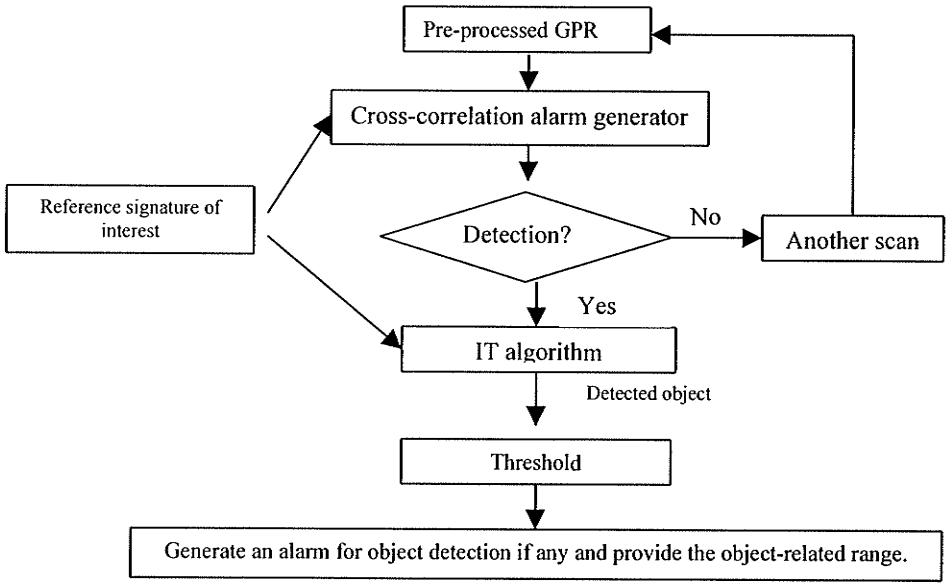

Figure 4-3-6 Object detection Block diagram with IT algorithm

The cross-correlation alarm generator is shown in Figure 4-3-7, as below:

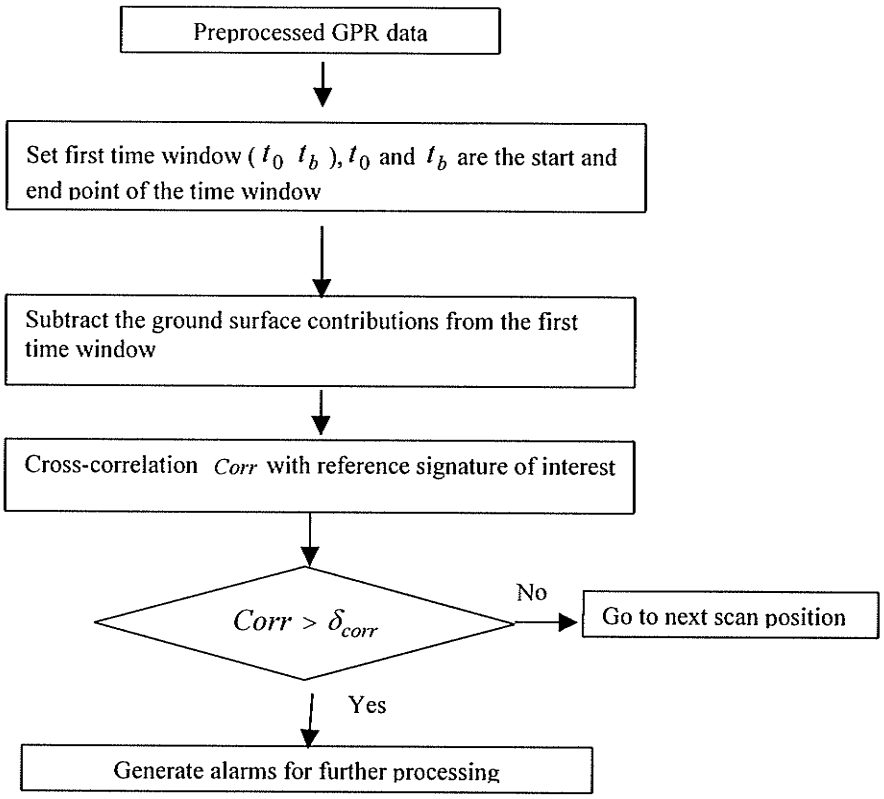

Figure 4-3-7 block diagram for cross-correlation alarm generator

Suppose $Corr$ is the cross correlation of the pre-processed GPR data with the reference signature $t_{signature}(\omega_i)$. The cross-correlation alarm generator in Figure 4-3-6 generates an alarm if $Corr$ is greater than the threshold δ_{corr} (an estimated value with an adjustable factor we will discuss it later). The purpose of this alarm generator is to run the IT algorithm only on the alarmed scan positions, reducing the total time over the whole scanning area.

If the range resolution, dR, of the GPR system is high enough, then the first time window, used in the IT algorithm, is also helpful in the *cross-correlation alarm generator* to reduce part of ground surface contribution.

$$dR = \frac{v_g}{2B} = \frac{3 \times 10^8 / \sqrt{\varepsilon_r}}{2 \times 5 \times 10^9} \tag{4-3-13}$$

Here B is the bandwidth of current source. v_g is the propagation speed and ε_r is the relative dielectric constant of the propagation media. In our FDTD simulation, B is 5GHz and ε_r is 7, therefore, dR is 1.13cm. Because the shortest distance between the buried objects and the ground surface is 1.25cm, the range resolution is high enough to separate the ground surface from the closest object. This means that the first time window can be used to remove part of the ground reflection with no loss of any contributions from the objects.

δ_{corr} is calculated over a small area with no object buried.

$$\delta_{corr} = \frac{F_{scale}}{N} \sum_{i=1}^{N} Corr(i) \tag{4-3-14}$$

Where $Corr(i)$ is the cross correlation value at the scan position i, F_{scale} is a factor to adjust the threshold δ_{corr}, N is the number of scan positions for the threshold estimation. If F_{scale} is high, δ_{corr} will be high, and the number of generated alarms will be low. δ_{corr} is set high enough so that few alarms are generated over an area with no objects buried. But, If δ_{corr} is too high, a buried object, which generates a low reflection, i.e. low SNR, will not be detected. This is unacceptable. So δ_{corr} should be set low enough so that no buried object will be undetected.

We use ***Prep_GPR_data_group_noise***, in section 4.2.2, as the inputs of the cross-correlation alarm generator. Figure 4-3-8 shows the images of the inputs and the output of the alarm generator. There are 93 scan positions and only half of them are alarmed. The time for scanning this area is reduced by 50%.

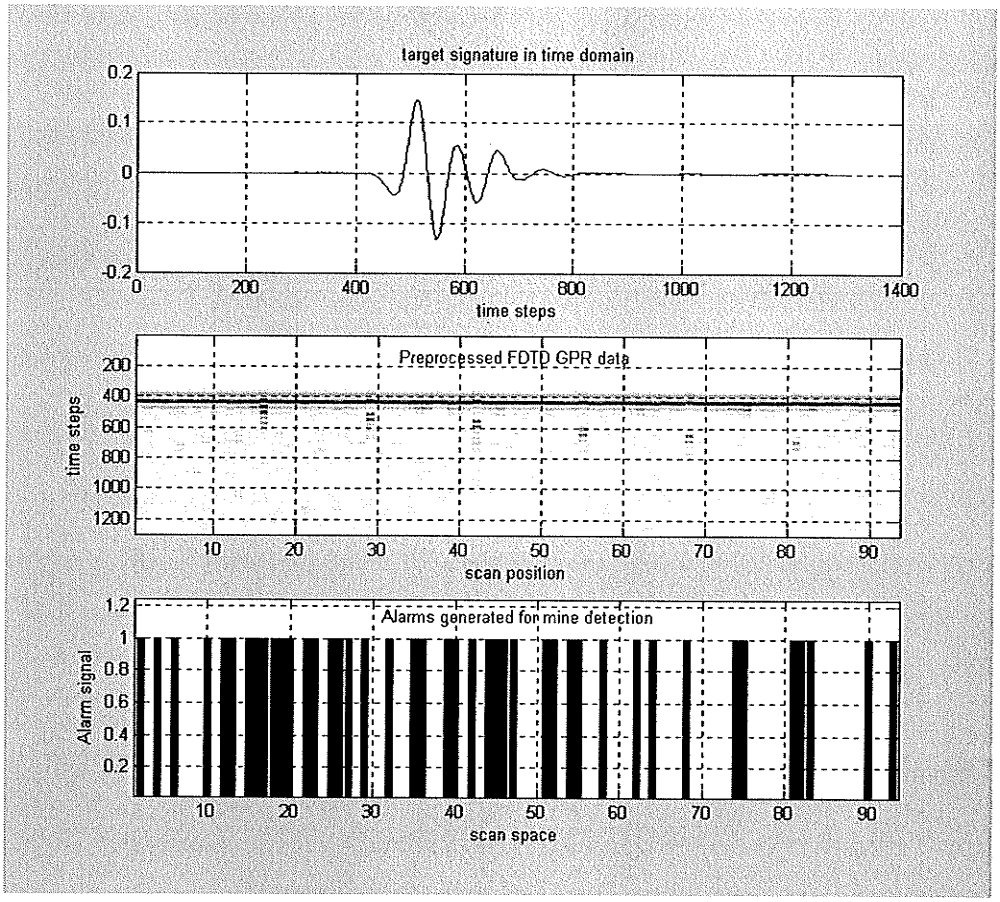

Figure 4-3-8 Inputs and output of the cross-correlation alarm generator

There are only six objects in ***Prep_GPR_data_group_noise***. We should be able to reduce the alarms further with a higher cross correlation threshold δ_{corr}. Table 4-7 and Table 4-8 are the simulation results with different thresholds for the number of object detection and the number of the false alarms over SNR.

Table 4-7 Alarms over SNR and object detection over SNR with F_{scale} 0.35

SNR	alarm #	object detected #	SNR	alarm #	object detected #
-5.169	15	10	-5.740	63	9
-5.092	15	10	-5.835	58	9
-5.166	20	10	-5.788	60	10
-5.175	17	10	-4.867	10	10
-5.334	34	10	-4.842	10	10
-5.329	25	10	-4.809	10	10
-5.452	21	10	-4.747	10	10
-5.503	19	10	-4.765	10	10
-5.490	29	10	-6.029	74	10
-5.462	31	10	-5.999	71	10
-5.604	30	10	-6.025	70	10
-5.603	40	10	-5.796	50	10
-5.57	41	10	-6.168	87	10
-5.625	40	10	-6.205	84	10
-5.763	63	10	-6.018	85	10
-5.874	56	10	-6.275	81	10
-5.840	56	10	-6.065	62	10

Table 4-8 Alarms over SNR and object detection over SNR with F_{scale} 0.40

SNR	alarm #	object detected #	SNR	alarm #	object detected #
-4.871	10	10	-5.551	22	10
-4.909	10	10	-5.856	31	9
-4.864	10	10	-5.720	34	8
-5.031	11	10	-5.744	33	9
-4.995	10	10	-5.855	37	10
-4.943	11	10	-5.847	25	10
-5.176	11	10	-5.769	26	10
-5.301	10	10	-5.687	32	10
-5.157	11	10	-5.976	51	9
-5.315	15	10	-6.089	33	9
-5.374	14	10	-5.957	49	10
-5.315	17	10	-6.0269	46	9
-5.320	20	10	-6.108	47	10
-5.333	17	10	-6.111	45	9
-5.540	18	9	-6.140	60	10
-5.647	22	8	-6.297	67	9
-5.590	31	10	-6.297	59	9

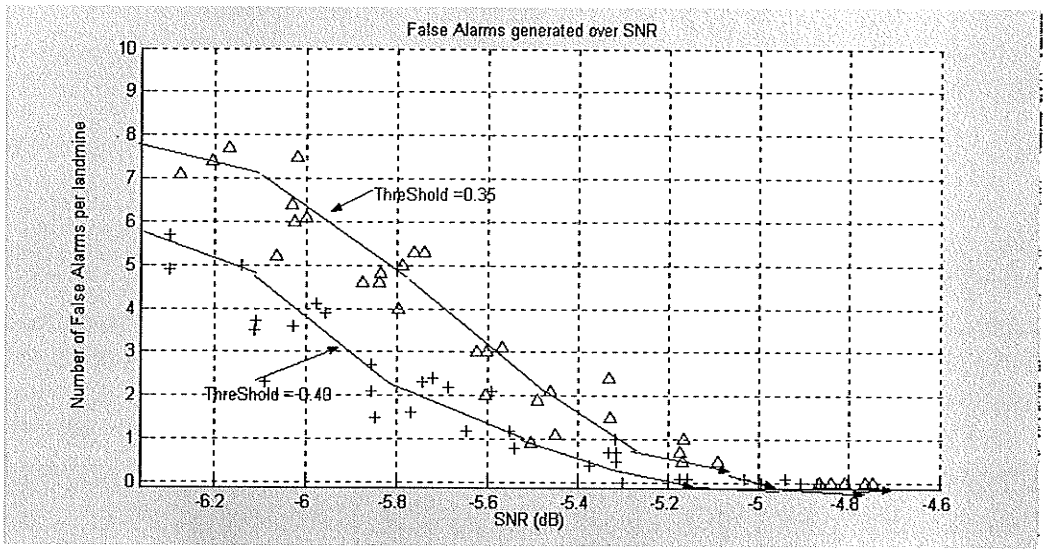

Figure 4- 3-9 Number of false alarms over SNR with different threshold factor

Table 4-7 and Table 4-8 indicates that if SNR<-5.3dB, the number of alarms are up to 30. The cross-correlation alarm generator yields good results if the SNR is high enough, SNR>-5.3dB. With the same SNR, the number of false alarms is decreased when compared with the LP alarm generator over the same SNR, see table 4-5. Figure 4-3-9 is created based on table 4-7 and table 4-8. It indicates that with the same SNR, increasing F_{scale} reduce the false alarms. A high threshold δ_{corr} is helpful in reducing the number of false alarms, but it also increases the number of buried objects undetected. With a low threshold δ_{corr} (F_{scale} = 0.35) and SNR >-5.5dB, the ratio of generated alarms per landmine is less than 3 and no landmines are undetected. The maximum number of generated alarms in table 4-7 is 34. The total number of scan positions is 93. Therefore, the number of the generated alarms over the total number of scan positions is up to 37% (34/93), i.e., the time consumption for this scan is reduced by 63%.

We applied the IT algorithm on the alarmed scan positions. The buried objects were detected as expected.

The image of the output of the IT algorithm is shown in Figure 4-3-10.

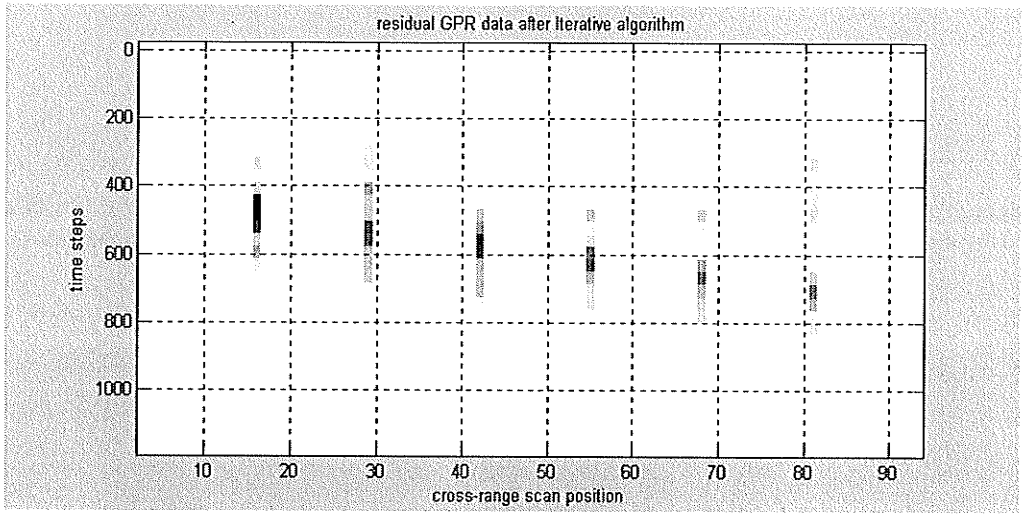

Figure 4-3-10 Image of pre-processed FDTD GPR data after IT algorithm

4.3.6 Summary

The IT algorithm was successfully implemented and the three main parameters of this method were correctly chosen. These three parameters are: i) the first time window selection for the ground surface contribution; ii) the rank estimation for ground contribution by the Prony technique; and iii) the start point for the object contribution by the Simplex method.

The implemented IT algorithm was applied to the pre-processed FDTD GPR data. The results indicated that the implemented IT algorithm decomposes the ground surface contribution from the contributions of the buried objects and detects the buried objects. This proves that the implemented IT algorithm works well with our simulated FDTD GPR data.

During our simulation, we found that this algorithm has an execution time problem. With an inner loop of 10 and an outer loop of 8, this algorithm takes up to 5

minutes to finish the detection over a scan position. In order to solve this problem, we introduced the cross-correlation alarm generator to generate an alarm on a cross-range scan position if the estimated measure is greater than a threshold. The IT algorithm is stimulated on an alarmed scan position only. By doing this, the detection time over an area of 93 scan positions can be reduced up to 70%.

Figure 4-3-11 is the recommended block diagram for buried object detection with DSP techniques discussed in this chapter. The use of these DSP techniques on measured GPR data for landmine detection is presented in Chapter 5.

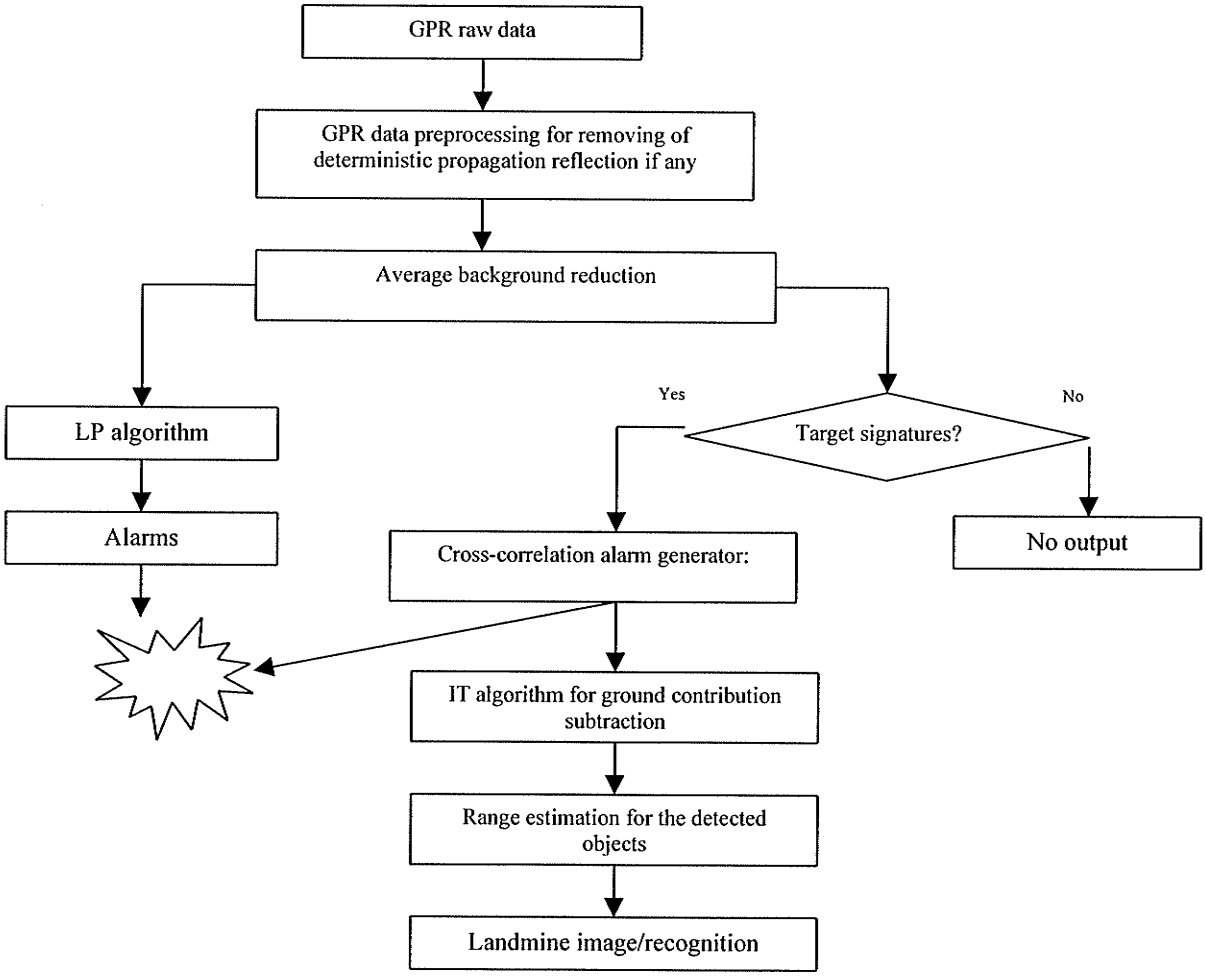

Figure 4-3-11 Recommend Block diagram for landmine detection

Chapter 5 Experiments on the Measured GPR data

In Chapter 4, we discuss the implementation of the LP algorithm for general object detection and the IT algorithm for object-oriented object detection. These two algorithms can detect the landmines with FDTD GPR data. In this chapter, we first introduce the collection of the measured GPR data with our lab set-up and pre-process them. And then, we apply these two algorithms for landmine detection.

5.1 GPR raw data collection

The system function block is shown in Figure 1-1 and is detailed in [19]. A Network Analyzer generated stepped frequency signals from 1GHz to 12.4GHz. The number of frequency steps is 501. One horn antenna attached to the moving cart is used for both signal transmission and receiving. In this work, GPR raw data or measured GPR data refers to the directly received data from the input of the Network Analyzer and is collected in frequency. At each cross-range scan position, GPR raw data is recorded and then downloaded to a PC. With this microwave Network Analyzer, the range resolution $R_{resolution}$ for the waveform through lossy sand is:

$$R_{resolution} = \frac{v_g}{2B} = \frac{3e^8 / \sqrt{\varepsilon_r}}{2 * 11.4GHz} = 0.74\text{cm} \qquad (5\text{-}1\text{-}1)$$

ε_r is 3.15, see [5].

Controlled by the PC, the moving cart moves evenly across the cross-range direction. The horn type antenna moves from right to left or left to right along the beam, covering a total cross range distance of 3m with various step sizes. Moving the antenna across the beam is called "a scan". The sandbox is bottomed with absorbing material to reduce the reflection from the room floor.

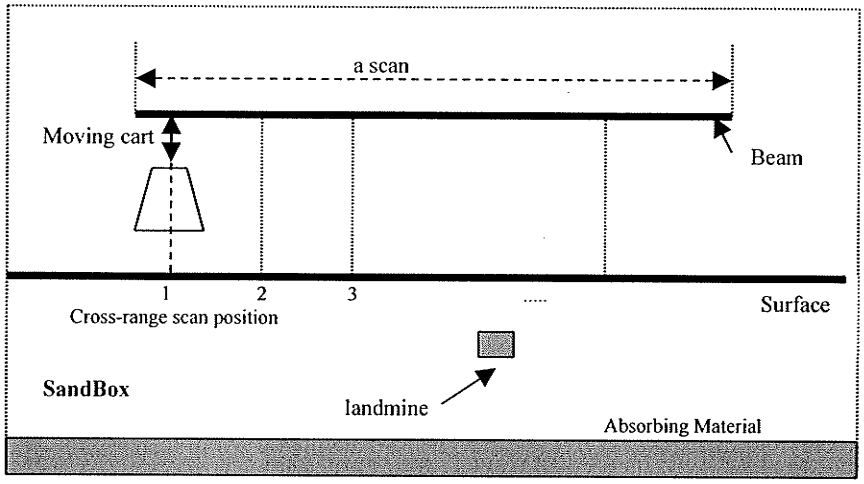

Figure 5-1-1 Illustration of conceptual geometry block for GPR raw data collection

One scan of GPR raw data, *NA_raw_data.mat,* was collected with a landmine buried under the sand with no buried rocks, as shown in Figure 5-1-1. The scan was performed across a beam of 140cm long. There are 116 scan spaces with a step size of 1.2cm approximately. Figure 5-1-2 is the waveform of the GPR raw data in time domain. Figure 5-1-3 is the image of the GPR raw data along the beam. There are no noticeable differences among the received raw GPR data at different scan positions.

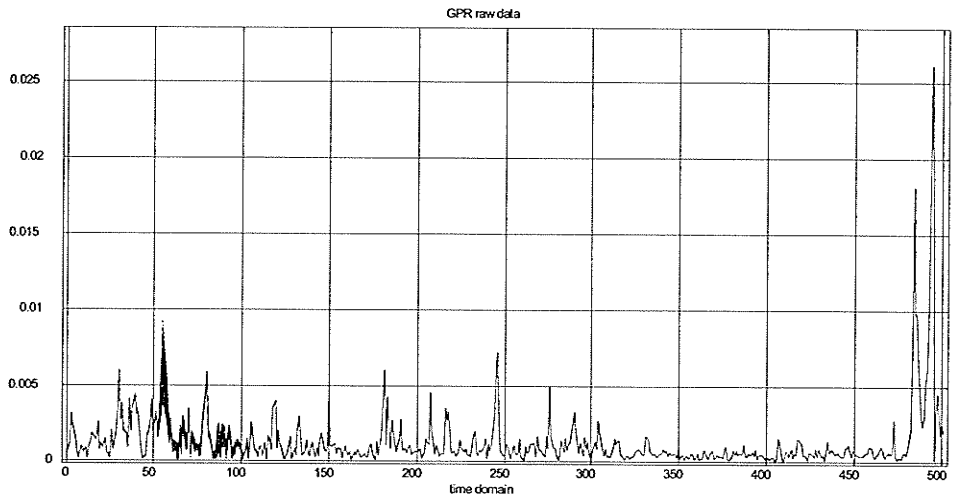

Figure 5-1-2 GPR raw data collected from sand with rocks and landmine

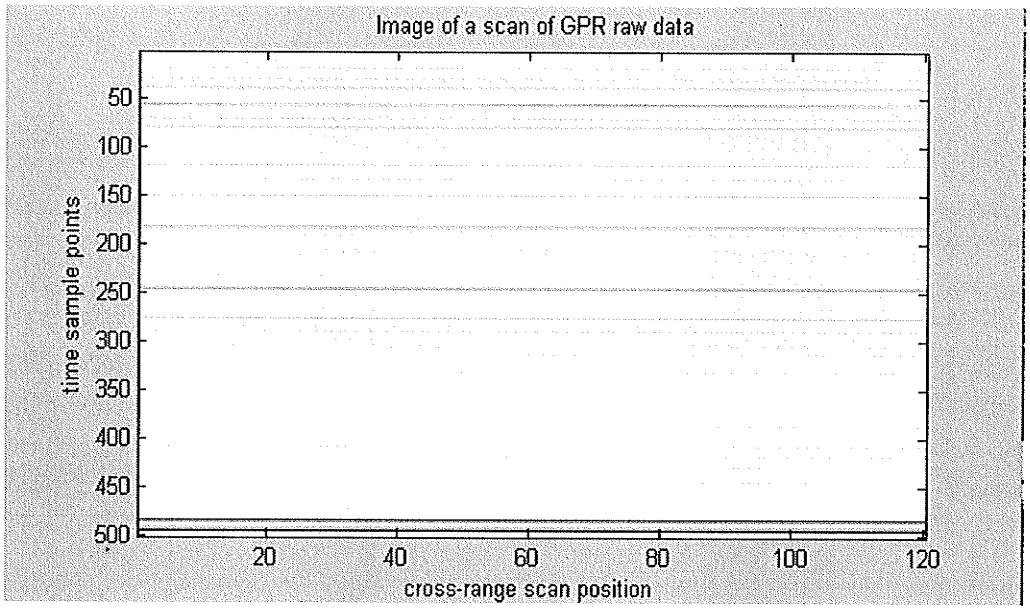

Figure 5-1-3 Image of a scan of GPR raw data

As with our simulation with FDTD GPR data, these raw GPR data must be pre-processed in order to apply signal-processing techniques for landmine detection.

5.2 Data pre-processing

We perform a few scans, and we noticed that there was little change in a scan of GPR raw data after time sample point 120. The Sandbox is 27cm deep. Range resolution $R_{resolution}$ is 0.74cm. It takes about 36 time sample points for the micro waveform to reach the bottom of the sandbox from the sand surface.

$$\frac{R}{R_{resolution}} = \frac{27}{0.79} \approx 36 \tag{5-2-1}$$

If the time sample point for the sand surface is located at 50, then the major contributions from the sandbox will be from the time sample point 50 to the time sample point 122 (50+2*36). The GPR raw data after the time sample points 122 are the contributions

mainly from the stable surroundings. Therefore, the GPR raw data, after time sample point 122, was filtered out by setting them to zero. After this processing, the scan of GPR raw data is denoted as *NA_raw_data_122*, as shown in Figure 5-2-1. As for the time sample points for the sand surface, it is an experimental value. It depends on the distance between the antenna and sand surface, and the time delay caused by the length of the cable attached from the antenna to the Network Analyzer as well.

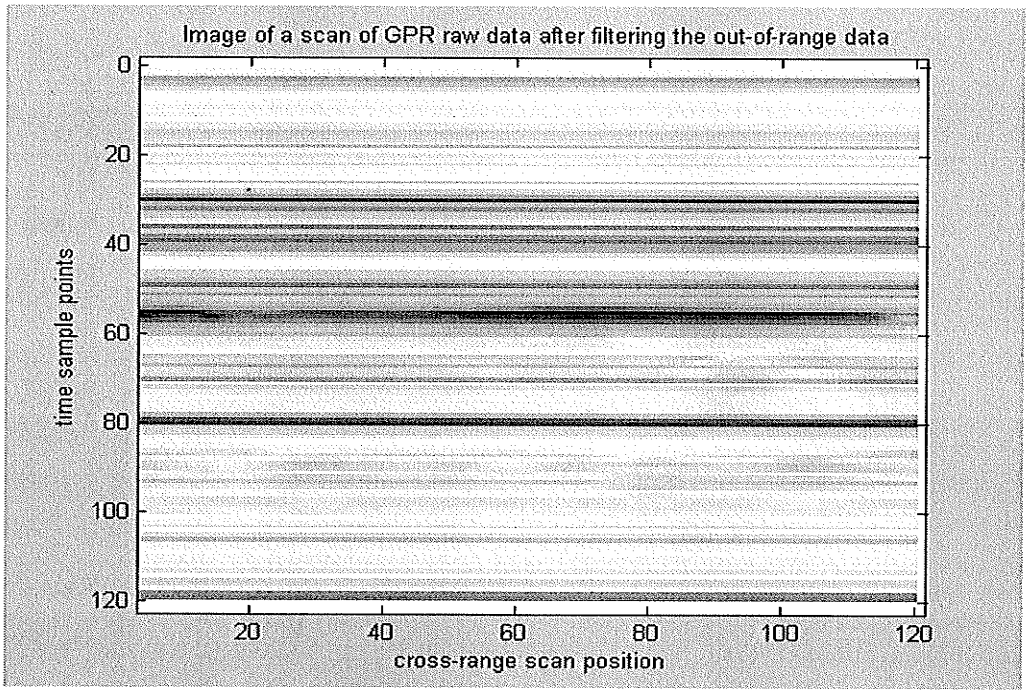

Figure 5-2-1 Image of a scan of GPR raw data after the out-of-range data is filtered

GPR raw data consists of two major signals: the deterministic signal and the statistical signal. The statistical signal is a random distribution from the reflecting objects like rocks, landmines and rough sand surface. The deterministic signal is the contributions by the stable surrounding objects with very slow change from a scan position to the nearby scan position, comparing with the disturbance caused by the small

objects. We defined clutter as the contributions from any reflection objects, except the contributions from the landmines.

5.2.1 Decomposition of deterministic propagation clutter

In FDTD simulation, the ground surface contributions can be reduced by the linear algorithm based on layer geometry model. Figure 5-2-2 is the output of the linear algorithm with GPR raw data, *NA_raw_data_122*, as its input. The prediction order is 24. The estimated coefficients are obtained based on the sand-only area.

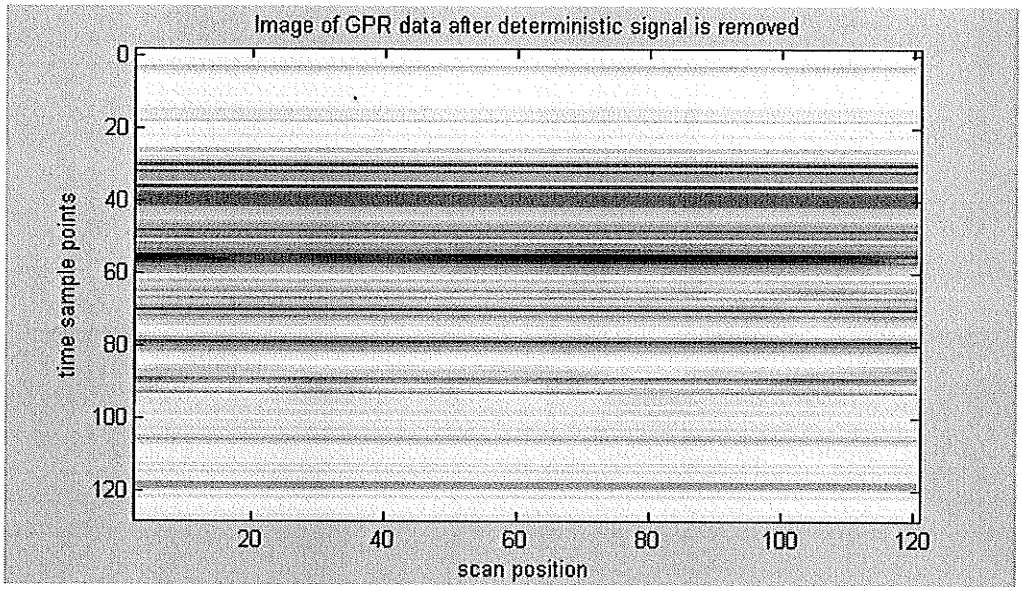

Figure 5-2- 2 Image of GPR raw data after deterministic signals are removed

Comparing Figure 5-2-2 with Figure 5-2-1, we do not notice any improvement. Changing the prediction order did not improve the result. This indicates that the received GPR raw data is not linear predicable in the same sense found using the algorithm with layered geometry model.

5.2.2 Average background estimation

Figure 5-2-1 demonstrates that background signals from unknown sources through the whole scan are very strong and has no significant change except the area from time sample point 50 to 60. The background noise in a small area is considered stable, which can be removed from the GPR raw data. Let $gPRdata(i)$ be a vector representing GPR raw data at the scan position i.

$$\boldsymbol{gPRdata}(i) = \{GPRdata(t_j, i), j = 1,..., m\} \tag{5-2-2}$$

m is the number of total sample points. In our case, m is 501. t_j is the time sample point. $GPRdata(t_j, i)$ is the GPR data sampled at time t_j at the scan position i. The background noise $\overline{backGround}(i)$ is the average of GPR raw data over N scan positions.

$$\overline{\boldsymbol{backGround}}(i) = \frac{1}{N}\sum_{i=1}^{N} \boldsymbol{gPRdata}(i) \tag{5-2-3}$$

In a large cross-range area, adaptive background average is used in order to adjust the various changes in the environments.

$$\overline{\boldsymbol{backGround}}(k) = \sum_{i=1}^{N} \boldsymbol{gPRdata}(k-i) \times AdapC(i), k > N \tag{5-2-4}$$

$AdapC(i), i = 1,2...,N$ are adaptive parameters chosen by:

$$\sum_{i=1}^{N} AdapC(i) = 1 \tag{5-2-5}$$

$AdapC(i)$ is adjusted according to the roughness of the sand surface. If $N = 2$, $AdapC(1) = \alpha$, $AdapC(2) = 1-\alpha$ and $\overline{backGround}(1) = gPRdata(1)$, then we have:

$$\overline{\boldsymbol{backGround}}(k) = \alpha \times \overline{\boldsymbol{backGround}}(k-1) + (1-\alpha) \times \boldsymbol{gPRdata}(k) \tag{5-2-6}$$

The residual GPR data $r_{pp}(k)$ at k scan position is obtained by removing the estimated background noise from the GPR raw data.

$$r_{pp}(k) = gPRdata(k) - \overline{backGround}(k) \qquad (5\text{-}2\text{-}7)$$

Figure 5-2-2 is the implementation block diagram for the adaptive background noise estimation.

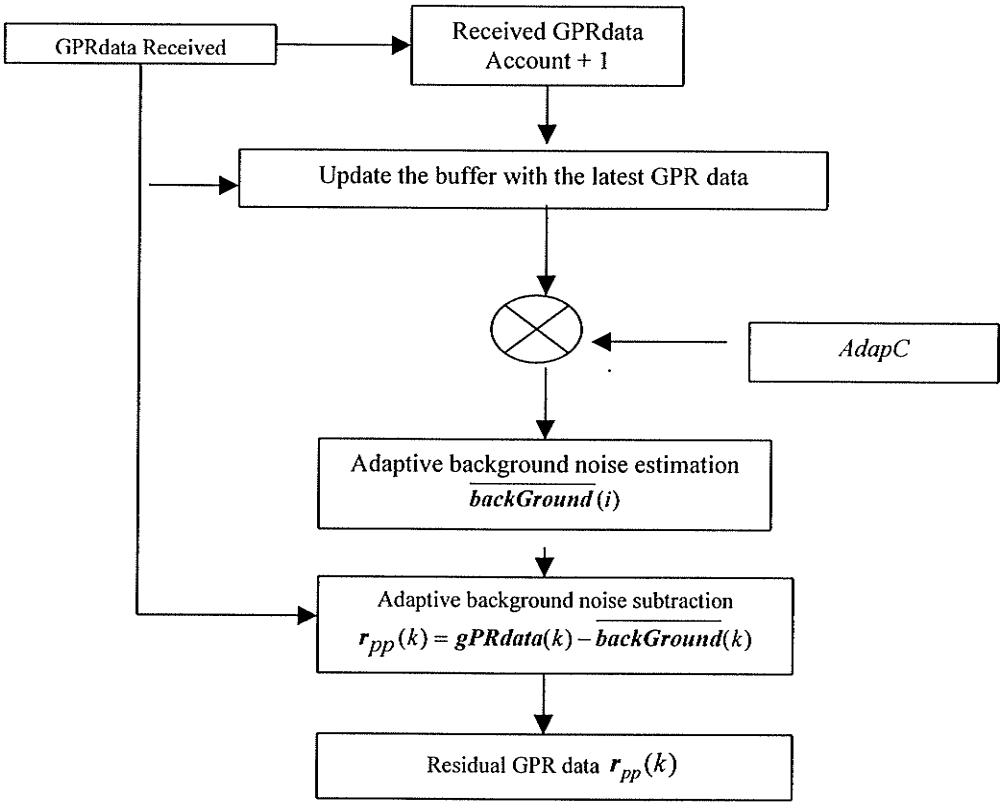

Figure 5-2-3 the block diagram of background estimation and removal

Figure 5-2-4 is the residual GPR data after the background noise with adaptive coefficients of [0.1 0.35 0.55] is removed. It indicates that the big disturbance under sand surface is located from scan position 80 to 100. It is the place where a landmine is buried. The landmine image becomes clear after subtracting the adaptive background noise. In our current set-up with dry sand and the flat surface or rippled surface, changing the adaptive coefficients makes no significant difference among the images of the

residual GPR raw data. This is because our sand environment is a homogeneous-like media. The residual GPR data after this pre-processing, called pre-processed GPR raw data, can be used for further processing.

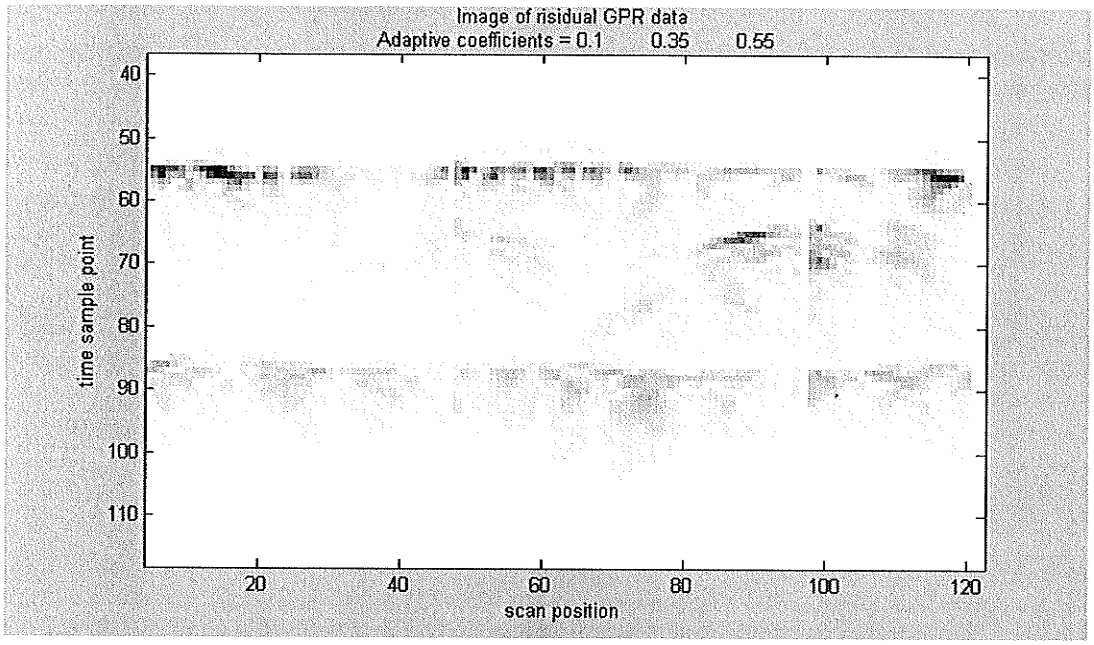

Figure 5-2-4 Image of residual GPR data after pre-processing

5.3 Experiments with the LP algorithm

NA_raw_data_E3_B is a scan of GPR raw data from a master database. There are 7 objects scattered under the sand surface. Figure 5-3-1 is the pre-processed GPR raw data as the input of the LP algorithm for general landmine detection. In this collection, the sand surface is roughly located at time sample point 110. The major contributions from the sandbox are from time sample point 110 to 180. The prediction order was set to 5 and the average number was set to 10 for the alarm threshold estimation. The alarm generator threshold is 1.5. Then, seven alarms were generated, located at the scan position 11, 13, 38, 66, 78, 88 and 89 as shown in Figure 5-3-2. There were two

landmines roughly centred at 119cm and 80cm. Because there are 118 scan positions over 140cm, the landmines' scan positions are calculated by:

$$scan\_position = mine\_position*118/140cm \quad (5\text{-}3\text{-}1)$$

The landmines are located at scan position 67 and 100.

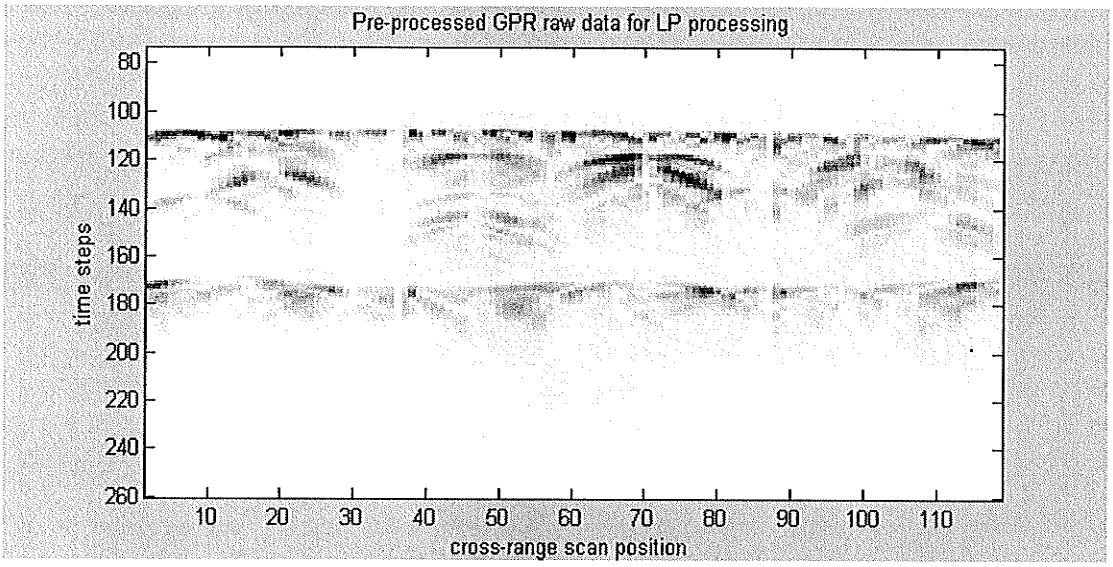

Figure 5-3-1 Image of pre-processed GPR raw data as the input of LP for landmine detection

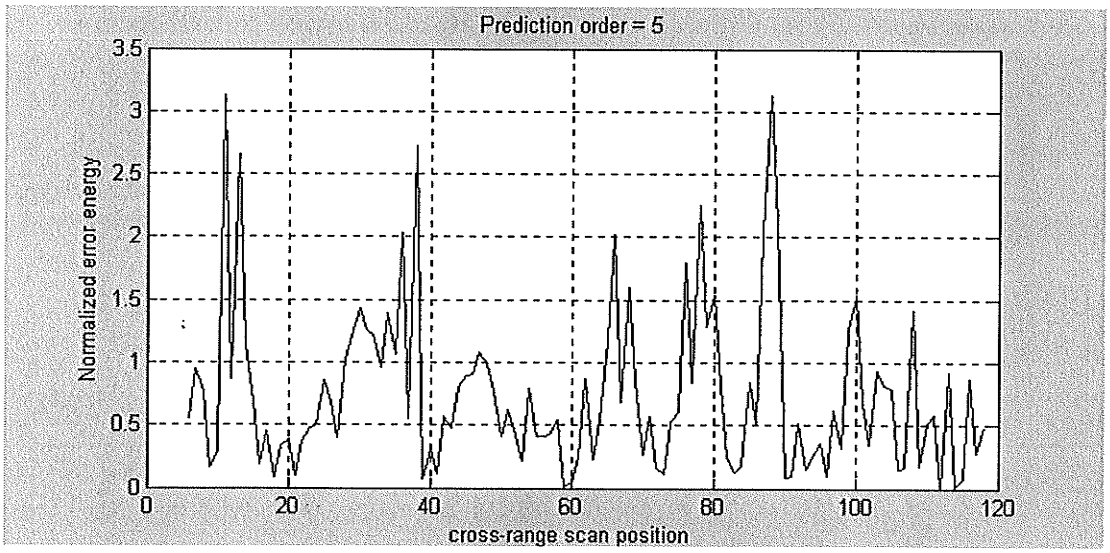

Figure 5-3-2 Output of LP algorithm for landmine detection

Alarms at nearby scan positions are considered as one alarm area, i.e. two alarms generated at scan position 11 and 13 are considered as one alarm area, and alarms located at scan positions 88 and 89 as another single alarm area. The results then are:

- 5 false alarm areas generated,
- A landmine located at 67 is detected,
- A landmine at 100 is missed.

Note that the landmine scan position 67 could be 66 due to the inaccuracy in the measured GPR data. Lowering the threshold to 1.2, we obtain 13 alarms located at scan positions:

[(11 13), 38, (66 68), (76 78 79 80), (88 89), (99 100), 108]

The results are:

- 7 false alarm areas generated,
- A landmine located at 67 is detected,
- A landmine at 100 is detected.

Figure 5-3-2 indicates that there are six cluttered peak areas:

Area 1: from scan position 11 to 13,

Area 2: from scan position 30 to 38,

Area 3: from scan position 62 to 68,

Area 4: from scan position 76 to 80

Area 5: scan position 100.

Area 6: scan position 108.

Because the LP algorithm is a general method for landmine detection, no knowledge of the landmine shape and size is considered. With pre-processed *NA_raw_data_E3_B*, and the threshold of 1.2, the LP algorithm generates six alarmed areas for further landmine determination. With some knowledge of the buried landmines, the alarms can possibly be reduced further. Based on the above results, we concluded that with our lab set-up, the LP algorithm can detect landmines with some false alarms. The lower the threshold is set, the more alarms will be generated.

5.3.1 Improvement of the LP algorithm

GPRdataStore_rawData.mat is a scan of GPR raw data collected with high cross-range resolution and a single buried square landmine. No rocks were buried. Figure 5-3-3 is the image of the GPR raw data after pre-processing. Setting the prediction order to 5 and the average number to 10, we expect the peak alarms generated around scan position 50 and scan position 65. The LP algorithm's output is shown in Figure 5-3-4.

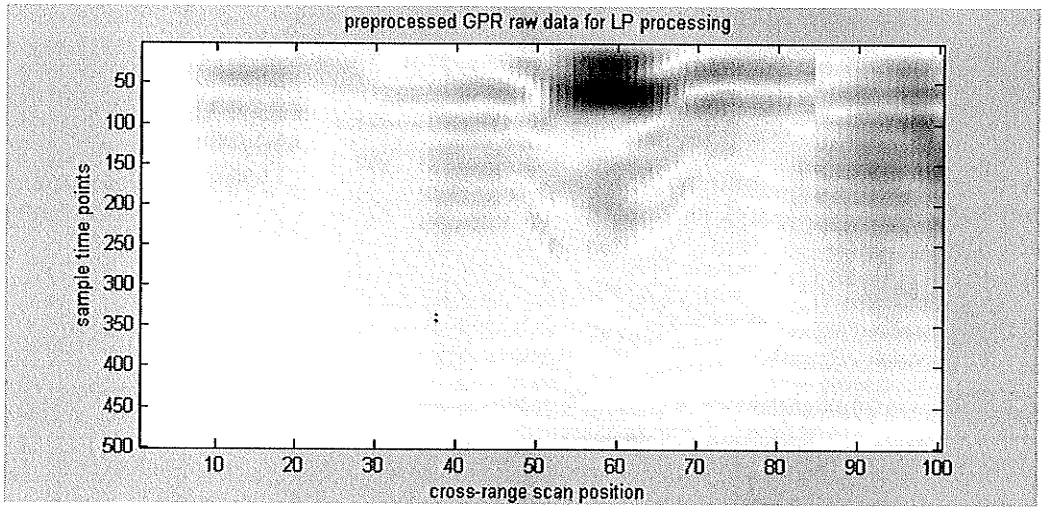

Figure 5-3-3 Image of pre-processed GPR data with a buried object under the sand surface

Figure 5-3-4 indicates that the LP algorithm detects the significant error energy at the scan position 50, and some small energy changes scattered at the scan position 55, 62, 67 and 85. The results are within our expectation. Figure 5-3-5 to Figure 5-3-7 are the outputs of the LP algorithm with different prediction orders. We notice that from prediction order 5 to 18, the strongest alarm is at scan position 50, the left edge of the landmine. If the prediction order is higher than 22, then the strongest alarm switches to scan position 60 from scan position 50, the right edge of the landmine, see Figure 5-3-6. For prediction orders of 20 to 21, the results are messed up far from satisfactory, as shown in Figure 5-3-7.

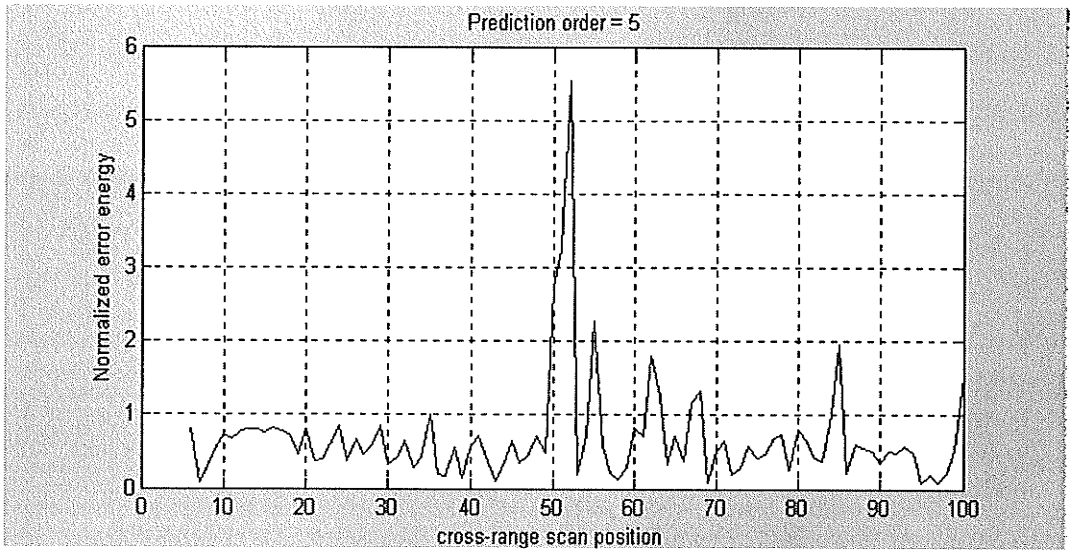

Figure 5-3-4 output of LP algorithm

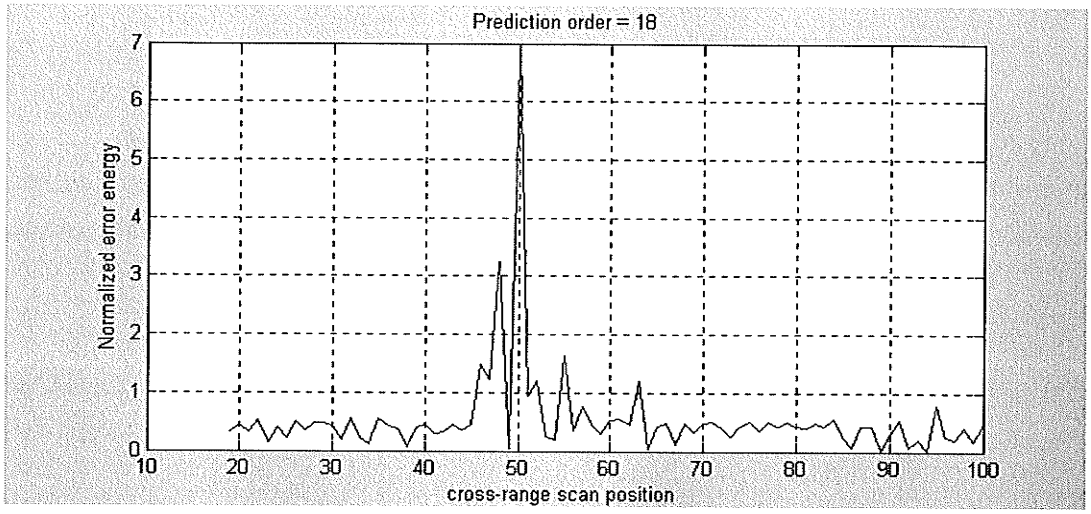

Figure 5-3-5 output of LP algorithm

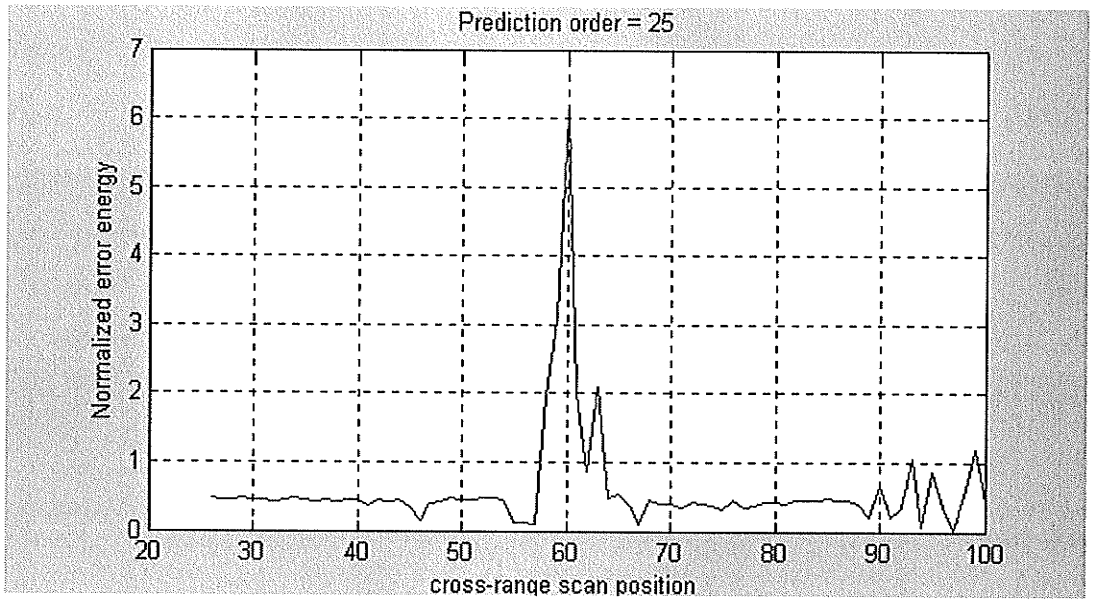

Figure 5-3-6 output of LP algorithm

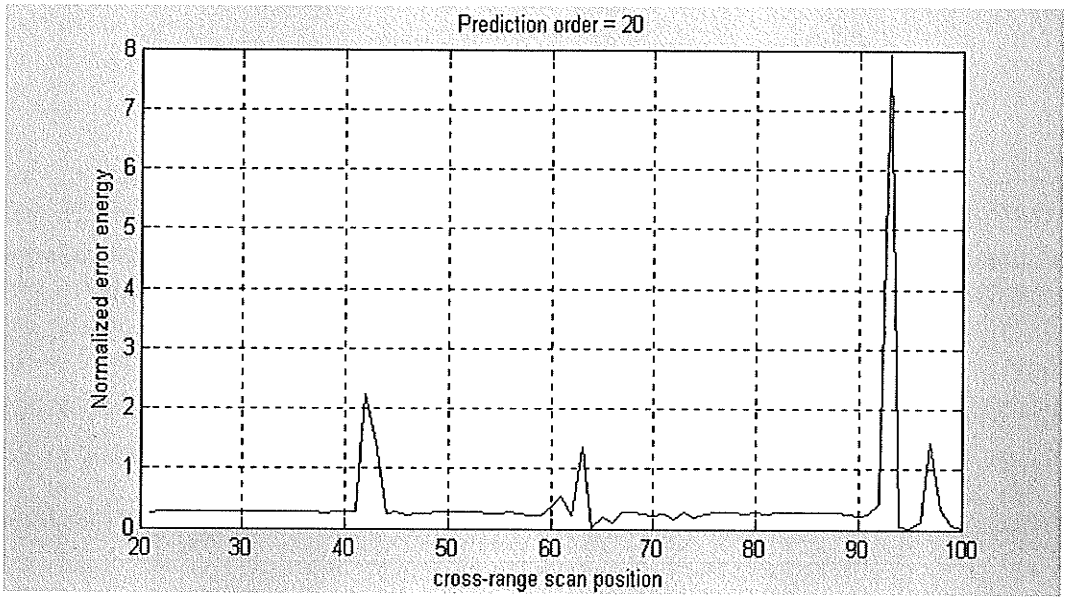

Figure 5-3-7 output of LP algorithm for landmine detection

The above results indicate that in the above case, with prediction order of 20, the original LP algorithm has trouble to set an alarm for the obvious buried landmine.

Figure 5-3-8 to Figure 5-3-11 are the outputs of the improved LP algorithm with different prediction orders. If the prediction order is less than 10, it alarms at both right edge and left edge of the buried object. If the prediction order is above 10, it generates one error energy peak area located from scan position 50 to 60, i.e. the position of the landmine. This indicates that the improved LP algorithm obtains better results for this case than the original LP algorithm.

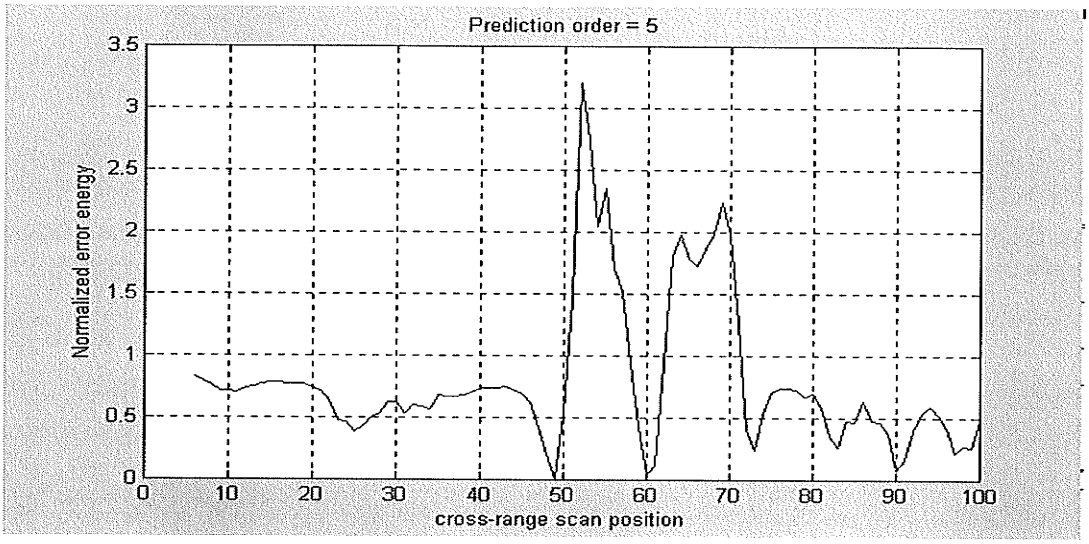

Figure 5-3-8 output of improved LP algorithm

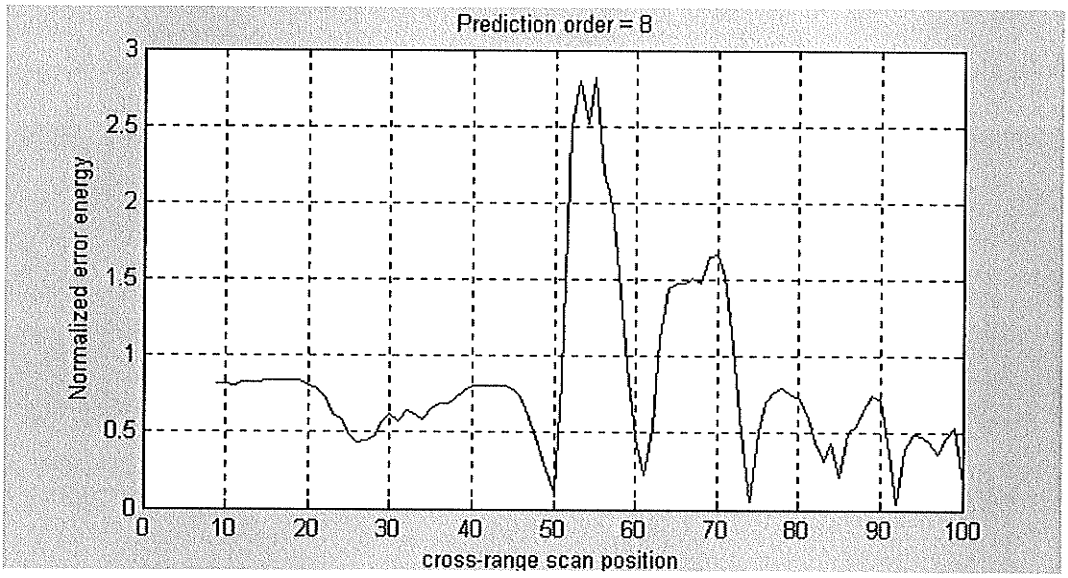

Figure 5-3-9 output of improved LP algorithm

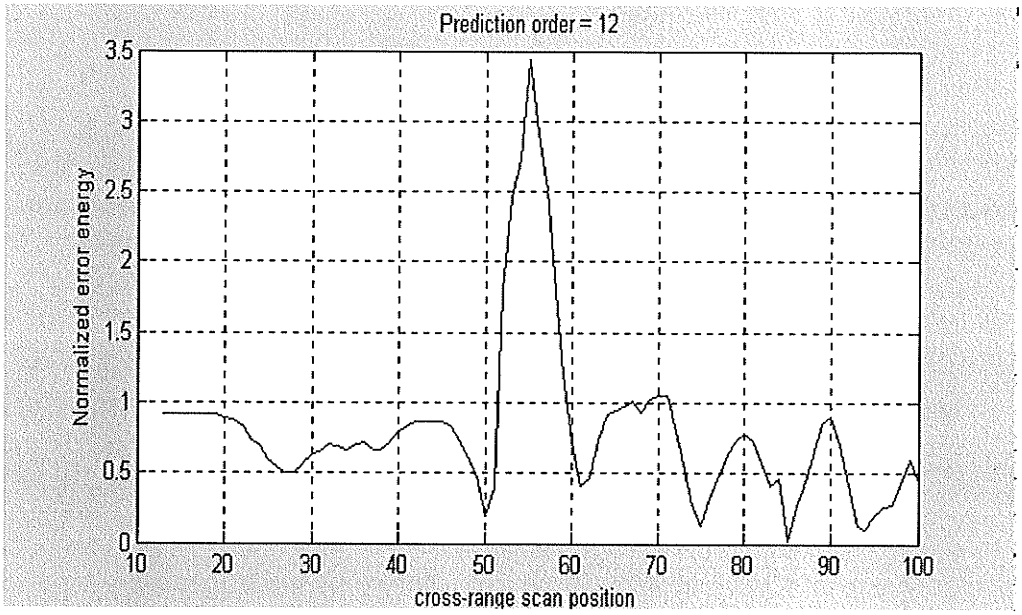

Figure 5-3-10 output of improved LP algorithm

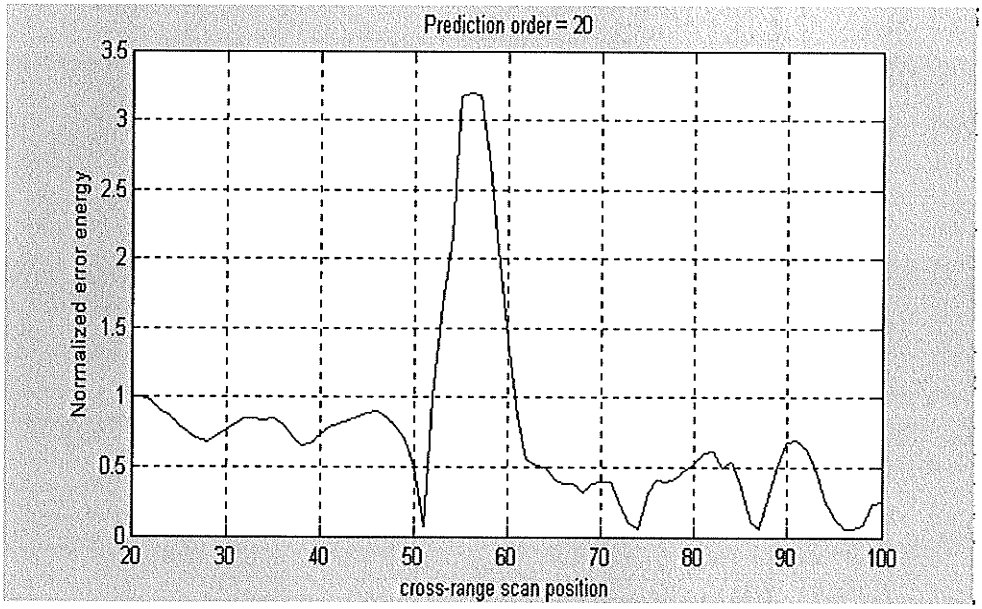

Figure 5-3-11 output of improved LP algorithm

Figure 5-3-12 is the image of the pre-processed *NA_raw_data_E3_B* used as the input of both the original and improved LP algorithms. We expect the highest error

energy to appear from 60 to 80. There are rocks scattered under the surface, so there should be some low error energies scattered, at scan locations from 10 to 20, from 40 to 50, from 60 to 80 and probably 100.

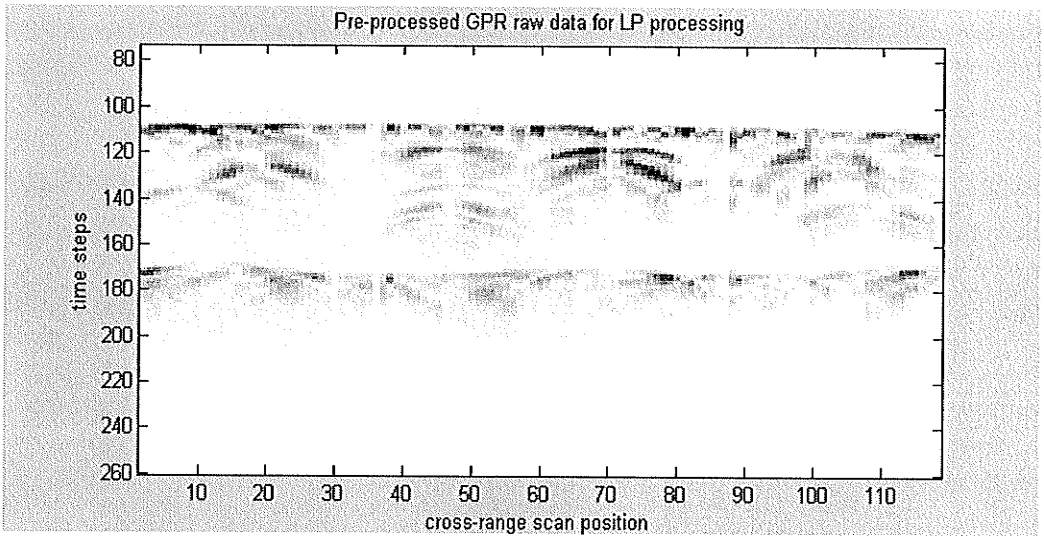

Figure 5-3-12 Image of pre-processed GPR raw data as the input of LP algorithms

The prediction order was set to 5. Figure 5-3-13 and Figure 5-3-14 are the outputs of the original and improved LP algorithms of the pre-processed GPR raw data, *NA_raw_data_E3_B*, from the Master database. Figure 5-3-15 and Figure 5-3-16 are the outputs of the original and improved LP algorithms for a prediction order of 8.

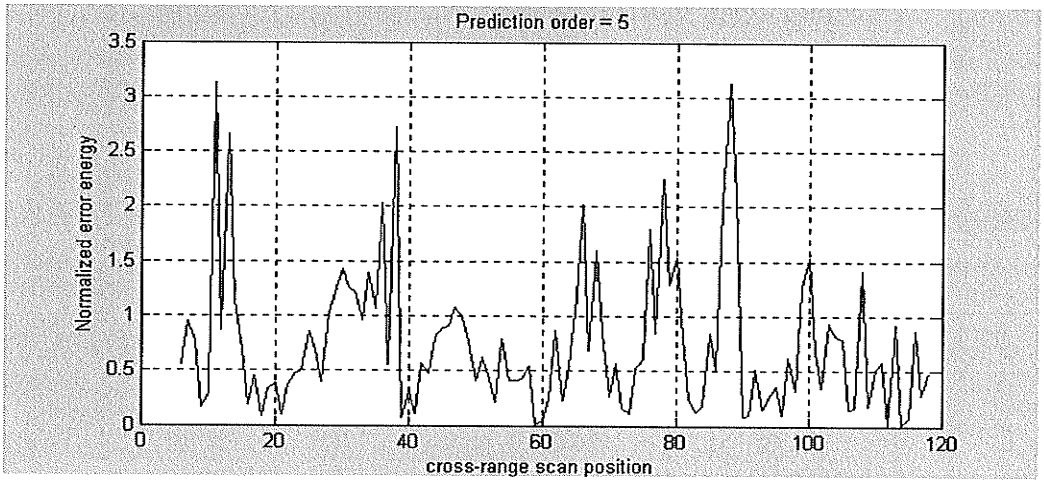

Figure 5-3-13 Output of LP algorithm for landmine detection

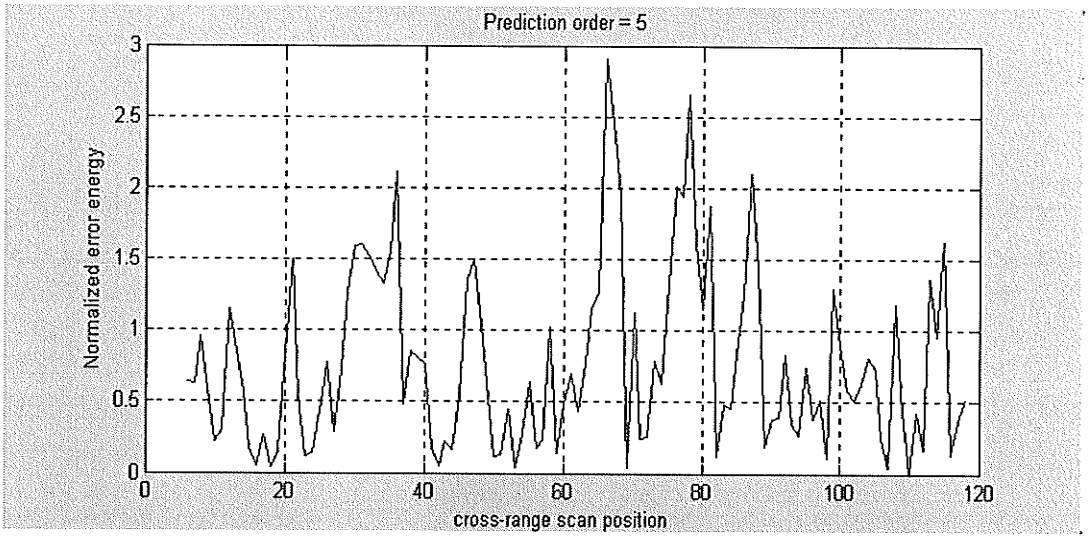

Figure 5-3-14 Output of improved LP algorithm for landmine detection

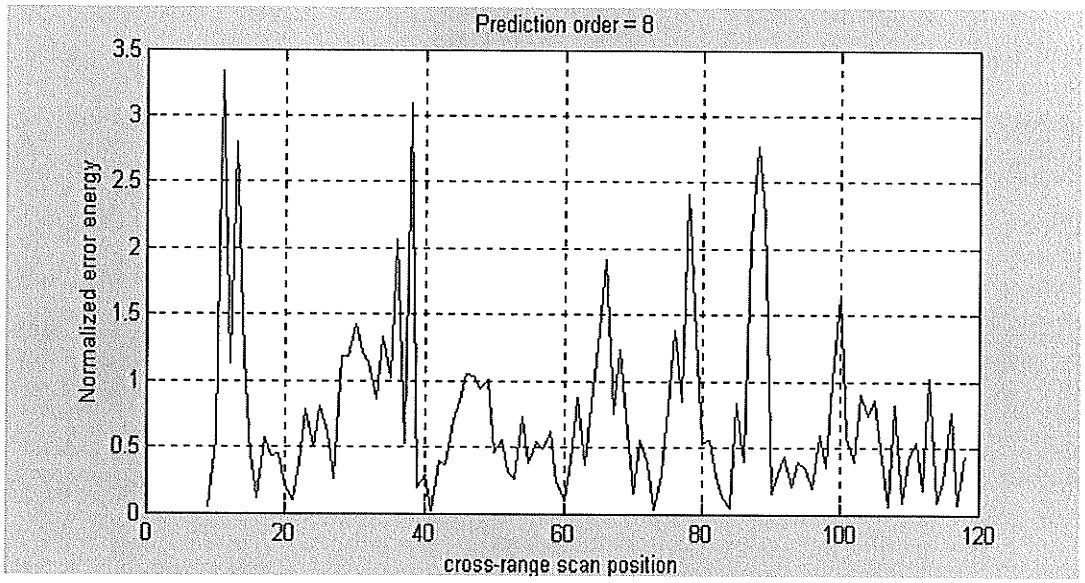

Figure 5-3-15 Output of the LP algorithm for landmine detection

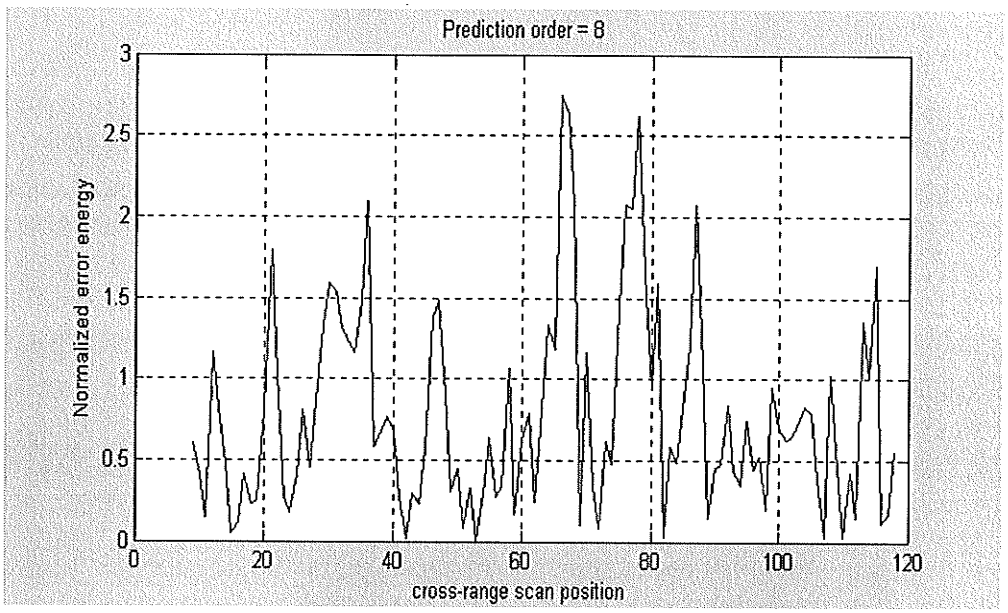

Figure 5-3-16 Output of improved LP algorithm for landmine detection

Comparing the above results, both the original and improved LP algorithms are able to generate alarms in the expected areas. However, the improved LP algorithm obtained better results than the original LP algorithm [10] as can be seen from the highest error energy located from scan position 60 to 80.

The following tables are created by the original/improved LP algorithms for the false alarms and landmine detection as a function of the threshold ($\xi'_{threshold}$).

Table 5-1 false alarms vs. threshold by the original LP algorithm with prediction order 5

$\xi'_{threshold}$	False alarm areas	Landmine detected
1.1	5	2
1.3	4	2
1.5	4	1
1.6	3	0

Table 5-2 false alarms vs. threshold by improved LP algorithm with prediction order 5

$\xi'_{threshold}$	False alarm areas	Landmine detected
1.5	6	2
1.6	4	2
1.8	1	1
2	1	1
>2	0	1

Table 5-3 false alarms vs. threshold by original LP algorithm with prediction order 8

$\xi'_{threshold}$	False alarm areas	Landmine detected
1.1	4	2
1.3	4	1
1.5	4	0

Table 5-4 false alarms vs. threshold by improved LP algorithm with prediction order 8

$\xi'_{threshold}$	False alarm areas	Landmine detected
1.1	5	2
1.3	4	2
1.5	2	1
>2	0	1

Table 5-5 false alarms vs. threshold by LP algorithm with prediction order 15

$\xi'_{threshold}$	False alarm areas	Landmine detected
2.2	2	0
2.0	4	1
1.8	4	2
1.5	6	2
1.3	9	2

Table 5-6 false alarms vs. threshold by improved LP algorithm with prediction order 15

$\xi'_{threshold}$	False alarm areas	Landmine detected
>2	0	1
1.8	1	1
1.5	3	1
1.3	5	1
1.1	6	2

From the above results, we can conclude that

- The improved LP algorithm obtained better results than the original one.
- The lower the threshold ($\xi'_{threshold}$) is set, the more false alarm areas are generated.
- With the improved LP algorithm, the square landmine is detected with fewer false alarms generated than using the original LP algorithm.
- For a rounded landmine, because its reflection is very low, it has to be detected with lower thresholds. Unfortunately, many false alarm areas are generated with a very low threshold. Because of this, the work presented here was focussed on the square landmine that was available. Detection of the smaller rounded mine was left for future research.

5.3.2 LP algorithm with adaptive technique

With a time varying environment, the adaptive LP algorithm is needed to adjust its results in response to the environment changes. Data was collected with a landmine, located between scan position 5 (left edge of the landmine) to 10 (right edge of the landmine). Some rocks are scattered in the scan area. The scan positions are separated 2.5cm apart. Figure 5-3-17 is the image of this pre-processed data. The peak error energies are expected to be at the scan position around 5 to 10 and 20 to 26.

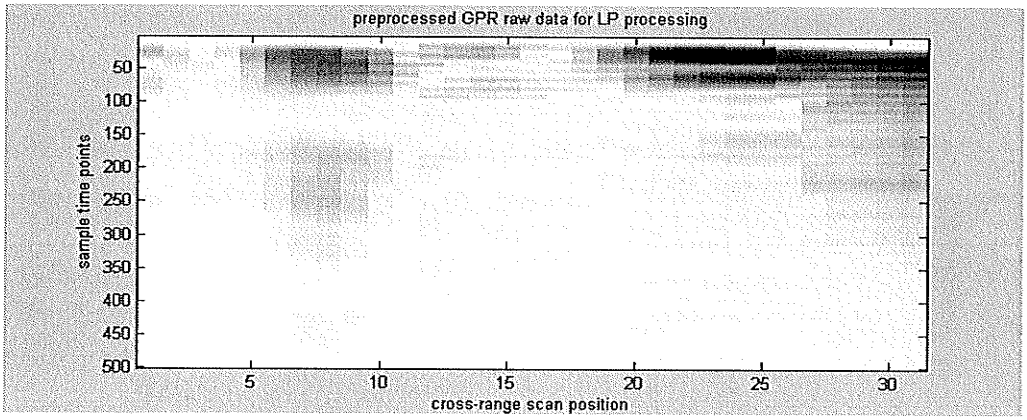

Figure 5-3-17 Image of pre-processed GPR raw data with a buried landmine and rocks

Because the location of the landmine is in the training area, the LP algorithm with no adaptive processing detects the right edge of the landmine, but fails to detect the left edge of the landmine. In this case, we set the prediction order to 3, the adaptive coefficient λ (refer to section 3-2-2) to 0.015. The output of the adaptive LP algorithm is shown in Figure 5-3-18. Figure 5-3-19 is the output of the LP with no adaptive technique.

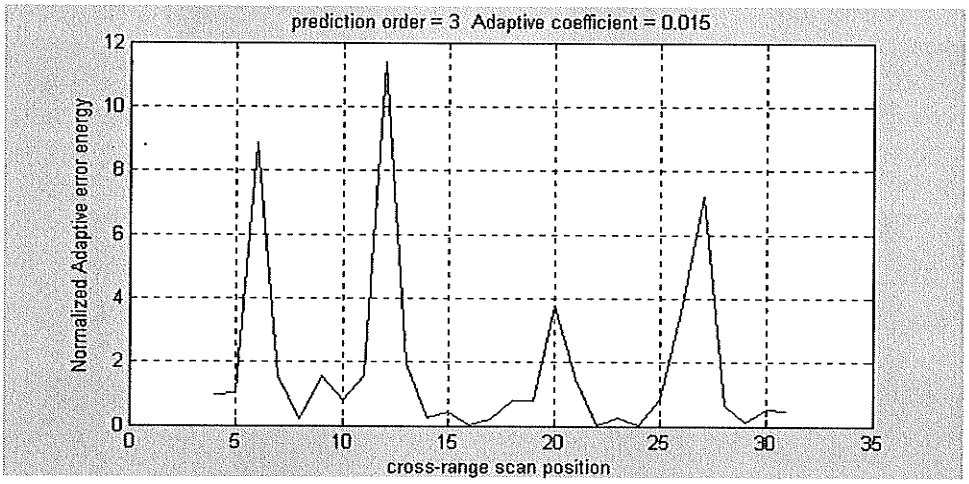

Figure 5-3-18 output of adaptive LP algorithm

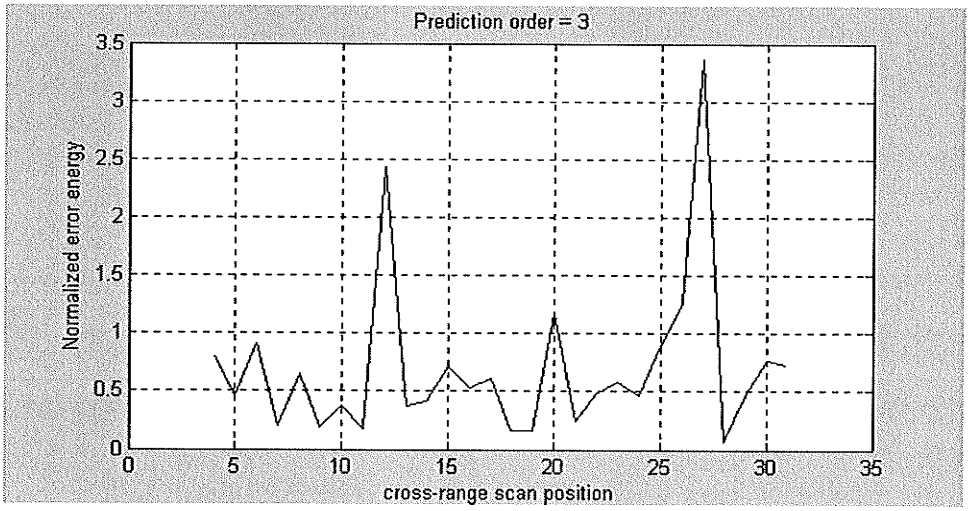

Figure 5-3-19 output of original LP algorithm with no adaptive technique

Figure 5-3-19 indicates that the LP algorithm without the adaptive technique failed to detect the error energy change at cross-range scan position 5, but alarmed the error energy at the scan position 12. With the adaptive technique, the adaptive LP method is able to generate alarms at the scan position 6, 12, 20 and 27, corresponding to the disturbance made by the landmine and the rocks as can be seen in Figure 5-3-17.

There are no significant differences among the outputs of the adaptive LP algorithm if the adaptive coefficient is less than 0.15 and the prediction order is less than 5, as can be seen in Figure 5-3-20 to Figure 5-3-22.

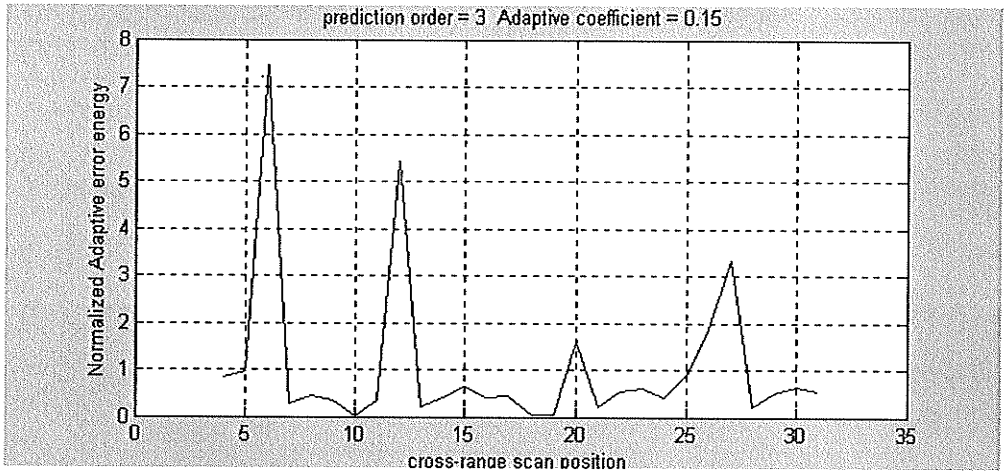

Figure 5-3-20 output of adaptive LP algorithm

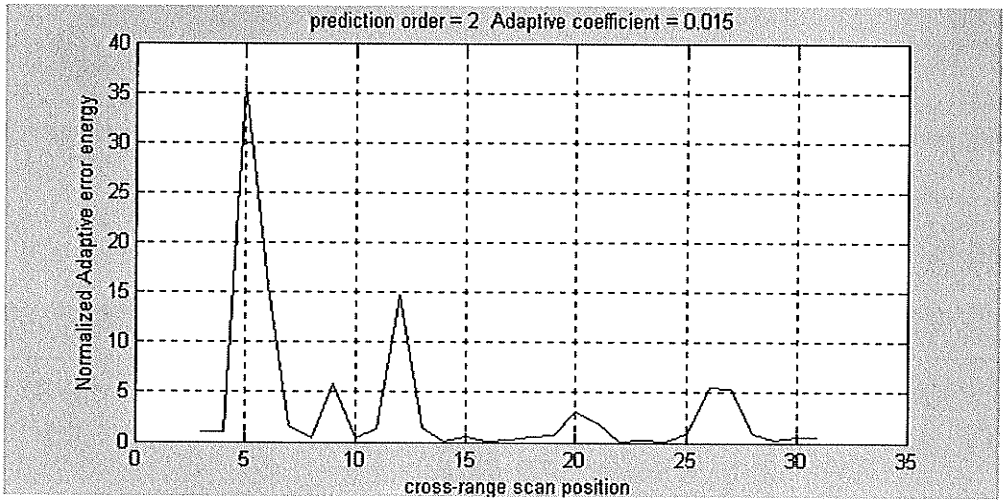

Figure 5-3-21 output of adaptive LP algorithm

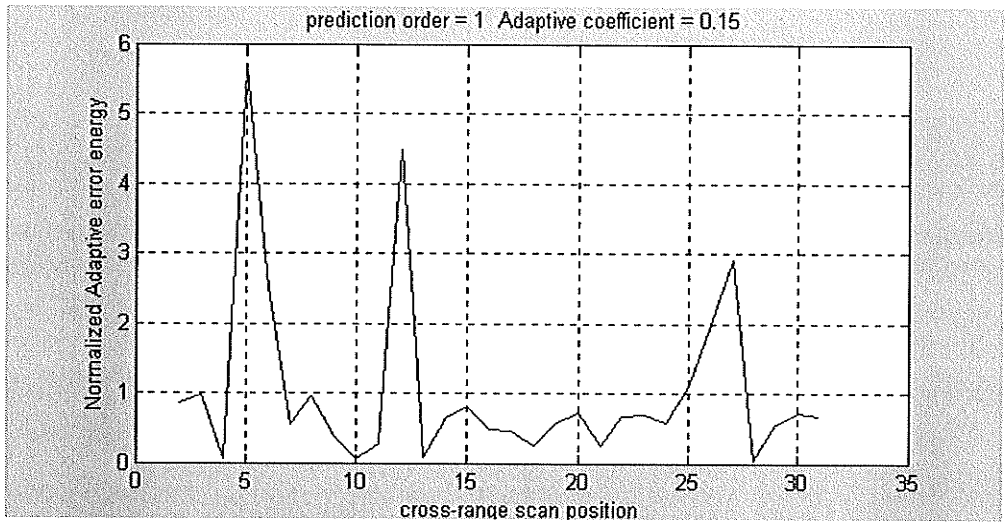

Figure 5-3-22 output of adaptive LP algorithm

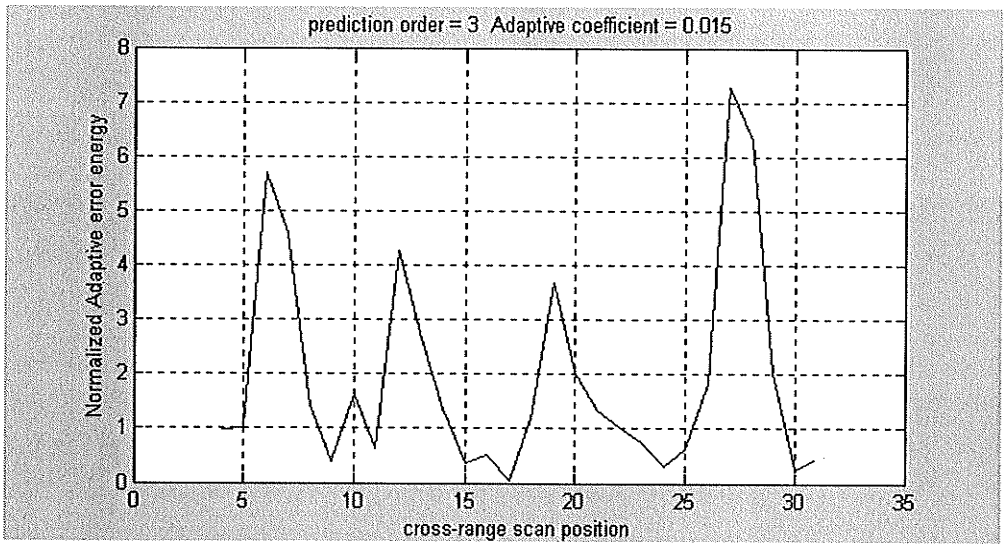

Figure 5-3-23 output of improved adaptive LP algorithm

Figure 5-3-23 is the output of improved LP algorithm with adaptive coefficient 0.015. Comparing with Figure 5-3-16, we can see that the improved, adaptive LP algorithm generates better results than the original, adaptive LP algorithm. The strongest error energy is located at the scan position 26 and 27. The adaptive coefficient is an

experimental value. With the same data, we obtain good results if the adaptive coefficient is in the range of [0.01 0.2].

The data used has a low cross-range resolution of 2.5cm. The pre-processed GPR raw data, *NA_raw_data_E3_B* from the Master database, has a higher cross-range resolution of 1cm or so. The higher cross-range resolution means a lower change in the GPR data from the nearby scan position. Figure 5-3-24 is the output of the adaptive LP algorithm with the pre-processed GPR raw data, using *NA_raw_data_E3_B* as its input. Comparing Figure 5-3-24 and Figure 5-3-15, if the normalised error energy threshold is 1.5, we can see the alarmed areas in both figures are the same. This indicates that the adaptive technique does not improve the results. This is because the cross-range resolution (1.2cm) in the pre-processed *NA_raw_data_E3_B* is high enough so that there is no big changes in nearby scan positions.

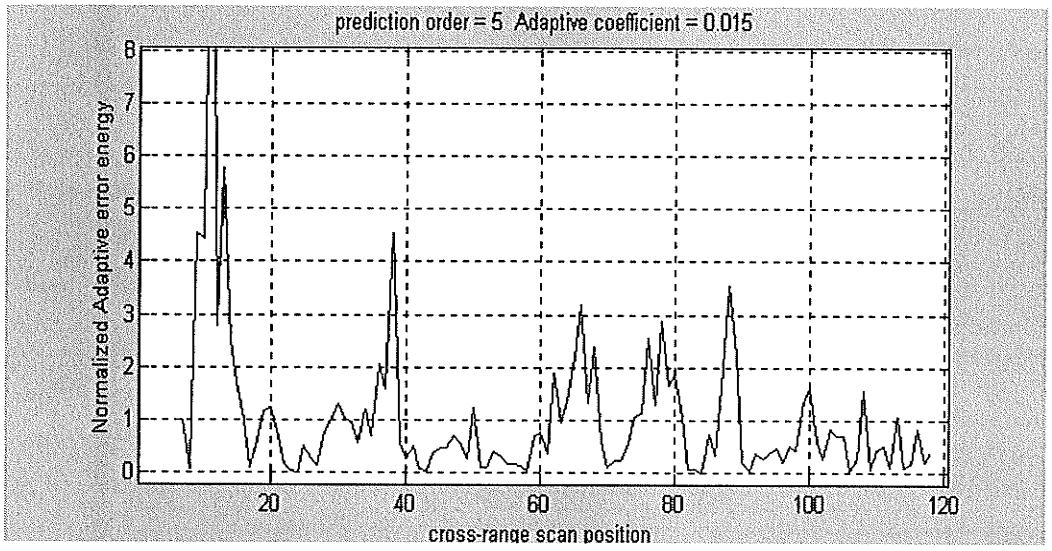

Figure 5-3-24 Output of original adaptive LP algorithm

Figure 5-3-25 is the output of improved LP algorithm with the adaptive technique. The results are not improved.

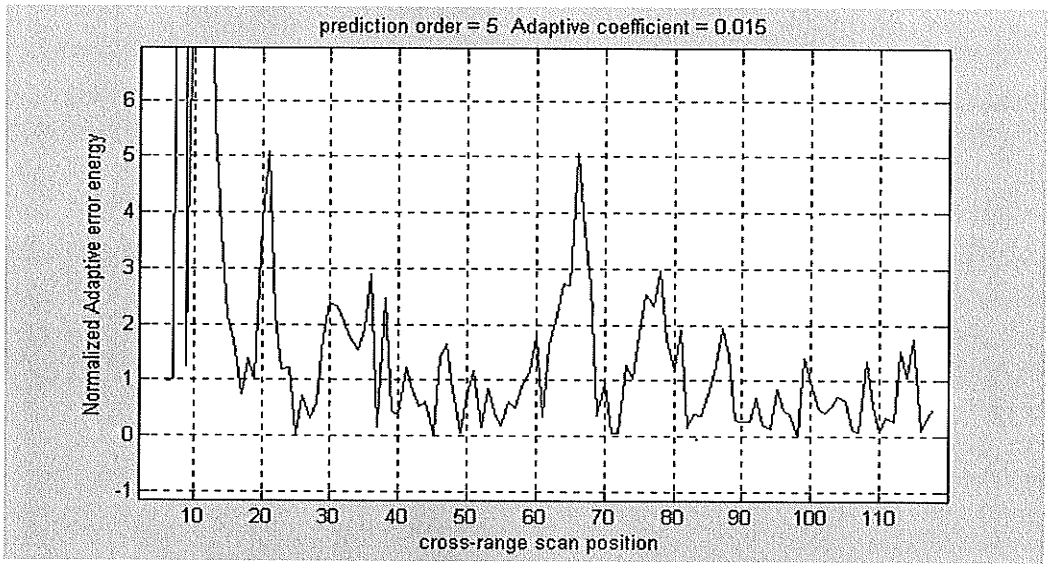

Figure 5-3-25 output of improved LP algorithm

In summary, the adaptive LP algorithm is used to adjust its results in response to the various environment changes. If the cross-range resolution is low, i.e., the distance between the closest scan position is big, the contribution from the surroundings changes quickly and then the adaptive technique is used in response to this change. The adaptive coefficient is an experimental value. With our lab collected GPR raw data, the adaptive coefficient is chosen in the range of [0.01 0.2]. The adaptive LP algorithms are able to generate alarms for landmine detection.

5.4 Summary of experiments with LP algorithm

GPR raw data with our GPR system were collected. These GPR raw data must be pre-processed before any further processing for landmine detection purpose is done. The pre-processing techniques we used are the filtering technique, which filters the out-of-range contributions, and the average background estimation method.

With pre-processed GPR raw data and without any previous knowledge of landmines, the LP algorithm can generate alarms. The lower the alarm threshold is set, the more the alarms are generated. If the threshold is not lower enough, a landmine with low energy contribution may not be detected. With a very flat surface, we find that in one case of high cross-range resolution, the original LP algorithm could detect one edge of the landmine, but fails to detect the other edge or unable to detect the buried landmine. With the improved LP algorithm, better results are obtained.

Finally, we experimented with the pre-processed GPR raw data with rocks scattered under the surface to simulate the environment changes in the fields. The adaptive LP algorithm is able to generate alarms for the buried landmines.

If a landmine is located at the area used for parameter training, the LP algorithm fails to detect the starting edge of the landmine. Using a reduced prediction order, the adaptive LP algorithm is able to detect the contributions from the buried landmine and rocks. In varying environment, the adaptive LP algorithm works better than the LP algorithm without adaptive processing.

Chapter 6 Experiments of the IT algorithm on Measured GPR Data

Using FDTD simulations, the implemented IT algorithm can decompose the residual ground surface contributions in the pre-processed GPR data and detect the simulated landmines. The cross-correlation alarm generator is introduced to solve the time consuming problem of this algorithm. In this section, we will apply the pre-processed GPR raw data to the cross-correlation alarm generator to generate alarms and then use the IT algorithm on the alarmed scan positions for the landmine detection.

6.1 Landmine signature

The reference signature of the landmine is an important feature when using the cross-correlation alarm generator and the IT algorithm. In FDTD simulation, the reference signature is obtained by subtracting the ground-only contribution from the contributions of the ground and the landmine, as mentioned in section 4-1-3. Similarly, with the pre-processed GPR raw data, the reference signature is obtained by subtracting the reflection of a deep buried landmine from the pre-processed sand-only GPR data with time gating.

Figure 6-1-1 shows the image of the pre-processed GPR raw data for the landmine signature subtraction. The landmine contribution is clearly visible. Using a time gate from 8 to 20, we obtained the reference signature.

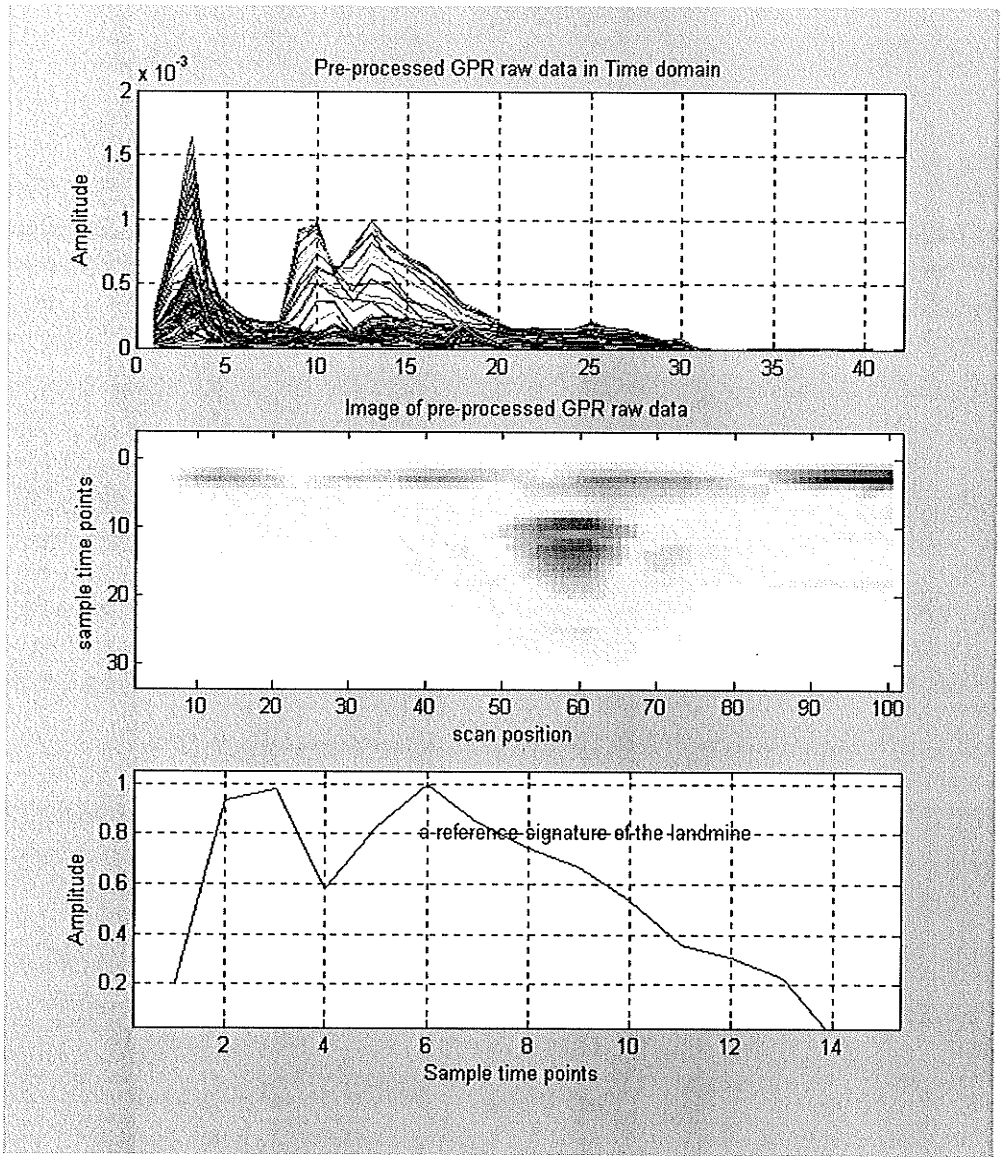

Figure 6-1-1 pre-processed GPR raw data and a reference signature of interest

6.2 Cross-correlation alarm generator

The threshold in the alarm generator is calculated at the first few free spaces, i.e. no landmine is buried at these scan positions. Figure 6-2-1 shows the image of the preprocessed GPR raw data collected with the landmine and two rocks buried in the sand.

There are 31 scan positions in total. The threshold scale F_{scale} is set to 1.1. There are 17 alarms generated. The IT algorithm is run only at the alarmed scan position. The calculation time for alarmed scan positions vs. total scan positions is reduced by 45%, $(1-\frac{17}{31}=45\%)$.

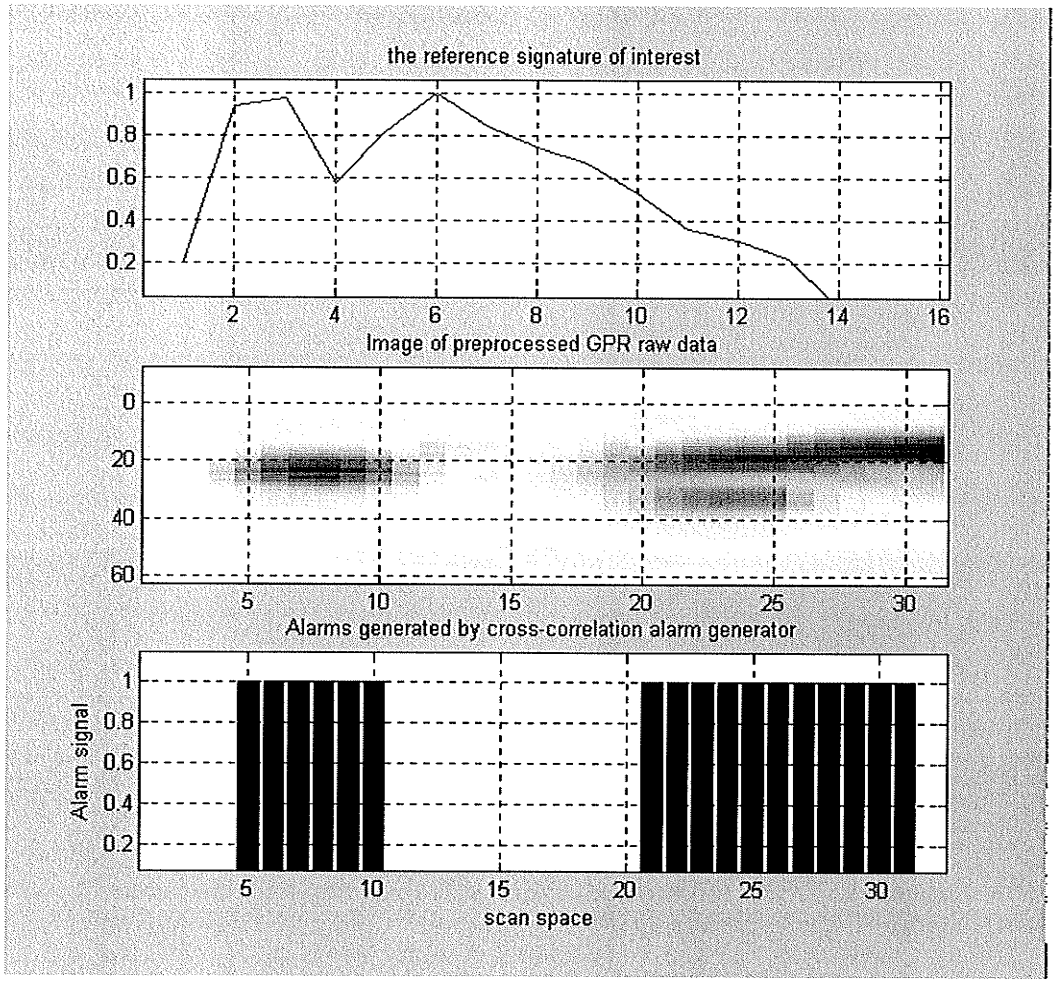

Figure 6-2-1 Illustration of alarms generated by the cross-correlation alarm generator

In Figure 6-2-2, the GPR raw data is collected with two big rocks and 5 small rocks under the surface. With 21 scan spaces and threshold scale F_{scale} of 1.1, there are

12 alarms generated. The calculation time for alarmed scan positions vs. total scan positions is reduced by 42%.

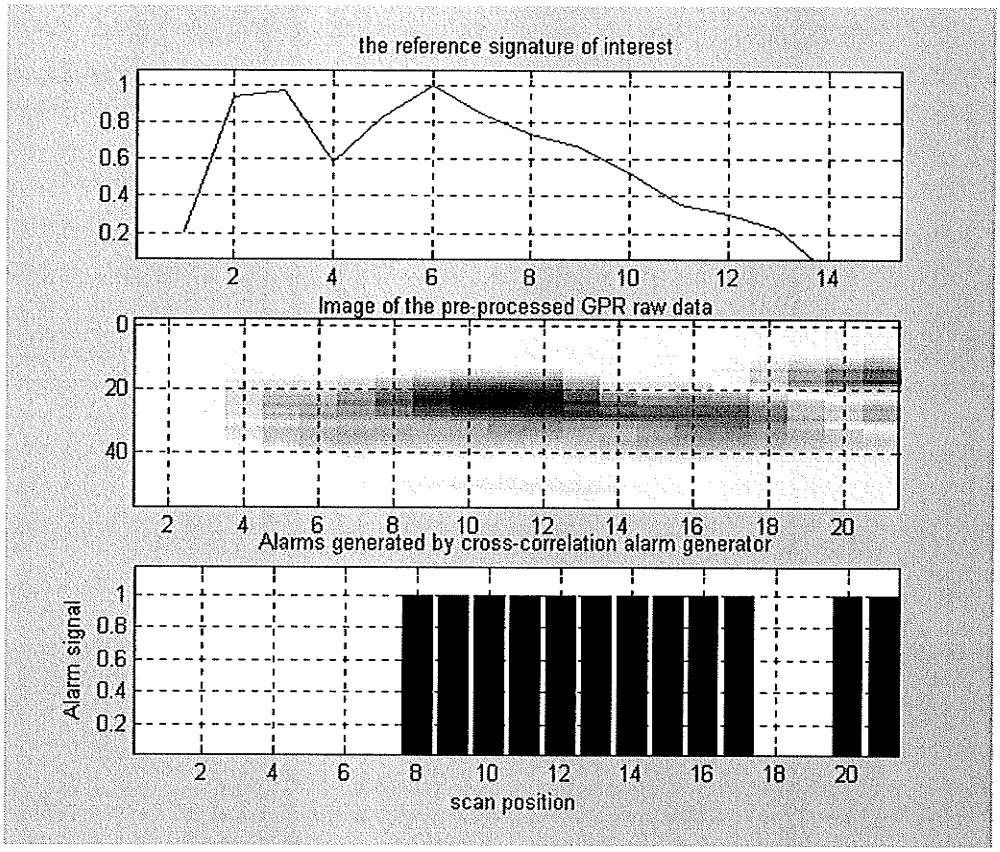

Figure 6-2-2 Illustration of alarms generated by the cross-correlation alarm generator

In Figure 6-2-3, the GPR data was collected in an unknown environment. With 118 scan positions over a 140cm beam. The threshold scale was set to 1.2, and 43 alarms were generated. The calculation time for the alarmed scan positions vs. total scan positions was reduced by 63%.

In summary, the cross-correlation alarm generator uses a reference signature of the landmine to generate alarms, which prompt us to use the IT algorithm for further landmine detection. The detection time can be reduced by up to 63% comparing it with

the time consumed by using the IT algorithm for every scan position. If the threshold is set higher, the number of alarms generated will be lower.

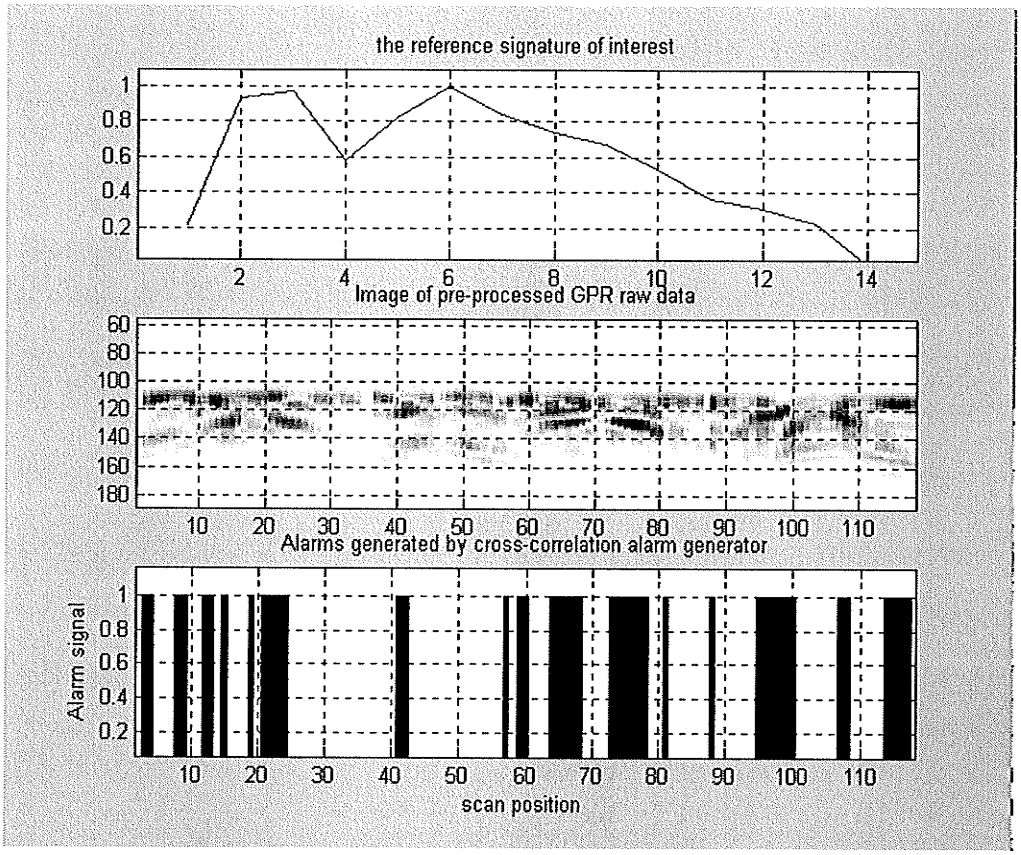

Figure 6-2-3 Alarm generated by cross-correlation alarm generator

6.3 Clutter decomposition, landmine detection and range estimation

At an alarmed scan position, the IT algorithm is used to decompose the clutter from the landmine's contribution, to further confirm the detection of a landmine and provide an estimated range. The propagation wave travels through the air (free space) and the sand. The distance between the antenna and the sand surface is variable. The estimation of the time delay from the sand surface to the buried landmine is critical for landmine

range estimation. Once the estimated time delay is obtained, the range for the landmine can be calculated accordingly.

6.3.1 Sand surface and range estimation

The microwave network analyzer does not provide the time sequence, as was the case in the FDTD simulation. The time delay for the contributions from the sand surface must be estimated first. In our lab set-up, the antenna is placed close to the sand surface to minimize the contributions from unknown sources. By doing this, we expect the strongest reflected signal to be the sand surface. Therefore, the sand surface is selected at the sample time point where the strongest signal is located.

An example of the pre-processed GPR raw data is shown in Figure 6-3-1. It has 21 scan positions along the flat sand surface, with a landmine, two big and five small rocks buried. The strongest signals for all of the scan positions are located at the same sample time point 13. The GPR waveform beyond the peak varies at different scan positions. They are the contributions received from the sand. A small peak at the sample time point 38 is explained as the contribution from the sandbox bottom or floor.

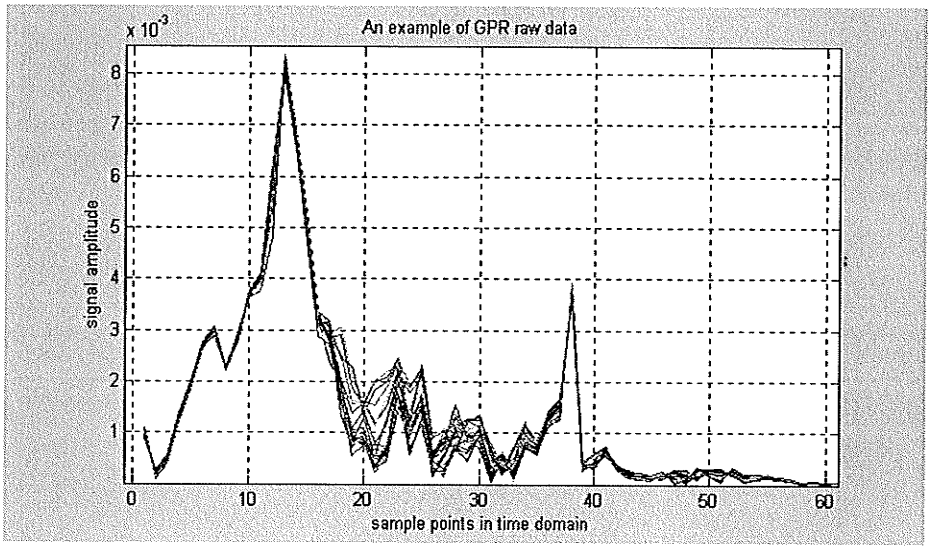

Figure 6-3-1 an example of GPR raw data before average background is removed

Once the sand surface sample point is located, we can set the first time window for the clutter estimation. The Prony technique, with an estimated rank, is used to estimate the time delay $t_{surface}$ for the sand surface contributions. If the time delay for the landmine contributions is denoted as $t_{landmine}$, then the range of the buried landmine will be:

$$R = v_g \times dt = v_g \times (t_{landmine} - t_{surface})/2 \tag{6-3-1}$$

v_g is the propagation speed. Because the network analyzer's frequency bandwidth is 11.4GHz, the time resolution is:

$$\delta_t = \frac{1}{11.4GHz} = 0.08772 \quad \text{ns} \tag{6-3-2}$$

The range resolution is defined as the minimum distance that we can identify the two separated objects. Because the time delay is two-way propagation time, the range resolution is calculated by:

$$\delta_R = \frac{\delta_t \times v_g}{2} = \frac{\delta_t \times c}{2 \times \sqrt{\varepsilon}} = \frac{4.366e^{-11} \times 3e^8}{\sqrt{3.15}} = 0.00738\text{m} = 0.738\text{cm} \tag{6-3-3}$$

where c is the propagation speed in free space and ε is the dielectric constant of the media. ε is set to 3.15 as specified in [15]. With this GPR raw data, the estimated time resolution is 0.08731909765204ns, close to the theoretical value δ_t in equation (6-3-2). The maximum range estimation error is $\delta_R/2$, i.e., 0.368cm. If the landmine is buried at a distance R, the range distortion is defined as $R \pm \delta_R$. Figure 6-3-2 is the image of the preprocessed GPR raw data, as shown in Figure 6-3-1. There is a landmine buried around 5cm deep, centered at the scan position 11. The sample time point for the landmine is

estimated at 20. Therefore, the estimated range of the landmine is $\delta_R \times (20-13) = 5.1\text{cm}$. The estimated range for the landmine is within the range distortion $5cm \pm 0.368cm$.

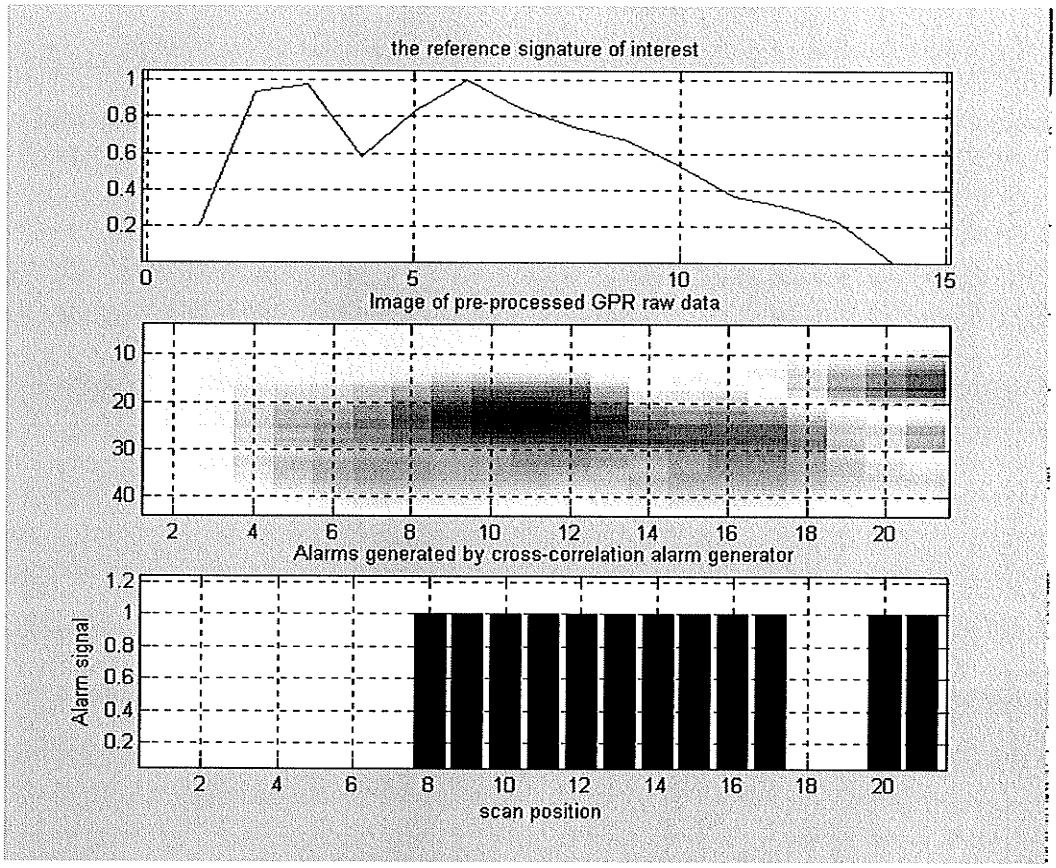

Figure 6-3-2 the image of preprocessed GPR raw data

6.3.2 Initial experiments with IT algorithm

With the pre-processed GPR raw data, shown in Figure 6-3-2, used as the input, the cross-correlation alarm generator generates 12 alarms over 21 scan positions. The IT algorithm decomposes the clutter and detects the objects on the alarmed scan positions. Figure 6-3-3 is the output of the IT algorithm with the threshold $\delta = 0.1$. The estimated objects include some rocks and the landmine. The detected areas are listed as below:

Scan positions	8	9~12	13	14~15	17	21
Detected area #	1	2	3	4	5	6

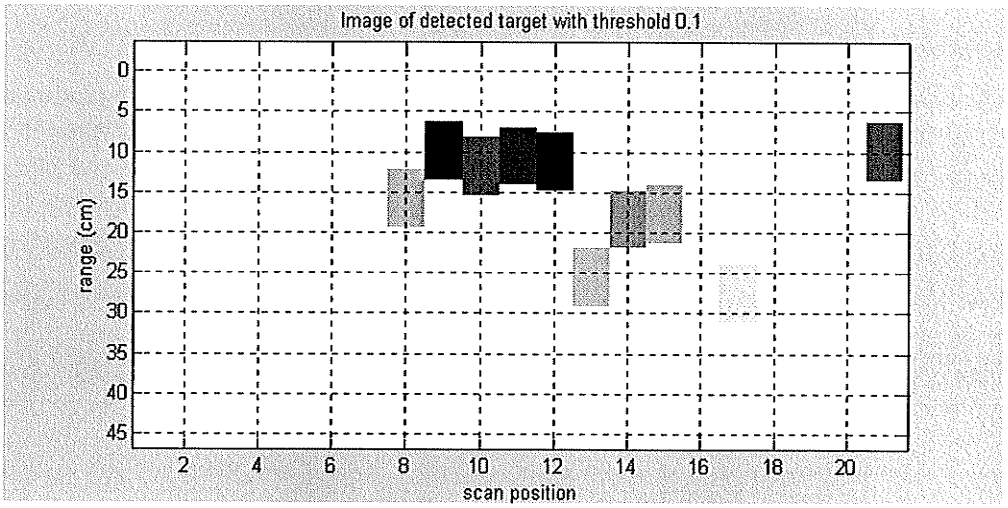

Figure 6-3-3 the output of the IT algorithm

The geometry characteristics of the landmine are helpful to reduce the false alarm rate further. Most landmines are symmetric. The landmine we used is 14cm long, 6.5cm wide and 3.5 thick. The GPR raw data, used in this thesis, was collected along the beam with the landmine face up, as shown in Figure 6-3-4.

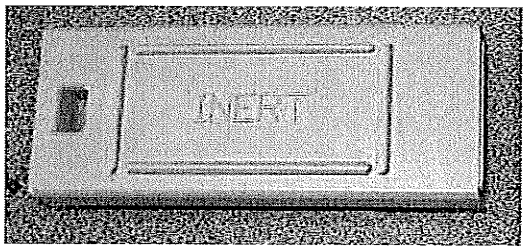

Figure 6-3-4 plastic anti-personal landmine used in our lab experiments

In this experiment, the landmine covers at least three continuous scan positions due to the cross-range resolution of 2.5cm. In Figure 6-3-3, the contributions from continuous

scan position 9 to 12 are stronger than the signals from the other alarmed scan positions. We can conclude that a landmine is detected at the scan position 9 to 12, buried about 6cm to 8cm deep. There are 1cm to 3cm differences in range estimation. The reasons could be measurement errors, waveform distortion by the rocks or imperfect of landmine signature.

6.3.3 More experiments

Figure 6-3-5(a) shows a pre-processed GPR raw data from the Master database. The cross-correlation alarm generator generates 40 alarms over a total of 118 scan positions. Figure 6-3-5(b) is the image of the estimated objects by the IT algorithm. The detected areas are listed in table 6-1.

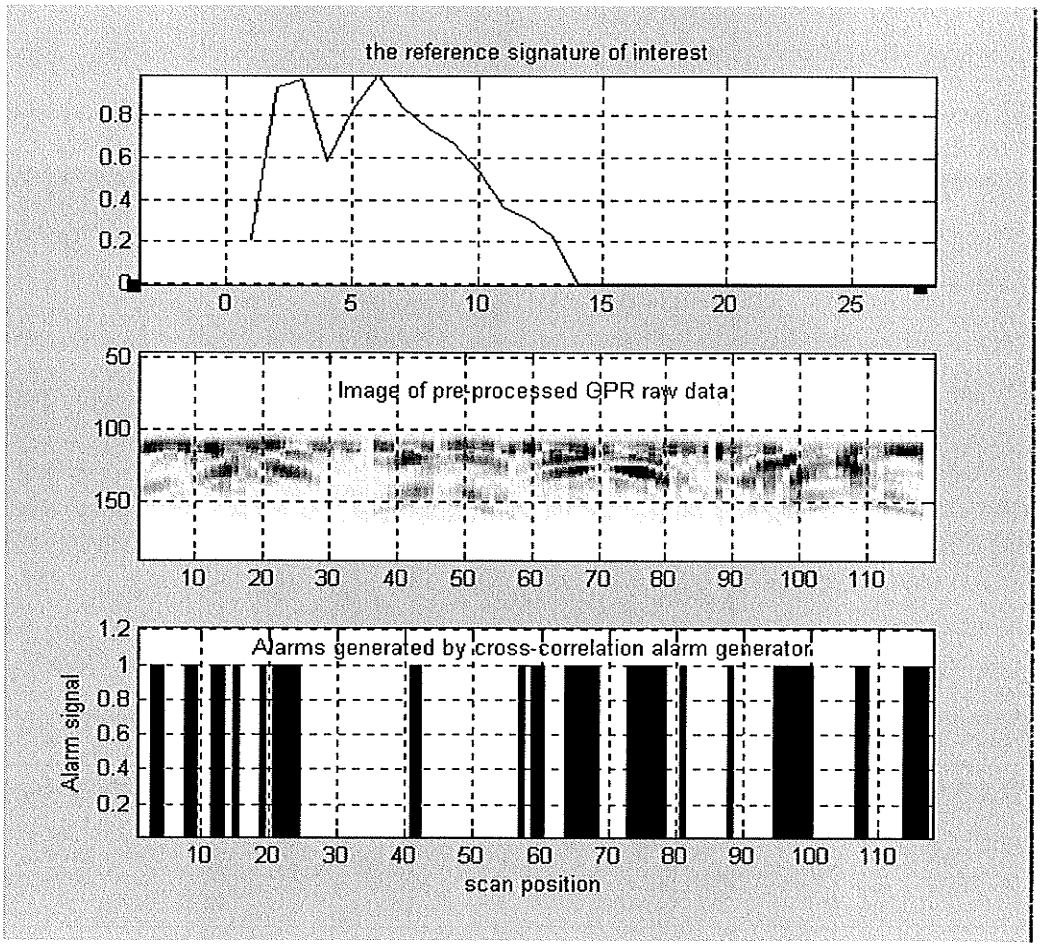

Figure 6-3-5(a) an example pre-processed GPR raw data for the IT algorithm

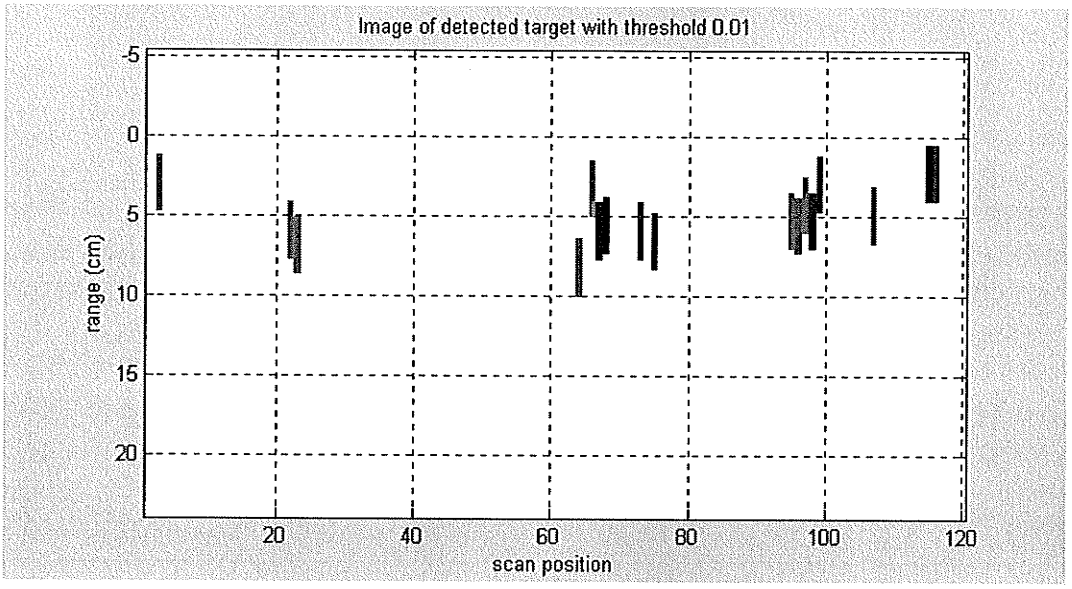

Figure 6-3-5(b) the output of the IT algorithm

Table 6-1 estimated objects from Figure 6-3-5(b)

Detected area #	Scan positions	Range (cm)
1	3	1
2	22 and 23	4~5
3	64 to 75	4~5
4	95 to 98	3.5
5	107	3
6	115 and 116	0.5

The cross-range resolution is approximate 1cm. The landmine should cover more than five continuous scan positions. The detected areas #3 and # 4 are two possible areas containing buried landmines. Table 6-2 is the geometry model (see Appendix III for geometry structure) for the GPR raw data collection. It indicates that a square landmine is buried 3cm deep centred at cross range scan position 80cm (scan position 67) and a round landmine 1cm deep at 119cm (scan position 100). There are ten rocks scattered around.

We conclude that the square landmine is detected, located at scan position from 64 to 75, with estimated depth of 4cm. The area #4 is a false alarm caused by the contributions from the rocks.

Geometry model: Table 6-2

	X(cm)	Y(cm)	Z(cm)	Scan position
Square Mine	80	59	3	67
Round Mine	119	59	1	100
Rock 1	123	50	5.5	103
Rock 2	95	70	6	80
Rock 3	53	58	3.5	44
Rock 4	78	34	4	65
Rock 5	30	21	5	25
Rock 6				
Rock 7	125	30	5	105
Rock 8				
Rock 9	69	65	5.5	58
Rock 10				
Rock 11	20	51	2	16
Rock 12	10	59	5.3	8
Rock 13	100	39	2.5	84

Figure 6-3-6 shows another pre-processed GPR raw data from the Master database. The cross-correlation alarm generator generates 52 alarms over 118 scan positions. Figure 6-3-7 is the image of the estimated objects by the IT algorithm. The detected areas are listed in table 6-3.

Table 6-3 estimated objects from Figure 6-3-7

Detected area #	Scan positions	Range (cm)
1	12	8
2	38 and 38	0.5
3	57 to 61	4~6
4	72	4
5	91	5.5
6	103	5

The detection result is that a landmine is buried at scan positions 57 to 61, with the estimated depth of 4 to 6cm.

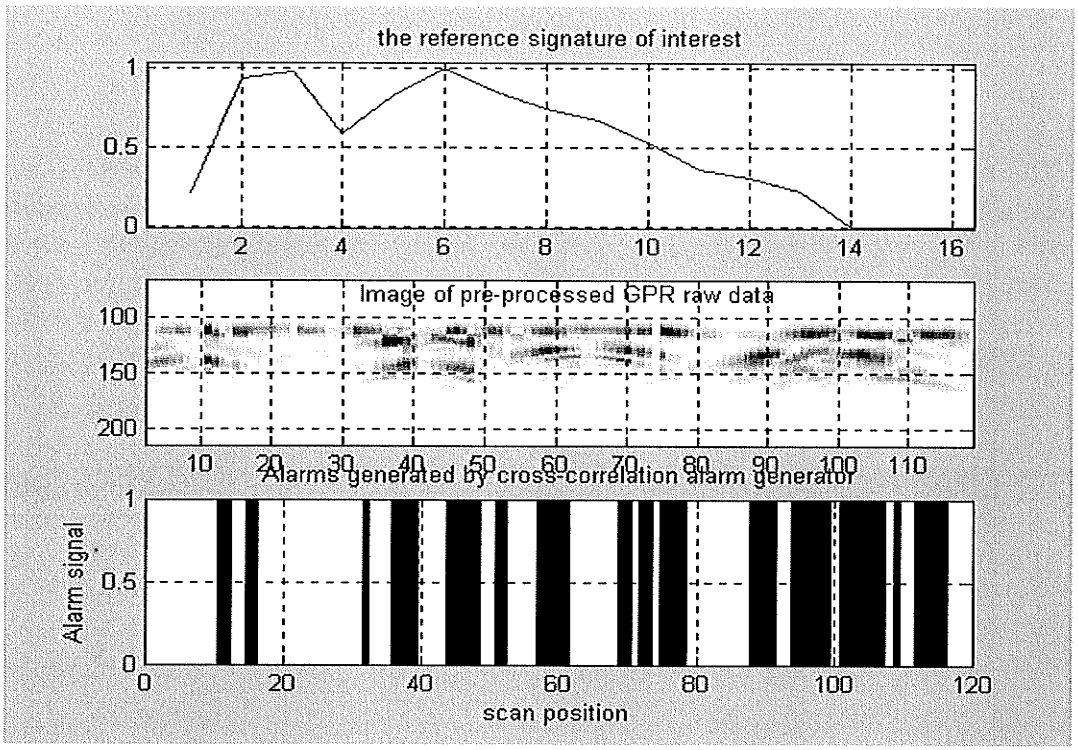

Figure 6-3-6 an example pre-processed GPR raw data for the IT algorithm

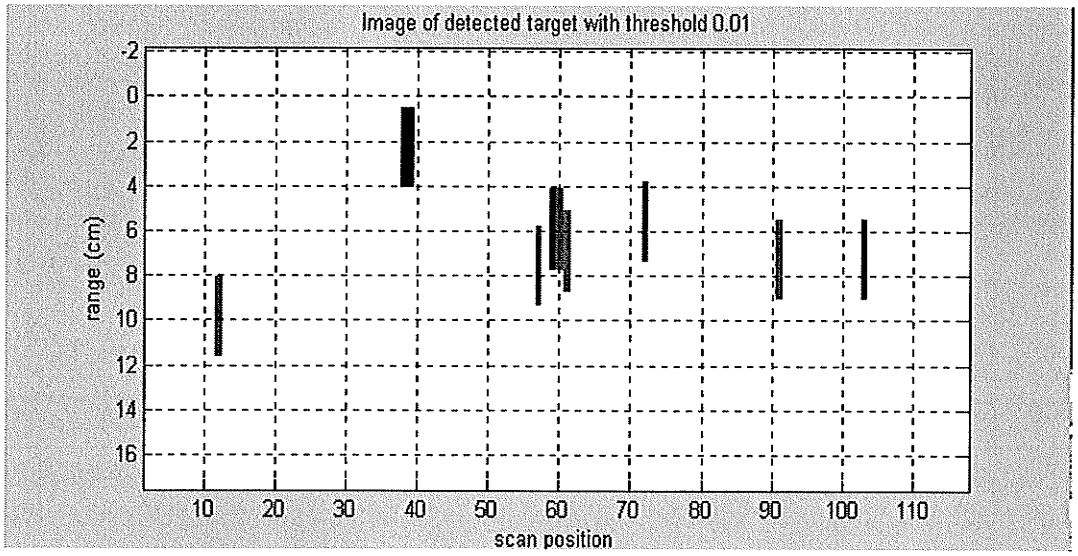

Figure 6-3-7 the output of the IT algorithm

6.4 Summary of experiments with IT algorithm

Using an ultra-bandwidth microwave network analyzer (1GHz to 12.4GHz), range resolution of around 0.7cm can be obtained. This resolution allowed us the use of early time gates to decompose part of the contributions from the sand surface and apply a cross-correlation alarm generator. The data at scan positions selected by these alarms was further processed using an IT algorithm. With the pre-processed GPR raw data, the cross-correlation alarm generator can reduce the time consumption of this IT algorithm significantly by up to 60%, depending on an experimental alarm threshold. The time delays for the sand surface and the detected objects were estimated. The estimated range of the landmine is within the range distortion. With many different sized rocks scattered in the sand, the IT algorithm was able to detect the square landmine and provided an estimated range.

Chapter 7 Conclusions and Future Work

The effort of this research was to develop DSP algorithms to be used in data collected by the GPR system built at the University of Manitoba, for landmine detection. In this thesis, the linear prediction algorithm and the IT algorithm combined with a cross-correlation alarm generator were investigated.

The DSP algorithms, implemented for GPR data pre-processing, are the linear prediction algorithm for the deterministic signal reduction based on the layered ground model and (adaptive) average background estimation. The linear prediction algorithm for the deterministic signal reduction based on the layered ground model was found to be more suitable for FDTD GPR data. With the lab collected GPR raw data, the average background estimation method could effectively remove the background noise.

Two alarm generators, the LP algorithm and the cross-correlation alarm generator, were implemented. With both FDTD GPR data and lab-collected GPR raw data, the LP algorithm with/without adaptive technique generated alarms at scan positions where buried landmines were located. The improved LP algorithm obtained better results than the original one. The landmine detection and false alarm rates were studied for different SNR values. With both FDTD GPR data and lab-collected GPR raw data, the cross-correlation alarm generator generated alarms at scan positions where landmines were buried. The cross-correlated alarm generator generated more alarms than the LP algorithm with a good landmine detection rate for high SNRs (greater than –5.5dB).

The IT algorithm was applied at the alarmed scan positions. This reduced the time consumption introduced by the IT method. With FDTD GPR data and lab-collected GPR raw data, the implemented IT algorithm decomposed the clutter, reduced alarms and

provided estimated ranges for the detected objects. The sand surface time delay was estimated in order to estimate range more accurately.

Using FDTD GPR data, the simulations verified the adequacy of these algorithms for landmine detection. Experiments with the measured GPR data proved that these implemented DSP algorithms were able to detect the square landmine. Ranges of the buried objects were also estimated.

Other contributions of this thesis included the following. The linear prediction algorithm for deterministic signal reduction based on layered earth model was introduced. We improved the LP algorithm to obtain a better result for the general alarm generation. Using the cross-correlation alarm generator reduced the time consumption by the IT approach. We developed the dynamic rank method for clutter estimation. The surface time delay was introduced in order to calculate the ranges of the detected objects.

Currently, FDTD GPR data is obtained based on a simple model. Further study may be needed to create more complex models with simulated rocks and rough surfaces for the GPR data simulation. Our experiment efforts were focussed on the detection of a square non-metal landmine buried in dry sand with scattered rocks. Future work may consider the application of these methods with different landmines under different propagation media.

Appendix I

Simplex Method and LSE Method for Target parameters estimation

- **The Simplex Method**

MATLAB function ***fminsearch*** uses the simplex search method to find the minimum of a scalar function of several variables, starting at an initial estimate. It is generally referred to as unconstrained nonlinear optimization.

fminsearch($myfun, x_0, options, p_1, p_2, ...$) starts at the point x_0 and finds a local minimum x of the function described in $myfun$. x_0 can be a scalar, vector, or matrix. It passes the problem-dependent parameters p_1, p_2, etc., directly to the function myfun.

Let

$$x = [real\ (Ar) \quad imag\ (Ar) \quad \gamma \quad t_r]$$

$$p_1 = [\omega; \quad T(\omega)]$$

$$p_2 = R(\omega)$$

Where A_r is a complex number representing the scattering factor in the damped exponential model [5]. γ represents the damping factor, and t_r represents the time delay. $T(\omega)$ is the reference signature. ω is the frequency. We use **fminsearch** to search the optimized parameters that minimizes the error in equation (3-4-2).

- **Least Square Error (LSE) method:**

MATLAB function **lsqcurvefit** solves nonlinear curve-fitting (data-fitting) problems in the least-squares sense. That is, giving the input data x_{data} and the observed output y_{data}, we find coefficients x that "best-fit" the following equation.

$$\min_x \frac{1}{2}\left\|F(x, x_{data}) - y_{data}\right\|^2 = \frac{1}{2}\sum_i \left\|F(x, x_{data_i}) - y_{data_i}\right\|^2$$

Where x_{data} and y_{data} are vectors and $F(x, x_{data})$ is a vector valued function.

$$x = \text{lsqcurvefit}(myfun, x_0, x_{data}, y_{data})$$

Starts at x_0 and finds parameter x to best fit the nonlinear function myfun(x, x_{data}) to the data y_{data} in the least-squares sense. y_{data} must be the same size as the vector (or matrix) returned by myfun(x, x_{data}).

Let

$$x = [real(Ar) \quad imag(Ar) \quad \gamma \quad t_r]$$

$$x_{data} = [\omega; \quad T(\omega)]$$

$$y_{data} = R(\omega)$$

Where A_r is a complex number representing the scattering factor in the damped exponential model [5]. γ represents the damping factor, and t_r the time delay. $T(\omega)$ is the reference signature. ω is the frequency.

- **Simplex Method and LSE method for the x parameter estimation**

Both **Simplex method** and **Least Square Error (LSE) method** are useful for solving the nonlinear problem in (3-4-3). **fminsearch** is unconstrained nonlinear optimization, and **lsqcurvefit** is the best-fit for the problem in the least-squares sense. **lsqcurvefit** may only give local solutions , and the function " myfun " to be minimized must be continuous. **fminsearch** can often handle discontinuity, particularly if it does not occur near the solution. In our case, the estimation of the start point may not near the solution, so the **fminsearch** is a better choice.

- **Simulation results**

Data generator:

Set $x=[real(Ar)\ \ imag(Ar)\ \ \gamma\ \ t_r]$ to different values and add noise into the landmine's contribution $A_r e^{-\omega\gamma_r} e^{-j\omega t_r} T_r(\omega)$, which is defined as ***myfun***.

$$y_{data} = A_r e^{-\omega\gamma_r} e^{-j\omega t_r} T_r(\omega) + noise \qquad \text{(A-1)}$$

The additional noises are normal random numbers with zero mean and standard deviation N_{level}.

Parameters estimated with no noise:

Set N_{level}=0, $A_r = 0.23 + j0.54$, time delay t_r=1.3, and the damping factor γ=2.1 in equation (A-1). The estimate parameters by **fminsearch** and **lsqcurvefit** are $x=[0.23\ \ 0.54\ \ 2.1\ \ \ 1.3]$. This is correct.

Parameters estimated with noise added:

Set $x=[0.23\ \ \ 0.54\ \ \ 2.1\ \ \ \ 1.3]$ as the original parameter x_0. N_{level} is chosen in the range from 0.01 to 0.15. With each N_{level}, we generates ***estX0***$=[real(estAr)\ \ imag(estAr)\ \ est_\gamma\ \ est_t_r]$as the estimated start point for the estimation of x_0 in both **fminsearch** and **lsqcurvefit** functions.

The estimated start points with different N_{level} values are shown at the top four charts of the following Figure. The blue lines are the original parameters in the vector x_0. The green curves are the estimated start points, i.e.,

$$estX0 = [real(estAr)\ \ \ imag(estAr)\ \ \ est\_\gamma\ \ \ est\_t_r].$$

We can see that the differences between the original parameters and corresponding components in ***estX0*** are increased as N_{level} is increased.

The middle four charts of the Figure are the outputs of **lsqcurvefit** function. The blue curves are the original parameters. The red curves are the estimated parameters with the original parameter vector x_0 as the start point. The green curves are the estimated parameters with the estimated parameter vector *estX0* as the start point.

The bottom four charts of the Figure are the outputs of the **fminsearch** function. The blue curves are the original parameters. The red curves are the estimated parameters with the original parameter vector x_0 as the start point. The green curves are the estimated parameters with the estimated parameter vector *estX0* as the start point.

We can see that LSE method is sensitive to the start point of the parameters. With the original parameter vector x_0 as the start point, the output of **fminsearch** function, Simplex method, is almost the same as the output of **lsqcurvefit** function, the LSE method. However, with the estimated parameters *estX0*, the results from the Simplex method are much better than the results from the LSE method. The output of **fminsearch** function is constantly optimized to the original parameters x_0.

Conclusion

The difference between the estimated start point *estX0* and the original start point x_0 increases as the noise deviation, N_{level}, increases. With the Least Square Error (LSE) method, the search of the start point is important. The errors between the estimated parameters and the original parameters increase as the noise deviation increases. The Simplex Method is less sensitive to the start point as the LSE method does. Comparing with the LSE method, the Simplex method gets better results in the parameter estimation for equation (A-1).

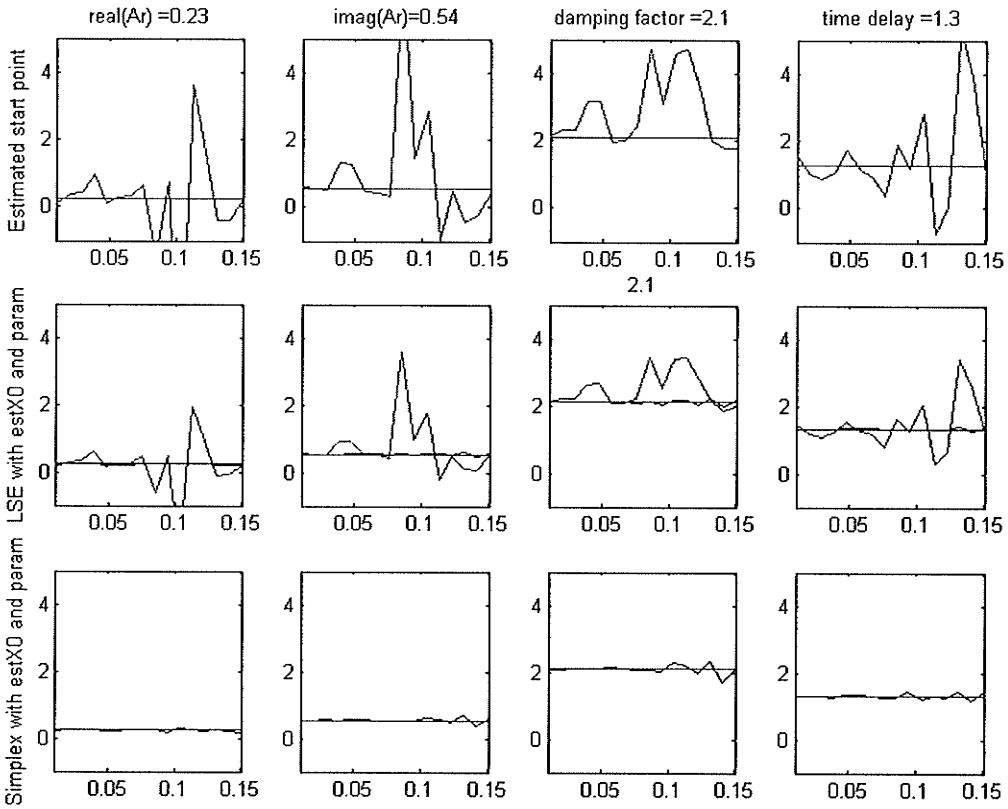

N_{level}

Blue line ---------- the original parameters
Green line ---------- Estimated parameters with the estimated start point
Red line ---------- Estimated parameters with the original start point

Appendix II

An example of the problem model for FDTD simulated GPR data

```
*************************************************************************
***
* Input data file for GPR
* March 11 2003
* GPR problem, Test
*************************************************************************
*
.Problem size: lower_x, upper_x, lower_y, upper_y, lower_z, upper_z
0 240 0 33 0 240
*
.Number of time steps and output frequency of the data
1000 300
*
.Space increment: delta_x, delta_y, delta_z
1
0  240  0.0025
1
0  33  0.0025
1
0  240  0.0025
*
.Test point T1
80 16 50 3 T1
*
.Test point T2
85 16 50 3 T2
*
.Test point T3
90 16 50 3 T3
*
.Directory to which output the files
./Example/
*
.Boundary conditions: specify with characters ('e' or 'a')
aaaaaa
*
.Mur ABC: 1 - first order; 2 - second order
2
*
.Object Ground
16 224 16 17 100 220 7 1.0 0.01
*
.Object bomb
116 124 16 17 130 132 3.5 1.0 0.01
*
.Isource dipole
3 120 121 16 17 20 21 1.0 1.0 0.0 0.0
dgaussian
1.0 1e-9 1.75e-10
*
.End: end of file
```

Appendix III

The following geometry is used in the experiments setup.

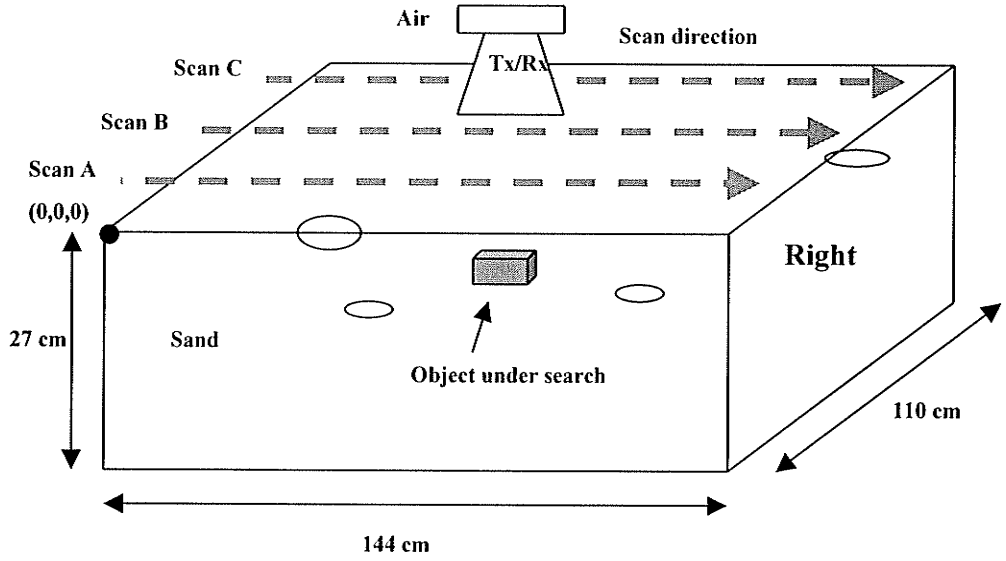

Fig. 2. Scanning set up

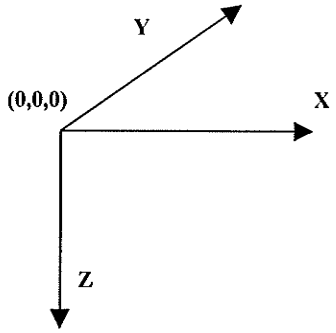

Fig. 3. 3-D Coordinate system adopted

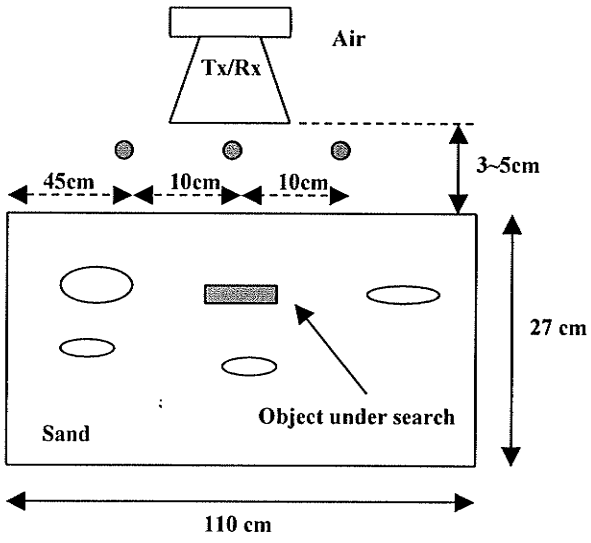

Fig. 4. Side view (right side) of scanning setup

Appendix IV

The coefficients of linear prediction algorithm for alarm generator
The derivation of equation (3-2-3)

$$\xi(n) = e(n)^* C^{-1} e(n) = [y(n) - \tilde{y}(n)]^* C^{-1} [y(n) - \tilde{y}(n)]$$
$$= [y_w - Y_w(n)a]^* [y_w - Y_w(n)a]$$

Where
$y_w(n) = wy(n)$
$Y_w(n) = wY(n)$
$C^{-1} = w^* w$

Take the derivative with respect to a and set to zero

$$\frac{\partial \xi(n)}{\partial a} = (-Y_w(n)^*)[y_w - Y_w(n)a] + [y_w^* - a^* Y_w(n)^*]\{-Y_w(n)\} = 0$$

We have:

$$(-Y_w(n)^*)[y_w - Y_w(n)a] = [y_w^* - a^* Y_w(n)^*]Y_w(n)$$
$$(-Y_w(n)^*)y_w + Y_w^*(n)Y_w(n)a = y_w^* Y_w(n) - a^* Y_w(n)^* Y_w(n)$$
$$Y_w(n)^* y_w + y_w^* Y_w(n) = Y_w^*(n)Y_w(n)a + a^* Y_w(n)^* Y_w(n)$$
$$Y_w(n)^* y_w + [Y_w^*(n) y_w]^* = Y_w^*(n)Y_w(n)a + \{[Y_w(n)^* Y_w(n)]^* a\}^*$$

Comparing the both side of the above equation, we obtain:

$$Y_w(n)^* y_w = Y_w^*(n)Y_w(n)a$$

If $Y_w^*(n)Y_w(n)$ is invertible, then we have:

$$a = [Y_w^*(n)Y_w(n)]^{-1} Y_w(n)^* y_w$$

References:

1. Ashley, S. (1996) Searching for landmines, *Mechanical Engineering, Vol. 118, No. 4,62*, found at http://www.unb.ca/ME/LTMD/LANDMINE.htm

2. Alan V. Oppenheim, "Applications of digital signal processing", *Massachusettes Institute of Technology Cambridge.*

3. K.S.Kunz. R.J. Luebbers, "The Finite Difference Time Domain Method for Electromagnetics", *CRC Press, Florida, 1993*

4. L.van Kempem, H.Sahli, 'Signal Processing Techniques for Clutter Parameters Estimation and Clutter Removal in GPR data for landmine detection," *ETRO Dept, IRIS Research group, 0-7803-7011-2/01, @2001 IEEE.*

5. Andria van der Merwe and Inder J. Gupta, "A Novel Signal Processing Technique for Clutter Reduction in GPR Measurements of Small, Shallow Land Mines," *IEEE Transactions on Geoscience and Remote Sensing, Vol.38, No. 6, Novemember 2000*

6. H. Brunzell, "Detection of shallowly buried objects using impulse radar," *IEEE Trans. Geosci. Remote Sensing, vol.37, pp.875-886, Feb. 1999*

7. A. Guantilaka and B.A. Baertlein, "asubspace decomposition technique to improve GPR imaging of anti-personnel mines," The Ohio State University ElectroScience Laboratory.

8. Ross W. Deming, "Automatic Buried Mine Detection Using the Maximum Likelihood Adaptive Neural System," *Processings of the 1998 IEEE.*

9. A. Farina and A. Protopapa, "New results on linear prediction for clutter cancellation," *IEEE trans, Aerosp. Electron, May 1998*

10. K.V. Ho and Paul D. Gader, "A Linear Prediction Landmine Detection Algorithm for Hand Held Ground Penetrating Radar," *IEEE transactions on Geoscience and remote Sencing," Vol.40, No. 6, June 2002*

11. Paul D. Gader, Miroslaw Mystkowski and Yunxin Zhao, "Landmine Detection with Ground Penetrating Radar Using Hidden Markov models," *IEEE Trans. On Geoscience and remote sensing, Vol. 39, No.6, June 2001*

12. Dragana Carevic, "Wavelet-based method for detection of shallowly buried objects from GPR data," *Surveillance Systems Division, Australia.*

13. Xiaoyin and Eric L. Miller, "On the use of Constrast Stretch and Adaptive filter to Enhance Ground Penetrating Radar Imagery," *Center for Subsurface Sensing and Imaging Systems, Northeastern University, Boston, MA 02115.*

14. Lagarias, J.C., J. A. Reeds, M. H. Wright, and P. E. Wright, "Convergence Properties of the Nelder-Mead Simplex Method in Low Dimensions," *SIAM Journal of Optimization, Vol. 9 Number 1, pp. 112-147, 1998.*

15. Ivor L. Morrow and Piet van Genderen, " Effective Imageing of Buried Dielectric Objects", *IEEE Transactons on Geoscience and remote sensing, vol. 40, No. 4, April 2002*

16. Landmines, Mine Action News form the United Nations, *vol. 3.2, 4th Qtr, 1998*

17. "Hidden Killers: The global landmine crisis," *U.S. Dept. State Rep., Publ. 10575, Washington, DC, Sept. 1998*

18. Scott Peters, Ian Jeffrey, Colin Gilmore and Derek Collions, "Design Construction and Testing of a Ground Penetrating RADAR System for use in Landmie Detection", *Department of Electrical and Computer Engineering at University of Manitoba*

19. Eduardo Corral, Hong Su and Peilin Yao, "GPR Master Database Collection of Objects Buried in Sand", *Department of Electrical and Computer Engineering at University of Manitoba*

20. M. Rahman and K.-B. Yu, "Total least squares approach for frequency estimation using linear prediction," *IEEE Trans. Acoust., Speech, Signal Processing*, vol. ASSP-35, pp. 1440–1545, Oct. 1987.